Controlled Release Films and Functional Surfaces Targeting Infection, Inflammation, and Bleeding

by

Anita Shukla

B.S., Chemical Engineering and Biomedical Engineering,
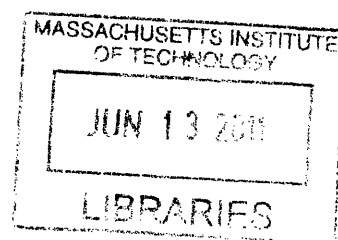Carnegie Mellon University, Pittsburgh, PA (2006)

M.S., Chemical Engineering Practice,
Massachusetts Institute of Technology, Cambridge, MA (2008)

SUBMITTED TO THE DEPARTMENT OF CHEMICAL ENGINEERING IN PARTIAL
FULFILLMENT OF THE REQUIREMENTS FOR THE DEGREE OF

DOCTOR OF PHILOSOPHY IN CHEMICAL ENGINEERING
AT THE
MASSACHUSETTS INSTITUTE OF TECHNOLOGY

JUNE 2011

Signature of Author...

Anita Shukla
Department of Chemical Engineering
May 11, 2011

Certified by..

Paula T. Hammond
Bayer Professor of Chemical Engineering and Executive Officer
Thesis Supervisor

Certified by..

Robert S. Langer
David H. Koch Institute Professor
Thesis Supervisor

Accepted by..

William M. Deen
Professor of Chemical Engineering
Chairman, Committee for Graduate Students

Controlled Release Films and Functional Surfaces Targeting Infection, Inflammation, and Bleeding

by

Anita Shukla

Abstract

Uncontrolled bleeding and infection are leading causes of patient morbidity and mortality following traumatic injury. Traditional pressure based methods of hemorrhage management are not suitable for incompressible or complex wounds. There is increasing interest in non-pressure based hemostatic dressings; however, many of these existing dressings are not amenable for use in complex sites and are often accompanied by adverse side effects. Additionally, patients are typically administered broad-spectrum antibiotics to prevent and eliminate existing infection. The systemic overuse of antibiotics has led to a worldwide increase in drug-resistant bacteria. As an alternative to these conventional treatments, local therapeutic delivery has the potential to effectively treat cellular dysfunction while avoiding drug toxicity.

This thesis focuses on developing degradable layer-by-layer (LbL) assembled multilayer films as local delivery coatings to address infection, inflammation, and bleeding. These films were engineered to deliver potent antibiotics such as vancomycin and exploratory drugs such as antimicrobial peptides, which prevent the development of drug resistant bacteria. Active films with large drug loadings and a range of drug release profiles were developed by taking advantage of film architectures, assembly techniques (spray versus dip LbL), and film component interactions. Due to the prevalence of infection and inflammation, degradable coatings for the concurrent release of antibiotics and anti-inflammatory therapeutics were also designed. These films have the potential to address a wide range of infection and inflammation requirements, from short term infection and inflammation eradication for trauma relief to infection prevention and long term inflammation mitigation from biomedical implants. All films were successfully applied to medically relevant substrates, including bandages and sutures, and were shown to be active *in vitro* against *Staphylococcus aureus* and cyclooxygenase. To address current complications with bleeding control, multilayer films were developed based on hydrogen bonding interactions found to occur between a polyphenol, tannic acid, and an essential clotting factor, thrombin. These thin films were used to coat a common clinically applied absorbent and porous gelatin sponge without reducing its liquid absorption capabilities. Coated sponges were shown to be highly effective in promoting hemostasis in a porcine spleen injury model. The therapeutic films developed in this thesis have the potential to be applied to any clinical substrate. Additionally, drug loading and release can be tuned based on the desired application.

Thesis Supervisor: Paula T. Hammond,
                      Bayer Professor of Chemical Engineering and Executive Officer
Thesis Supervisor: Robert S. Langer,
                      David H. Koch Institute Professor

For my loving parents,
Arun and Vinita Shukla

Acknowledgments

There are so many individuals I would like to thank that have made this thesis possible. First, I would like to thank my advisor, Professor Paula Hammond. Paula has been a wonderful mentor who has taught me so much during my years at MIT. She is a truly inspiring person who has always been tremendously supportive of me. I would also like to thank my co-advisor, Professor Robert Langer, who has been a great source of guidance during my thesis research. Additionally, I am grateful to my thesis committee members, Professor Greg Stephanopoulos and Dr. James Bradner, who have always been enthusiastic about my research, providing a unique perspective and invaluable suggestions.

I am indebted to all of the Hammond Lab members who have been wonderful colleagues and friends during my time at MIT. In particular, the Layer-by-Layer Drug Delivery Subgroup has been a great source of intellectual input throughout my Ph.D. In particular, I would like to acknowledge Dr. Mara Macdonald who personally mentored me as an early graduate student, helping me get started on my research. Mara continues to be wonderful mentor and a great friend. I would also like to thank Dr. Kevin Krogman for teaching me about spray layer-by-layer assembly. I am very grateful to my wonderful collaborators, Dr. Renée Fuller and Dr. Amanda Engler. The work described in Chapter 4 could not have been completed without Renée; she is a wonderful person and good friend. Amanda initiated a collaboration in which together we characterized her antimicrobial polypeptides (work described in Chapter 7). I have learned so much from Amanda and thank her for her collaboration and friendship. I am also greatly indebted to Ferrosan and in particular, Flemming Jensen, who has been a great collaborator and helped coordinate testing of the devices described in Chapter 6 of this thesis. I have also been very blessed to have worked with several talented undergraduates during my time at MIT. In particular, I would like to thank Sravanthi Puranam and Jean Fang, who continue to amaze me; they are two of the most driven and bright students I have encountered. I would also like to acknowledge all of the staff in Chemical Engineering and the Institute for Soldier Nanotechnologies for their help throughout my graduate career. I would especially like to thank Christine Preston whose kind smile, sense of calm, and organizational skills have always made my life so much easier.

Much of the reason I am at MIT is due to the support of several faculty members who I encountered in my years as an undergraduate student at Carnegie Mellon University. I would like to thank Professor Lynn Walker, who was my research advisor during my time at CMU. Thank you, Professor Walker, for telling me to get my act together if I ever wanted to get into a graduate school like MIT during my first semester at CMU. I would also like to thank Professor Krystyn Van Vliet who was my research mentor during a summer research experience for undergraduates program at MIT. Professor Van Vliet is a wonderful mentor and has continued to be very supportive of throughout my graduate career. Additionally, I would like to thank Professor Hadley Sikes, who has provided me with great mentorship and career advice during graduate school.

Last but not least, I would like to acknowledge my family and friends. In particular, I would like to thank my husband, Vikas Srivastava. Vikas balances me perfectly and has really been

Contents

Figures

16

Tables

Chapter 1

Introduction

Bleeding and infection are two major causes of patient morbidity and mortality following traumatic injury [1-3]. Traditional options for hemorrhage control include the application of pressure-based devices such as tourniquets and compressive bandages. However, these devices are often unsuitable for application to complex wounds or incompressible sites, and recently there has been much interest in the development of non-pressure based hemostatic dressings [1, 4]. Fibrin based glues and dressings have been used to augment the natural clotting cascade. However, fibrin products are not practical due to their short shelf-life, exorbitant prices, and risk of disease transfer. Zeolite-based powders have also been applied; they function by absorbing water and concentrating the clotting factors in a wound. Again, these powders are not ideal due to their lack of applicability in windy environments and the inherent exothermic reaction that accompanies their use, which is known to cause severe burns to surrounding tissue [1, 5]. Freeze-dried chitosan bandages have shown the greatest promise of currently available hemostatic dressings and have been adopted for use by the Department of Defense [2, 4]. The mode of action of these bandages is not entirely understood; however, their ability to promote hemostasis is thought to be due to their tissue adhesive properties, ability to cause vasoconstriction, and attraction of negatively charged red blood cells and platelets [1]. The primary drawback of these chitosan bandages is difficulty in application to complex non-planar wound sites [1].

To treat potential infection following injury, patients are typically administered broad-spectrum antibiotics orally or intravenously. This systemic exposure allows drug-resistant bacteria to flourish and greatly increases difficulty in treating infection [6]. In fact, in wounded soldiers, there is a close correlation with the increasing use of broad-spectrum antibiotics and a rise in antibiotic-resistant bacteria, such as methicillin-resistant *Staphylococcus aureus* (MRSA) [3]. Additionally, colonization of bacteria on implant surfaces or dead-tissue can give rise to biofilms, which further complicate treatment [7]. There has been much research in the area of localized antibiotic delivery methods to avoid systemic administration, particularly in the area of orthopedic devices, wound dressings, periodontal devices, and vascular grafts, to name a few [8].

Scaffolds and dressings embedded with the antimicrobials allowing for passive drug release [8-10], drug-loaded hydrogels [11], degradable coatings [12-14], and antimicrobial polymeric surfaces [15-19] have been developed. In many cases, these devices are unable to bear large drug loads without compromising device integrity. Often, there is inadequate control over drug release timescales and concentrations. This is especially concerning as prolonged exposure to antibiotics, particularly at concentrations that are below the minimum inhibitory concentration of the therapeutic against common bacteria, is directly implicated in causing drug resistance [6, 8].

It is clear that there is vast area for improvement in both the control of bleeding and the treatment of infection. Namely, for bleeding control, there is a need for an effective non-pressure based technology that is applicable to a variety of wound configurations. For infection treatment, local delivery methods that demonstrate superior control over drug release timescale and drug loading are needed.

1.1 Controlled Local Drug Delivery

Use of local drug delivery devices has the potential to alleviate many of the non-ideal outcomes of systemic drug delivery. Most often drugs are administered either topically, orally, intravenously, intramuscularly, subcutaneously, or sublingually. Local delivery offers significant advantages over these methods. These include requiring lower drug doses, a greater control over drug toxicity and bioavailability, potential for extended release, potential for control over drug release profile directly at the site, and requiring lower number of drug administrations during treatment [20, 21]. There are numerous local drug delivery devices currently approved by the United States Food and Drug Administration (FDA) that are routinely utilized. Some of the prominent areas of use include drug-eluting stents, catheters, orthopedic devices, and wound dressings [8, 20]. In most of these devices, polymers are utilized to both load and control drug release behavior. Commercial drug-eluting stents contain micron-scale coatings of polyisobutylene or polymethacrylate copolymers loaded with drug. In the case of the widely-studied sirolimus-releasing stent, CYPHER™ (manufactured by Cordis), drug loadings of approximately 140 µg/cm^2 are attained with a burst-release upfront followed by extended drug release up to 6 weeks. For antimicrobial catheters, two methods of functionalization have been employed, including dip coating of catheters in drug solution prior to use where drugs will adsorb onto and absorb into the catheter material, as well as drug impregnation prior to injection

molding or extrusion to produce the device [20]. To combat osteomyelitis, antibiotics are loaded into bone cement, polymethylmethacrylate (PMMA), or PMMA beads. PMMA bone cement is a non-degradable polymer in which drugs can be combined during the curing process, in which a solid and liquid component are combined immediately prior to use. The solid component contains the PMMA powder, an initiator, and the drug, while the liquid component contains the methyl methacrylate monomers. Upon mixing, the glassy polymer cement is formed within minutes accompanied by an exothermic reaction [8]. Drug release behavior from PMMA is governed by drug loading, porosity, surface area, and roughness [20]. Wound dressings are also another application of great interest for localized drug delivery and there are several currently approved devices in use. Acticoat® (manufactured by Smith and Nephew) is a gauze dressing with silver-coated polyethylene meshes on both the outer layers; wetting the gauze several times a day allows the release of antimicrobial silver to the wound site. To eliminate need for changing dressings, biodegradable dressings utilizing lactide-caprolactone copolymers have found utility in the clinic [20]. Aside from the few mentioned here, numerous other formulations and applications of local drug delivery devices are currently in clinical use.

Despite their widespread use, there are many areas for improvement of currently used drug delivery devices. Many of these devices release drug at concentrations that are sub-therapeutic which can exacerbate the condition and increase difficulty in treatment. This is especially prevalent with PMMA use, where often less than 10% of the loaded drug is eventually released from these non-degradable matrices [8]. Additionally, it has been shown that many of the organisms in contact or close proximity to the drug-releasing PMMA, develop resistance to the drug, most likely due to the sub-minimum inhibitory concentration drug exposure [20]. Also, there is often a lack of adequate control over drug delivery timescales, where prolonged drug exposure is problematic and may give rise to drug-resistance in the case of antibiotics. These limitations can often not be overcome with current design methods, due to the fact that the mechanical and functional properties of the drug loaded devices must be maintained. Most of the current methods do not allow for complex delivery profiles, such as sequential delivery of multiple therapeutics. In current devices, release is often a combination of drug diffusion and degradation or dissolution of polymer matrix [21], rather than a stimuli-responsive release. Additionally, as apparent with PMMA use, many of the current local delivery techniques are inherently harsh in regards to temperature or solvent used during device preparation [8]. This is

especially problematic when trying to incorporate sensitive components into these devices, such as proteins, which will denature at these conditions. Recognizing the benefits of controlled local drug delivery while trying to overcome the many drawbacks of current techniques, this thesis explores the development of therapeutic coatings using the layer-by-layer assembly technique to target infection, inflammation, and bleeding.

1.2 Layer-by-Layer Assembly

Layer-by-layer (LbL) assembly is used for the fabrication of polymer multilayer films [22]. In this technique, films are assembled by the sequential adsorption of materials with complementary functionality, including electrostatic interactions [22], hydrogen-bonding [23], and biological interactions [24]. Following each deposition step, a wash step is used to remove any non-specifically bound material. Functionality reversal at each deposition step allows the film to continue growing with each subsequent deposition [22]. Although dip LbL assembly, in which the substrate is submerged in deposition solutions allowing substantial time for diffusion and adsorption of species to the growing film surface, is the most common method of LbL assembly, both spray [14, 25-28] and spin LbL assembly [29] have also been explored. Spray LbL assembly, in particular, has shown great promise in achieving thin films in a time-effective manner by eliminating diffusion limitations of the LbL process. LbL assembly is an aqueous technique, and unlike many of its bulk coating counterparts, it is able to support the direct encapsulation of a variety of sensitive molecules and macromolecular species, including proteins [30-34], peptides [13, 35, 36], nucleic acids [24, 37-40], etc. This assembly technique has found utility in a variety of areas, including biological engineering, electrochromics, and fuel cells, amongst numerous others [41-47]. Additionally, due to ease of application, LbL films have been applied to a wide variety of substrates, including stents [37], electrospun materials [27], microparticles [38], mammalian cells [48, 49], biological tissues [50], etc. Properties of the materials and solvents used to assemble these films are critical in determining film characteristics, including molecular weight and degree of ionization, related directly to solution ionic strength and pH [13, 51-53].

1.2.1 Layer-by-Layer Assembly for Drug Delivery

Due to the fact that a wide range of species can be encapsulated and delivered from LbL assembled systems, these films are being examined extensively for various therapeutic applications [44]. Of particular interest to this thesis are films developed to deliver antimicrobials, anti-inflammatory drugs, and proteins. In specific, previous research has shown the incorporation and release of a variety of therapeutics from LbL films, including antibiotics such as gentamicin [12, 54, 55] and triclosan [56], chemotherapeutics such as doxorubicin [57], non-steroidal anti-inflammatory agents such as diclofenac [58], and proteins such as FGF-2 and BMP-2 [30, 31, 33, 34]. In much of this work, it has been shown that changing the number of layers allows for tunable drug loading.

Many groups have explored the encapsulation of drugs in these films by absorption after film assembly where the drug is not one of the direct building blocks of the film. For example, in one study bilayer films were composed of poly(L-lysine) (PLL) and hyaluronic acid, following which the film was soaked in paclitaxel allowing for absorption of the drug. These films had an anti-proliferative effect on a cancerous cell line [59]. In another recent study, a unique method of using LbL films to obtain antimicrobial drug incorporation and release was examined. In this study, bilayer films were assembled with poly(methacrylic acid) (PMAA) and poly(N-vinylpyrrolidone) (PVPON) which were subsequently crosslinked and the PVPON removed, leaving behind a PMAA hydrogel. Antimicrobial drugs, proteins, and peptides were incorporated post hydrogel formation via absorption. The drug release here was based on hydrogel swelling in response to changes in pH and ionic strength [55]. Others have explored the direct incorporation of the drug as a component of the LbL film. In one study, the antimicrobial peptide (AmP), defensin, was adsorbed as a layer into a bilayer film of poly(L-glutamic acid) (PGA) and PLL. The cationic defensin was deposited following an anionic PGA deposition, and PLL was needed in order to obtain complete charge reversal. Release of drug from these films was not quantified or examined; however, it was noted that bacteria needed to be in close contact with the film for antimicrobial activity to be visualized [35].

Rather than relying simply on passive release of drugs, stimuli-responsive drug release may be desirable. For example, biodegradable polypeptides including PLL and PGA have been used extensively in LbL films for this purpose. In one particular study, both TGF-β and BMP-2 were incorporated as layers into a PGA and PLL containing film and used to create polymeric

capsules. *In vivo* bone formation upon administration of these capsules was examined in mice. Film activity in this study was attributed to the enzymatic degradation of the PGA and PLL, liberating the active proteins [31]. In a similar study, films containing PGA, PLL, DNA, and cyclodextrins, were found to demonstrate *in vitro* activity only in the presence of cells and not due to passive release of drug [60]. Although these biodegradable polymers have been utilized extensively, their properties are often not as easily manipulated as entirely synthetic polymers, which has implications on drug loading and release properties of LbL films. Many researchers have therefore examined the use of synthetic degradable polymers in these films, such as hydrolytically degradable poly(β-amino esters) [61, 62]. The properties of these polymers can help tune the degradation rate of LbL films in the specific environment in which the films are applied. For example, the level of hydrophobicity of poly(β-amino esters) has been shown to greatly influence the mechanism of film degradation, including surface and bulk erosion, and the rate at which these processes occur [63].

It may also be desirable to sequentially deliver multiple therapeutics from a single LbL assembled film. Sequential drug delivery is complicated by the phenomena of interdiffusion which occurs when one or more components within a film architecture are sufficiently mobile within the underlying film during assembly, allowing rearrangement in the film structure [52]. Methods of blocking interdiffusion of one segment of a multilayer film from another have been examined in the form of thermally crosslinked barrier layers for the sequential delivery of macromolecular model therapeutics [64]. Additionally, current methods in the Hammond Lab at the Massachusetts Institute of Technology such as the incorporation of catechol modified polymers into LbL films have also shown great initial promise in controlling film component interdiffusion.

1.3 Thesis Overview

This thesis focuses on using LbL assembly to design device coatings that target infection, inflammation, and bleeding. The remainder of the thesis is divided into 7 chapters discussing the design of these coatings. In Chapter 2, a hydrolytically degradable polymer multilayer film is developed for the delivery of an AmP, ponericin G1. Several film architectures are designed in which the AmP is directly incorporated via its net cationic charge. Depending on film architecture, a variety of drug loadings are obtained and AmP is released over a timescale of 10

days with varying release profiles. The film-released ponericin G1 is found to maintain complete activity against *S. aureus*. Additionally, film-coated surfaces prevent bacterial attachment which may be useful in preventing biofilm formation [13].

Although AmP films are highly promising, production of natural AmPs is not cost-effective. As a viable alternative, Chapter 3 describes the use of dip and spray LbL assembly to develop hydrolytically degradable films for the delivery of a small weakly charged antibiotic, vancomycin. These films are found to have unprecedented drug loadings (up to 20 weight percent) and a variety of release profiles including bolus and linear drug release. Drug loading and release profiles are strong functions of both film architecture and LbL assembly technique (spray versus dip LbL). This work also provides insight into the importance of interdiffusion in these films for promoting non-electrostatic secondary interactions that are necessary for enhancing film stability [14]. Additionally, Chapter 3 describes studies on the long-term storage stability of these vancomycin containing films. These films are found to be highly stable at both room and elevated temperatures and entirely maintain vancomycin activity against *S. aureus*, providing a valuable alternative to typical intravenous formulations of the drug which are known to degrade at these conditions.

Chapter 4 describes the design of coatings aimed at simultaneously targeting infection and inflammation. These composite films are assembled using the antibiotic films described in Chapter 3 and modularly combining with LbL films previously developed for the delivery of diclofenac, a non-steroidal anti-inflammatory drug [58]. Studies uncovering novel interactions between vancomycin and diclofenac as well as other film components allow *a priori* prediction of the behavior of these composite films. Dip and spray LbL assembly are used to further control drug loading and release. The versatility of these films in coating medical devices, including bandages, intraocular lenses, and sutures is also demonstrated in this work, and complete retention of film-released therapeutic efficacy is demonstrated.

In Chapter 5, the vancomycin films developed in Chapter 3 are applied to a clinically relevant substrate, an absorbent and porous gelatin sponge, Surgifoam®. These sponges are typically used in combination with clotting factors, to promote hemostasis, and would clearly benefit from releasing antibiotics as well. A vacuum spray assembly technique is used to assemble vancomycin films on Surgifoam® in order to take advantage of the large surface area available for coating and minimize liquid exposure. The effect of the sponge on the drug loading

and release kinetics of these vancomycin films along with the effect of the film on the substrate are thoroughly examined. Overall, an increase in drug loading and release time is noted along with increased liquid absorption by film-coated sponges. This increased absorption is attributed to the hydrophilicity and absorptive quality of the vancomycin film. Additionally, the coated sponges show activity against *S. aureus* compared to no activity with uncoated sponges, as expected.

Chapter 6 describes the development of multilayer films aimed at promoting hemostasis. These nanoscale films are designed based on novel hydrogen bonding interactions found to occur between a polyphenol, tannic acid, and an essential clotting factor, thrombin. These films are developed primarily using spray LbL assembly. The growth and morphology of these protein films is thoroughly described. The films are also applied to Surgifoam®. In collaboration with Ferrosan these films are tested for both *in vitro* and *in vivo* activity. The Surgifoam® coated films are found to be highly active in promoting hemostasis in a porcine spleen injury model.

As previously mentioned, use of AmPs as antimicrobial therapies is often impractical. In Chapter 7, the development and testing of a cost-effective synthetic antimicrobial polypeptide is described. A library of these polypeptides is synthesized by the ring opening polymerization of γ-propargyl-L-glutamate N-carboxyanhydride and the alkyne-azide cycloaddition click reaction. The polypeptides range in length from 30 to 140 repeat units and have varied side group functionality, including primary, secondary, tertiary, and quaternary amines with hydrocarbon side chains ranging from 1 to 12 carbons long. Overall, these polypeptides are shown to have broad-spectrum antimicrobial activity against both Gram-positive and Gram-negative bacteria and also prevent bacterial attachment on functionalized surfaces. Additionally, these polypeptides display very low hemolytic activity, far lower than most natural AmPs, an initial test of their biocompatibility [19].

Finally, Chapter 8 concludes with a discussion of the primary conclusions from Chapters 2 through 7. Additionally, Chapter 8 provides suggestions for future work that may advance the current findings of this thesis.

Chapter 2

Controlling the Release of Peptide Antimicrobial Agents from Surfaces

2.1 Introduction

A sharp rise in the emergence of antibiotic resistant bacteria over the last several decades is of major concern. Methicillin-resistant *Staphylococcus aureus* (MRSA), which was initially found to be limited to hospitals, has become widespread in community settings during the last two decades despite efforts to contain its spread. Over time, staph resistance to several other classes of antibiotics is also being observed [65]. Additionally, soldiers returning from overseas are often seen to have contracted multi-drug resistant infections [3]. This vast spread in antibiotic resistance is due in part to the sophisticated mechanisms by which these bacteria gain resistance, including the ability of bacteria to exchange genetic material from one strain to another [65]. This exchange of genetic information is much more likely to occur upon repeated exposure to large concentrations of particular antibiotics. Current therapies, such as prophylaxis with broad spectrum antibiotics, only augment this critical problem [66]. For these reasons, a localized rather than systemic administration of antimicrobial agents is highly desirable.

Scientists have recently begun to understand the mechanisms behind the development of biofilms, which are a common source of infection. These sessile bacteria colonies develop on medical device surfaces and dead tissue. They damage surrounding tissues and lead to implant failure, while giving rise to planktonic cells and spreading infection [7]. Biofilms are rarely treatable with conventional antibiotics, and methods of resistance differ from those which planktonic cells have adopted [7, 67]. The most effective method for preventing biofilms, is to stop the initial bacterial attachment on the surface of the implant material. Bacteria attachment can be prevented by using appropriately functionalized implant coatings.

Localized antimicrobial delivery leads to time-effective handling of infection, while potentially eliminating issues associated with systemic toxicity and excessive exposure of healthy human bacterial flora to agents that may cause resistant bacteria to develop [68].

Localized antimicrobial delivery has been explored in the context of drug loaded orthopedic device coatings, cements, and wound dressings with conventional antibiotics in attempts to prevent biofilm formation and treat infections caused by planktonic bacteria [8]. Although controlled local release resolves some of the issues of systemic treatment, an additional challenge is the ability to gain therapeutic efficacy of antibacterial treatments while avoiding contributions to the rise in antimicrobial resistance. The systematic and controlled release of antimicrobial peptides (AmPs) provides a means to achieve this goal. These broad spectrum peptides are found as part of the innate immune system in eukaryotes, and are used as a first line of defense against invading pathogens. AmPs are active against Gram-positive, Gram-negative, and multi-drug resistant bacteria, and are also known to be antifungal and antiviral [69, 70]. The exact modes of action of these peptides remain to be elucidated; several proposed mechanisms [69-71] suggest that AmPs are very unlikely to cause the development of resistance. Additionally, it has been found that AmPs, such as lactoferrin, are able to block biofilm development [72]. AmPs might have this effect on biofilms due to their diverse modes of action and cellular targets [73]. Recognizing AmPs as a promising agent intended to combat and prevent infection and formation of biofilms, we have explored the controlled and extended delivery of AmPs from layer-by-layer (LbL) assembled polyelectrolyte multilayer films, which can coat a variety of materials for local delivery.

Layer-by-layer assembly of multilayer thin films is a versatile tool used in the past to formulate thin films for numerous applications such as drug delivery [12, 30, 40, 62, 64, 74, 75], biosensors [76], selective membranes, fuel cells [77], nanomechanical films, and electrochromic devices [41]. These films can be formed by exploiting electrostatic, hydrogen bonding, and covalent interactions between film components [22, 23, 78, 79]. Compared to other proposed methods of local drug delivery, such as the use of hydrogels, LbL films offer the ability to gain temporal control over drug release from a variety of substrates and the potential for pairing AmP release for sequential delivery of multiple therapeutic agents [64]. By incorporating hydrolytically degradable polymers into these films, surface erosion based temporal control of drug release can be attained. The family of cationic poly(β-amino esters) [61] has proven to be very useful for this particular application [43, 80]. These polymers have been shown to be effective in the delivery of several model drugs [62], proteins [30], antibiotics [12], and DNA [40]. Additionally, compared to other coating techniques, LbL assembly has the advantage of

being a gentle, aqueous assembly process, which has the ability to conformally coat virtually any substrate, with nanometer level control over the composition of the layers. An advantage of AmPs that enables facile assembly with negatively charged polymer systems is their largely cationic composition.

A few recent studies have recognized the need for local delivery of new antimicrobials, and have focused on AmP incorporation in LbL films. Non-degradable and non-eluting films were the focus of initial studies in which LbL films containing antibacterial and antifungal cationic AmPs were assembled [35, 81]. These films were found to have strong action against various Gram-positive and Gram-negative bacteria and fungi placed in contact with the resulting film surfaces. The results attributed importance to the initial bacterial adhesion to the film and the resulting proximity of the peptide to promote bacteria killing; no drug was found to elute from the films. A more recent study looked at construction of a film containing a hydrophobic AmP, and qualitatively determined that this AmP was partially leached from the non-degradable film system and remained active in solution over a timescale of 24 hours. These films also exhibited strong activity against Gram-positive bacteria; this action was attributed to both the contact of bacteria with the film surface as well as activity of released peptide in the surrounding media [36]. The level of control in peptide loading and release timescales that are required in applications that could benefit from such antimicrobial films has thus far not been demonstrated; the introduction of thin film coatings that can release AmPs in a controlled manner are therefore of interest for biomedical coating and wound healing applications.

With the initial successes of AmP incorporation in LbL films, there remain challenges in achieving sustained AmP release from surfaces with a highly tunable amount of drug loading. It is also important to achieve fully decomposable films that erode completely in the body for applications such as coatings on degradable bandages, sutures, and medical implants. For these purposes, we examined a previously unexplored aspect of local delivery of AmPs: delivery from degradable polymer films. As mentioned earlier, use of degradable LbL films allows for temporal control over drug release as well as a potential for sequential release with a multitude of agents, including those needed for hemostasis and wound healing, as well as tissue regeneration and repair. A form of the natural AmP, ponericin G1, was the focus of this study. Found in the venom of predatory ants, the ponericin family has shown strong activity against a wide range of bacteria, including *S. aureus*, and has low hemolytic activity [82]. Here, we demonstrate for the

first time, the incorporation and release of an AmP from a hydrolytically degradable polymer thin film formulated using LbL assembly. It is well known that factors such as degree of ionization, molecular weight, and secondary interactions can affect film assembly [51, 52, 83-85]. Considering this and in attempts to tune antimicrobial delivery properties via nanolayer film composition, we have examined several different architectures for ponericin G1 film assembly and explored the effects of varying the alternating polyanion on film growth properties.

2.2 Materials and Methods

2.2.1 Materials

Poly(β-amino ester) 2 (poly 2) was synthesized as previously described [61, 86] (molecular weight, M_n = 6.7 kDa). Chondroitin sulfate sodium salt was purchased from TCI International (Tokyo, Japan; M_n estimated using water GPC to be approximately 85 kDa). Alginate (M_n = 120 – 190 kDa) was purchased from Sigma-Aldrich (St. Louis, MO). Dextran sulfate sodium salt (M_n = 500 kDa) was purchased from Polysciences (Warrington, PA). Silicon substrates (test grade, n type) were obtained from Silicon Quest International (Santa Clara, CA). Ponericin G1 was synthesized by the Massachusetts Institute of Technology Biopolymers Lab (Cambridge, MA) with amino acid sequence: GWKDWAKKAGGWLKKKGPGMAKAALKAAMQ [82] and an amidated C-terminus. All agents were utilized as provided without further purification. Deionized water (18.2 MΩ, Milli-Q Ultrapure Water System, Millipore) was used for all washing steps during film construction and substrate preparation. Sodium acetate buffer (3 M, tissue culture grade) was purchased from Sigma-Aldrich (St. Louis, MO). Dulbecco's phosphate buffered saline (PBS, 0.1 M) was purchased from Invitrogen (Carlsbad, CA). *Staphylococcus aureus* 25923 was purchased from ATCC (Manassas, VA). Cation-adjusted Mueller Hinton Broth (CaMHB) and Bacto agar were obtained from BD Biosciences (San Jose, CA). Human umbilical vein endothelial cells (HUVEC) were obtained from Lonza (Walkersville, MD), while NIH 3T3 embryonic murine fibroblasts were obtained from ATCC (Manassas, VA). All reagents for HUVEC culture were obtained from Lonza Clonetics, while reagents for NIH 3T3 culture were obtained from ATCC.

2.2.2 Polyelectrolyte and Peptide Solution Preparation

All polyelectrolyte solutions (poly 2, chondroitin sulfate, alginate, and dextran sulfate) were prepared at a concentration of 2 milligrams per milliliter (4.6 mM, 4.4 mM, 5.7 mM, and 5.0 mM with respect to poly 2, chondroitin sulfate, alginate, and dextran sulfate repeat unit, respectively) in 100 mM sodium acetate buffer (pH 5.1), created from 3 M stock. Ponericin G1 solutions were prepared at a concentration of 1 milligram per milliliter (0.31 mM) in 100 mM sodium acetate buffer (pH 5.1).

2.2.3 Layer-by-Layer Assembly

All films were assembled on clean silicon substrates. Prior to assembly, 2.0 cm by 0.7 cm substrates were cleaned using methanol and deionized water and dried under nitrogen. Substrates were plasma etched using air in a Harrick PDC-32G plasma cleaner at high RF level. Immediately following plasma etching, the substrates were submerged in cationic poly 2 solution. Substrates remained in this solution for at least 15 minutes. A tetralayer repeat architecture was then assembled on these substrates using a Carl Zeiss HSM programmable slide stainer. The architecture of the film is denoted as: (poly 2/polyanion/ponericin G1/polyanion)$_n$, where n represents the number of deposited tetralayer repeats. The first deposition step was a 10 minute submersion is poly 2, followed by three deionized water rinse steps (10, 20, and 30 seconds each). The substrate was then submerged in the polyanion of choice for the particular architecture being constructed for 7.5 minutes, followed by three deionized water rinse steps (10, 20, and 30 seconds each). After this the substrate was submerged in a 10 minute deposition step of the cationic therapeutic, ponericin G1. This was followed by two deionized water rinse steps (20 and 30 seconds each). Following these three deposition steps, the second step sequence of polyanion dipping and rinsing was repeated. Together these four deposition steps complete one tetralayer of the film. For the purposes of this work, $n = 75$, was found to be a reasonable number of tetralayers to realize differences between film architectures based on varying polyanions. The three architectures examined in this work were: (poly 2/alginate/ponericin G1/alginate)$_{75}$, (poly 2/chondroitin sulfate/ponericin G1/chondroitin sulfate)$_{75}$, and (poly 2/dextran sulfate/ponericin G1/dextran sulfate)$_{75}$, which vary only in the choice of polyanion used during assembly.

2.2.4 Film Growth and Degradation Characterization

The growth of all polymer films was tracked using a surface profilometer (KLA Tencor P-16). Films were built with a varying numbers of tetralayers and then scored using a sharp razor. This allowed for step height measurement and construction of film growth curves (five measurements were made per film and at least four films were examined per tetralayer number). The film thickness for each particular measurement was taken as an average over a 100 μm length. The final morphology of the films was also examined using a Dimension 3100 Nanoman atomic force microscope (Veeco Metrology, Santa Barbara, CA).

Film degradation was tracked by monitoring film thickness during the therapeutic release study described below. At predetermined times during the degradation, the film thicknesses were measured using a profilometer. Measurements were taken as described earlier for film growth.

2.2.5 Therapeutic Release Studies

Upon construction, films were dried under nitrogen and laid flat in a vial containing 500 μL of 0.01 M PBS at pH 7.4, completely submerging the film. These films were then incubated at 37 °C. At predetermined time points, the films were moved into a fresh 500 μL aliquot of 0.01 M PBS. Each sample therefore represents the release of film components for the duration of time for which the film was present in a particular PBS containing vial rather than a cumulative amount released over the entire test period. All release samples were immediately stored in a -20 °C freezer until they were analyzed and the amount of therapeutic quantified.

2.2.6 Therapeutic Quantification

The presence of ponericin G1 in each release sample was quantified using the inherent fluorescent properties of ponericin G1. Ponericin G1 is rich in tryptophan residues; it was found that excitation of peptide dissolved in PBS at 280 nm leads to a maximum emission at 355 nm. Fluorescence measurements were made using a Jobin Yvon Fluorolog-3 spectrofluorometer (HORIBA Scientific) and a Spectrosil quartz cuvette (315 μL volume, 3 mm path length; Starna Cells, Atascadero, CA). A calibration curve of ponericin G1 emission at 355 nm was constructed using known quantities of ponericin G1 dissolved in 0.01 M PBS, which was linear in the range of $2 - 62$ μg/mL ($R^2 = 0.9984$). Release samples were then examined using the

same technique. Comparing emission values of release samples to the calibration curve of peptide standards, the quantity of ponericin G1 in each release sample was calculated. It was found that the other components present in the release samples (polyanions and poly 2 degradation products) did not interfere with fluorometer readings at relevant concentrations (data not shown). All measurements were made in triplicate.

2.2.7 Bacterial Growth Inhibition Assays

Activity of the film release solutions against *Staphylococcus aureus* 25923 was also investigated. This particular strain was selected based on the recommendations of the Clinical and Laboratory Standards Institute [87]. The activity of film-released ponericin G1 and native non-film incorporated peptide was tested using a modified microdilution assay modeled after a similar technique reported by the Clinical and Laboratory Standards Institute [87]. For film release solution, films were allowed to soak in 1 mL of 0.01 M PBS for a duration long enough to release the entire contents of the film; film release was monitored using fluorometer measurements as described earlier. A serial dilution of release solution as well as a control solution of native peptide dissolved in 0.01 M PBS (after passing solutions through 0.2 μm sterile filters) with CaMHB was performed, to make a total of 8 dilutions of the peptide solutions in a 96-well polystyrene tissue culture plate. *S. aureus* in its exponential growth phase (3 to 4 hours following inoculation) was added to each of these dilutions at a final concentration of 10^5 CFU/mL (bacteria concentration was assessed with optical density measurements at 600 nm using an HP Agilent UV-Vis Spectrophotometer). Negative controls used 0.01 M PBS with no peptide and serial dilution in CaMHB with no final bacterial challenge. Positive controls were made similarly with bacterial challenge. All measurements were made in triplicate. The 96 well plates containing the test samples, negative, and positive controls were incubated at 37 °C with gentle agitation for 16-18 hours. Following this, a Biotek PowerWave XPS plate reader was used to monitor the optical density of the wells at 600 nm, corresponding directly to the cell density. A normalized bacteria density was computed for all test samples with the appropriate negative and positive controls using the following equation:

$$Normalized\ Bacteria\ Density = \frac{(OD_{600,\ sample\ avg} - OD_{600,\ negative\ control\ avg})}{(OD_{600,\ positive\ control\ avg} - OD_{600,\ negative\ control\ avg})}.$$

Bacterial inhibition was also assessed using an agar plate assay following the Kirby-Bauer protocol described by the Clinical and Laboratory Standards Institute [87]. Agar plates were made from CaMHB and Bacto agar. *S. aureus* in the exponential growth phase at a concentration of 10^8 CFU/mL was evenly applied over the agar surface. LbL films were placed face down on top of the bacteria coated agar. Negative controls of clean silicon substrates with no film coating were also placed on the agar. These plates were incubated for 16-18 hours at 37 °C. All films were examined for reduction in bacterial growth as compared to the negative control, using a Zeiss Axioskop 2 optical microscope with Zeiss AxioVision 3.1.2.1 imaging software. The digital images were subsequently processed using CellC, an automated image analysis software which allows determination of bacterial coverage area in each image [87]. A quantitative comparison of bacteria growth on and surrounding the film to growth on the uncoated substrate was conducted.

2.2.8 Bacterial Attachment Assay

Bacteria attachment capabilities on the surface of ponericin G1 films were examined using a method adapted from a protocol described by Tiller et al [16]. Films were placed face up in petri dishes and covered with a suspension of 10^6 CFU/mL *S. aureus* and allowed to incubate at 37 °C for 2 hours. Negative controls of clean silicon substrates with no film coating were also incubated under bacteria. Following incubation, each substrate was removed from the bacteria suspension and briefly rinsed in three separate sterile water washes. Each substrate was subsequently placed face down in an agar plate made of CaMHB and Bacto agar and incubated for 16-18 hours at 37 °C. All films were examined for bacteria attachment compared to the negative control using a Zeiss Axioskop 2 optical microscope with Zeiss AxioVision 3.1.2.1 imaging software. The digital images were processed using CellC [88].

2.2.9 Biocompatibility

Films were allowed to erode entirely for approximately 15 days (for alginate and chondroitin sulfate films) and 25 days (for dextran sulfate films) and elute contents in 1 mL of the appropriate cell culture media at 37 °C for two important wound healing cell lines, human umbilical vein endothelial cells and NIH 3T3 fibroblasts. Endothelial cell growth media, EGM-2 completed using supplements and suggested protocol (Lonza Clonetics, Walkersville, MD) was used in the release of samples intended for HUVEC. Dulbecco's Modified Eagle Medium

supplemented with 10% fetal bovine serum and 1% penicillin/streptomycin was used in release intended for NIH 3T3 fibroblasts. Complete media for each cell line was also incubated for the same duration of time as the released films with clean bare silicon substrates. Immediately prior to beginning cell viability testing, ponericin G1, dextran sulfate, chondroitin sulfate, and alginate, were all dissolved in fresh complete media for each cell line at a final concentration of 25 µg/mL. HUVEC and NIH 3T3 cells were plated at a concentration of 10,000 cells per well in a 96-well polystyrene tissue culture plate and allowed to incubate at 37 °C and 5% CO_2 in 100 µL of media per well for 24 hours. Media was then aspirated off the cells in each well, and the test media was added at a 100 µL volume per well. For each cell type, test media included: media from each of the three film release systems, media incubated with blank substrates (positive control for the release films), polyanions and ponericin G1 (25 µg/mL standards) dissolved in fresh media, and fresh media (positive control for polyanions and ponericin G1 standards). All test media solutions were passed through a 0.2 µm sterile filter. Negative controls containing no cells were also incubated with media at the start of the experiment. After an 18 hour incubation period with test media, an MTT assay (Sigma, St. Louis, MO) was performed to assess cell viability. MTT solution (10 µL) was added directly to the cells in test media, and the plate was incubated for 3 hours at 37 °C. Following this, media and MTT solutions were aspirated from each well and MTT solubilization solution (100 µL) was added to each well. A Biotek PowerWave XPS plate reader was used to monitor the absorbance of the wells at 570 nm (directly related to cell viability). Background absorbance of the plate at 690 nm was subtracted. Normalized cell viability was computed using the following equation:

$$Normalized\ Cell\ Viability = \frac{\left(Abs_{570-690,sample\ avg} - Abs_{570-690,negative\ control\ avg}\right)}{\left(Abs_{570-690,positive\ control\ avg} - Abs_{570-690,negative\ control\ avg}\right)}.$$

2.2.10 Statistical Analysis

In all studies reported in this work, four films were examined per specific experimental condition and the experiment was repeated at least three times. All data is reported as mean ± standard deviation. For growth profile compilation, five areas of each of the four films were examined per tetralayer number and experimental repeat. Atomic force micrographs were taken for three 10 µm by 10 µm areas per each film profiled; three independent films were examined

per polyanion. Bacteria inhibition and attachment experiments processed using CellC were conducted in triplicate, with three films examined per polyanion architecture.

2.3 Results and Discussion

2.3.1 Film Architecture and Morphology

Nanolayer assembly of thin films was accomplished using the electrostatic layer-by-layer approach which consists of alternating deposition of polymers with complementary functional groups. Multilayer films were generated by alternating an amine-terminated ponericin G1 peptide sequence which exhibits a net positive charge at physiological conditions, a hydrolytically degradable polycation from a series of poly(β-amino-esters), and an alternating non-cytotoxic polyanion. An amidated ponericin G1 was used to provide an additional positive charge at the film assembly conditions to assist in the assembly process. Many natural peptides in the ponericin family are also amine terminated [82]. Figure 2-1 shows the structure of each of the components used to build the films, a schematic of the LbL process, as well as the film architecture. Poly 2 has been shown to lead to longer release times and slower degradation rates in eroding multilayer films than those films composed with the similar poly(β-amino ester), poly 1, reported in previous work [61]; poly 1 has one less methylene group in its backbone. This slower release rate can be attributed to the increased hydrophobicity of poly 2 [58, 63, 86]. For these reasons, poly 2 was the focus of this work. In addition, preliminary data on films constructed using poly 1 (not reported here) led to unstable and rapidly disrupted film architectures.
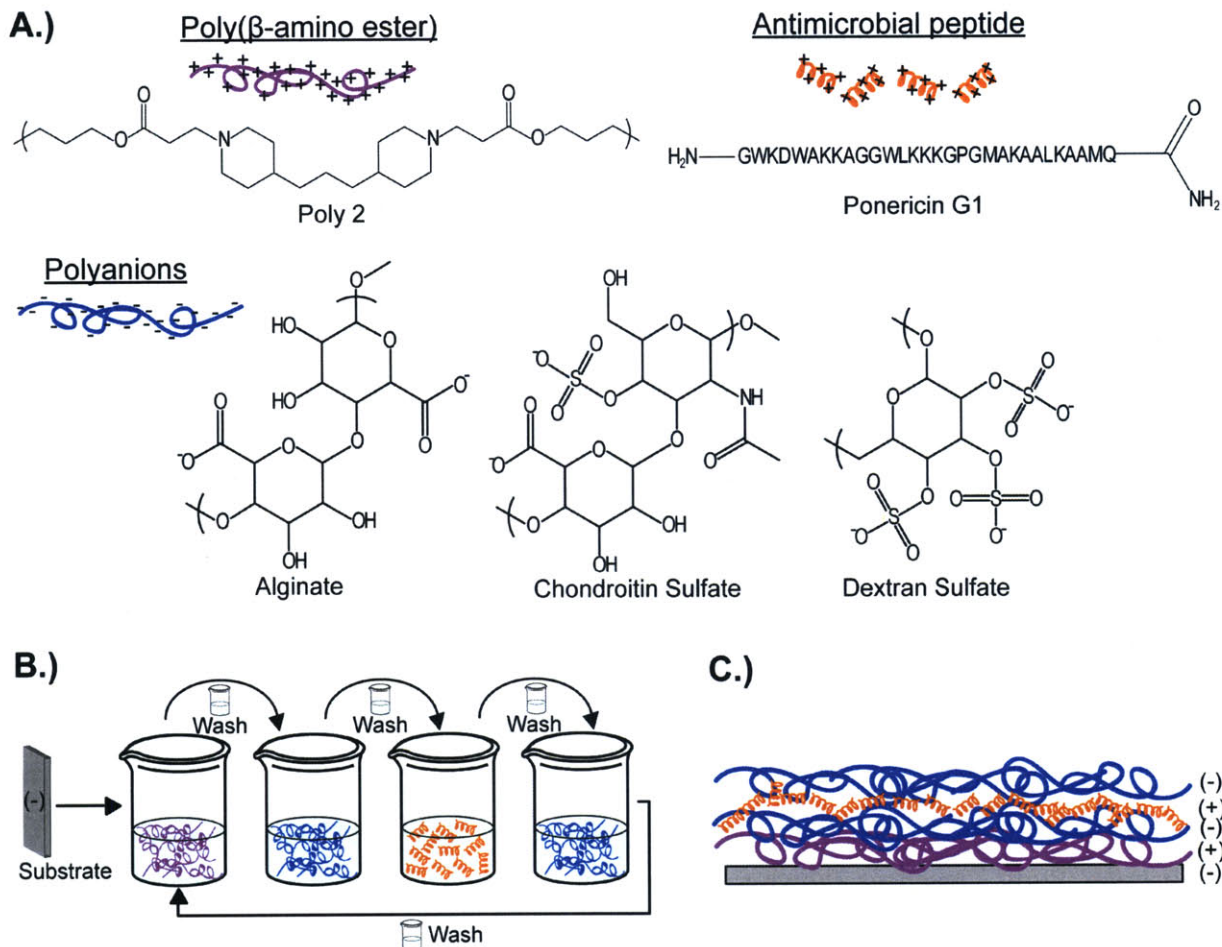
Figure 2-1: Film components, layer-by-layer film assembly, and film architecture. A.) Structure of poly 2, alginate, chondroitin sulfate, dextran sulfate, and ponericin G1. B.) LbL assembly process. C.) Single tetralayer of the 75 tetralayer films assembled in this study.

Polyanions in our study were chosen based on high surface charge density and the non-cytotoxic nature of glycosaminoglycans and polysaccharides. After an initial screening of several polyanions, chondroitin sulfate, dextran sulfate, and alginate were found to successfully build films with therapeutic ponericin G1 loading and were chosen for further investigation. Initially, films were constructed with three different film architectures to examine growth potential and final morphology. Seventy-five tetralayer films were deposited for each of the architectures examined: (poly 2/alginate/ponericin G1/alginate)$_{75}$, (poly 2/dextran sulfate/ponericin G1/dextran sulfate)$_{75}$, and (poly 2/chondroitin sulfate/ponericin G1/chondroitin sulfate)$_{75}$.

Figure 2-2A shows selected atomic force microscopy images representative of the entire film area for the seventy-five tetralayer films of all three architectures examined. AFM measurements gave RMS roughness values of: 26.035 ± 5.130 nm for dextran sulfate films,

69.410 ± 5.277 nm for alginate films, and 84.475 ± 10.978 nm for chondroitin sulfate films. The dextran sulfate films were noted to have a relatively uniform roughness over the entire film area, whereas alginate and chondroitin sulfate films have a non-uniform roughness, with large hills and valleys distributed throughout the films.
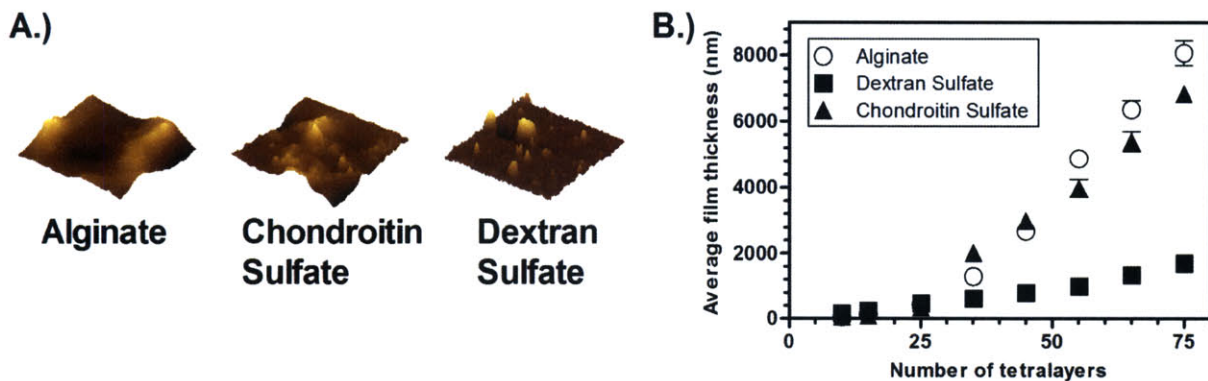
Figure 2-2: Film morphology and growth profiles. A.) Atomic force microscopy images (10 μm by 10 μm; z-scale = 500 nm. B.) Growth profiles of films based on polyanion used.

When comparing growth mechanisms for each of the three architectures, there are striking differences, as seen in Figure 2-2B. Film growth was tracked for each of the three systems at 10 and 15 tetralayers and at every 10 tetralayers following this, to a final value of 75 tetralayers. Dextran sulfate films show linear growth, characteristic of classic polyelectrolyte LbL systems with low or no interdiffusion of the polyion(s) into the film during the adsorption step, and typical for films in which high molecular weight or strong polyion charge density have been used [52, 85]. For both alginate and chondroitin sulfate films there are two phases of linear growth behavior with increasing number of layers. The following phenomenological equation describes this behavior:

$$t = X_1 n_o + \frac{1}{2}\left[(X_1 + X_2)(n - n_o) - (X_1 - X_2)\sqrt{(n - n_o)^2 + dn}\right].$$

Appendix A explains how this equation was derived.

Here, t is the thickness of the film, n is the number of tetralayers, n_o is the number of tetralayers at which the transition from phase 1 to 2 occurs, X_1 is the slope of the first linear phase, X_2 is the slope of the second linear phase (where X_1 is less than X_2), and d is a transition parameter that governs how abruptly or gradually the transition from phase 1 to 2 occurs ($d = 0$ gives an instantaneous transition at $n = n_o$). Assuming d to be zero, the parameters relevant to this equation were fit to the experimental data shown in Figure 2-2, and are presented in Table 2-

1, for each of the three polyanion systems investigated. In the alginate and chondroitin sulfate systems, the first linear growth phase exhibited a similar shallow slope (X_1) that spans the deposition up to 25 tetralayers. Dextran sulfate films showed a similar linear growth to the first linear growth phase of chondroitin and alginate films, and maintains this linear behavior throughout the tested range of $n = 10$ to 75 tetralayers. While dextran sulfate films grow with a continuous slope, both the alginate and chondroitin sulfate films undergo a 6 to 7 times increase in slope (X_2) at growth beyond $n_o = 25$ tetralayers.

Table 2-1: Growth and loading parameters based on polyanion used in AmP films.

Growth Parameters	Alginate	Chondroitin Sulfate	Dextran Sulfate
X_1 (nm/tetralayer)	25.00	19.44	22.45
X_2 (nm/tetralayer)	172.7	120.6	22.45
n_o (tetralayers)	25	25	0
Film thickness (nm)[a]	8100 ± 375	6850 ± 230	1700 ± 100
Ponericin G1 loading ($\mu g/cm^2$)[a]	147.2 ± 6.9	41.0 ± 4.9	20.2 ± 0.3
Ponericin G1 density ($\mu g/mm^3$)[a]	200 ± 10	60 ± 8	100 ± 7

[a]Values correspond to 75 tetralayer films.

This super-linear growth has been previously noted in LbL assembled films [89-91]; it has been observed in several films utilizing biological polymers such as polysaccharides, polypeptides, etc [78]. This growth behavior has been attributed to several interesting phenomena. Super-linear growth is likely to occur when a species that is being used in the LbL deposition process is easily able to interdiffuse within the underlying film. As the film grows, the lower layers rearrange due to this interdiffusion behavior. This restructured zone grows as more layers are deposited, and as it grows larger, it hinders species in the top layers from penetrating too deeply into the restructured zone. Therefore, the top zone, although undergoing interdiffusion, approaches a constant thickness and the system displays linear growth with much thicker increments per adsorption step or bilayer pair [53, 89, 90, 92]. This mechanism is dependent on several different factors that include the charge density of the polyion, its molecular weight, and its chemical composition and solubility in the underlying film matrix [52, 53, 78, 85], and is likely to govern the growth profiles seen in the alginate and chondroitin sulfate cases. A peptide such as ponericin G1 can easily diffuse into and out of an LbL

assembled thin film, given its significantly smaller size and charge density in comparison to the polyelectrolytes involved in film buildup.

At the same time, the dextran sulfate films do not seem to undergo a significant amount of interdiffusion and show a linear growth profile in the range of what was examined in this work. The alginate used had a molecular weight of 120-190 kDa, the chondroitin sulfate had a molecular weight of approximately 85 kDa, and the dextran sulfate had a much larger molecular weight of 500 kDa. As seen in Figure 2-1, both dextran sulfate and chondroitin sulfate are negatively charged due to the presence of sulfate groups in each of these polyanions, while alginate is negatively charged due to carboxylic acid groups. The linear growth seen in the case of the dextran sulfate film is attributed in part to the significantly higher molecular weight of dextran sulfate compared to the other polyanions investigated, as high molecular weight species undergo a much slower diffusion process that can eliminate interdiffusion observed during the time frame of the adsorption cycle [85]. There may be additional factors that impact the linear growth behavior of dextran sulfate in these systems as compared to chondroitin sulfate and alginate, including relative affinity of the macromolecules for the poly 2 or ponericin G1 components of the film.

2.3.2 Ponericin G1 Loading, Release, and Film Degradation

After determining that all of the films grew successfully, the release characteristics and hence the incorporation of ponericin G1 was studied. Figure 2-3 shows results of ponericin G1 quantification in film drug release samples incubated at 37 °C in phosphate buffered saline. Ponericin G1 was successfully incorporated and released from all three film constructs. The data for each film architecture, as presented in Figure 2-3B, were normalized to the total ponericin G1 released for that particular architecture. Examining the normalized release, it can be seen that chondroitin sulfate and alginate films have similar release profiles. This starts with a large release of 62 and 65% of the total therapeutic in approximately 24 hours, for chondroitin sulfate and alginate films, respectively. Meanwhile, films that contain dextran sulfate tend toward a linear release profile, particularly after the first several hours, taking nearly 4 days to release 60% of the film contents. All three film architectures continue to release some amount of therapeutic for up to 10 days.
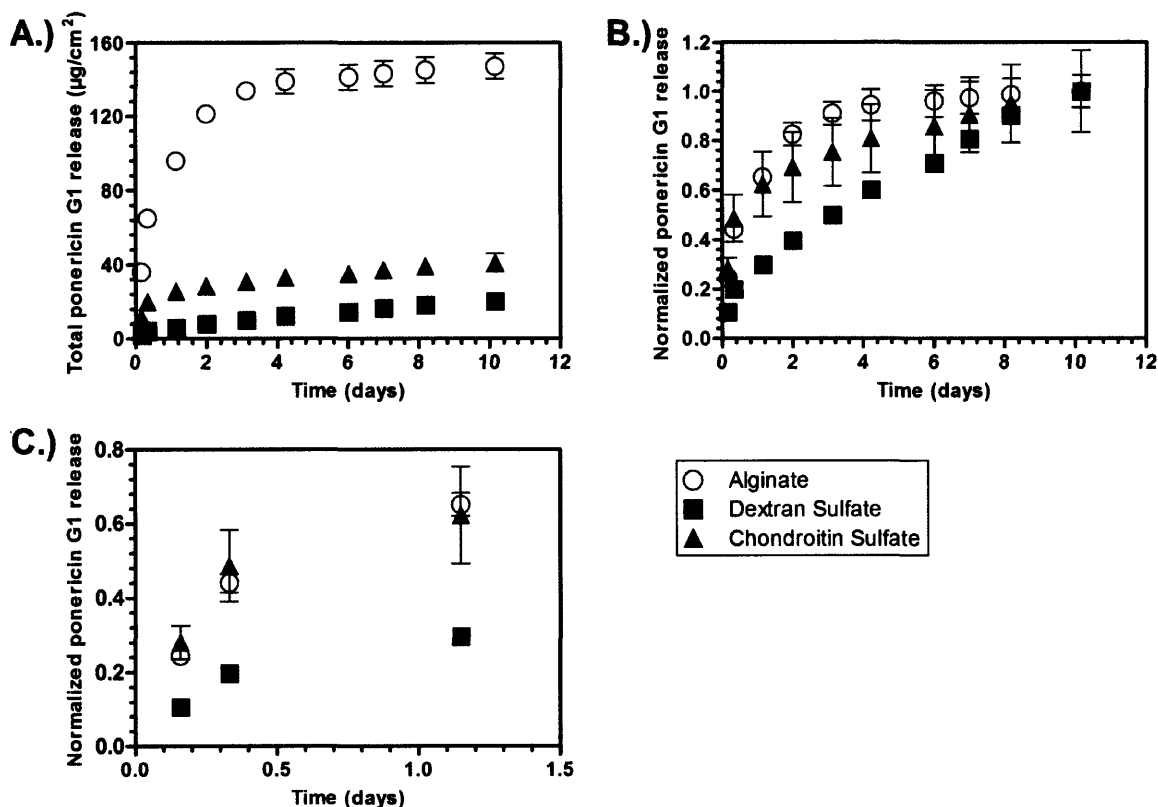
Figure 2-3: Ponericin G1 release versus time for 75 tetralayer films. A.) Total ponericin G1 released over time based on polyanion used in film. B.) Normalized ponericin G1 release profiles based on polyanion used in film. C.) Normalized ponericin G1 release over first 30 hours.

The thicknesses of the alginate, chondroitin sulfate, and dextran sulfate films were 8100 ± 375 nm, 6850 ± 230 nm, and 1700 ± 100 nm, respectively. Although the chondroitin sulfate films have a similar thickness and growth profile to the alginate films, they incorporated much less ponericin G1. Dextran sulfate films also incorporated significantly less ponericin G1 than both of the other film systems, which can be attributed in part to a linear growth profile and limited interdiffusion of peptide into the film as discussed earlier, leading to thinner films, and thus less total ponericin G1 incorporation for the same number of tetralayers. On examining the drug loading per film volume as shown in Table 2-1, it is evident that less ponericin G1 is loaded per volume of film deposited for dextran sulfate and chondroitin sulfate films compared to alginate films. At the same time, more ponericin G1 is loaded per unit film volume for the dextran sulfate system than for chondroitin sulfate. These observations suggest that in general ponericin G1 may interact more favorably with carboxylic acid groups (as in alginate) than with sulfate groups present in both dextran and chondroitin containing films, thus drawing larger

quantities of ponericin G1 into the film during its adsorption step. In general, interdiffusing systems are much thicker, and therefore there is larger overall drug loading for the alginate and chondroitin systems; however, chondroitin sulfate films, which grow similarly to the alginate films, incorporate less ponericin G1 per film volume than dextran sulfate films. This indicates that the primary factor in determining increased ponericin G1 loading in alginate films is not the super-linear growth mechanism, but rather the specific interactions between ponericin G1 and alginate. It has been shown that amino acid residues are capable of forming hydrogen bond interactions with glycosaminoglycans which contain carboxylic acid functional groups [93]. It is therefore possible that carboxylic acid groups are able to participate in hydrogen bonding interactions that are abundant in the case of alginate, but limited in fully sulfonated molecules such as dextran sulfate It also appears that the linearly growing dextran sulfate film has a high density of ponericin G1, although it grows linearly and is thus thinner at the same number of tetralayers. The super-linear growth builds thicker films faster, but leads to lower overall concentrations of ponericin G1 in the chondroitin sulfate film, suggesting that much of the tetralayer composition is polymer for this case. This variation in AmP release with choice of polyanion suggests that extending the release of these systems and capitalizing on their loading characteristics can lead to highly controlled release and effective films.

While drug loading appears to be related primarily to the particular interactions between film components, the varying release profiles seem to be strongly related to the film growth properties, which lead to linear versus super-linear growth as discussed earlier. Films with super-linear growth, lead to a large release of ponericin G1 in a short duration of time early in the release process. This can be attributed to the fact that during super-linear growth, most of the peptide localizes near the top of the film due to the nature of interdiffusion, causing greater accumulation of the diffusing species in the final layers of the film. There is a large diffusion based driving force for this drug to leave the film when placed in a phosphate buffer solution containing no peptide at a pH of 7.4. Figure 2-4 shows the degradation profiles for each of the films.
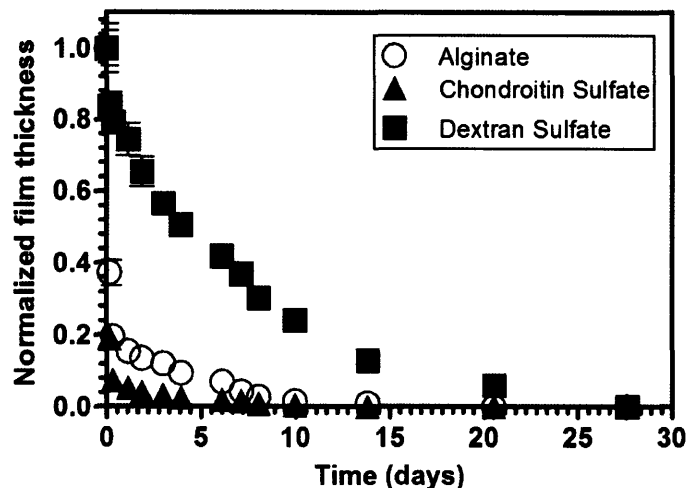
Figure 2-4: Normalized film thickness versus time of films starting at 75 tetralayers.

For the two film systems exhibiting super-linear growth, the large efflux of peptide from the top layers destabilizes the film and a large bulk of the film thickness is also lost during this time. Approximately 85% of the alginate film thickness and 95% of chondroitin sulfate film thickness is lost in the first 24 hours. The thicknesses of the remaining alginate and chondroitin sulfate films decrease linearly with 2% and 1% of the original film thickness left at 10 days, the point at which all film systems have completely finished releasing peptide. This film degradation profile is similar to the drug release profile, which becomes more linear after the top portion of the film is shed early on due to film destabilization. In the case of the dextran sulfate film, 49% of the film thickness is lost in the first 4 days; this corresponds well with the 3.5 day period it takes for the dextran films to release 50% of the incorporated ponericin G1. Notably, at 10 days, nearly 25% of the dextran film thickness remains, although almost all of the peptide has been released. This finding likely suggests that there may be some outward diffusion of peptide in this system that occurs during the assembly or the release process. The rapid release of ponericin G1 could be further exacerbated by the nature of interdiffusing multilayer thin films, for which rearrangement during film assembly may lead to layers void of ponericin G1 at the base of the film and an enrichment of the interdiffusing species, such as AmP, at the top of the film. This is a phenomenon which has previously been noted in interdiffusing LbL films [91].

In dealing with infections, the initial burst release that is seen with the chondroitin sulfate and alginate films is highly desirable. This large bolus of drug released in a short timescale could be used to rapidly eradicate any bacteria that are present. The smaller doses that follow

may help eliminate any residual bacteria. In cases where a more sustained and regular release of drug is needed, the dextran sulfate configuration appears more desirable, particularly if applied with sufficient numbers of tetralayers. There are a wide range of infection treatment needs [66], and therefore, having the range of control over AmP loading and release that is demonstrated in this paper is a valuable asset.

2.3.3 Bacterial Growth Inhibition

We have examined the alginate containing film, which showed the highest drug loading, for efficacy in *Staphylococcus aureus* growth inhibition, using a liquid microdilution assay. *S. aureus* was chosen as a Gram-positive strain of bacteria that is a common source of infection. By examining a standard sample of non-film incorporated ponericin G1 and comparing it with bacterial inhibition activity of cumulative alginate film release solution, the effects of the LbL assembly technique and release process on the peptide were examined. Figure 2-5 shows a comparison of the normalized bacterial inhibition of film released ponericin G1 and the amine-terminated native ponericin G1 against *S. aureus*. Figure 2-5A shows the response of a ponericin G1 standard against *S. aureus*. The minimum inhibitory concentration (MIC) of amine-terminated ponericin G1 is in the range of 11-22 μg/mL. Figure 2-5B shows that film released ponericin G1 over a span of the 10 day release time from alginate films exhibits an MIC in the range of 15-30 μg/mL, overlapping with the MIC of native ponericin G1. Therefore, film-released ponericin G1 retains comparable activity against *S. aureus* compared to the native peptide. Dextran sulfate and chondroitin sulfate containing films did not show a marked bacterial inhibition with this same microdilution assay due to their lower loading and release capacity as compared to the alginate films. However, in incorporating similar antimicrobial peptides with lower MICs against *S. aureus*, bacterial inhibition is expected to be noted for these films also. Furthermore, the loading of the current films can be increased by increasing the number of layers and thus, the thickness of the films.
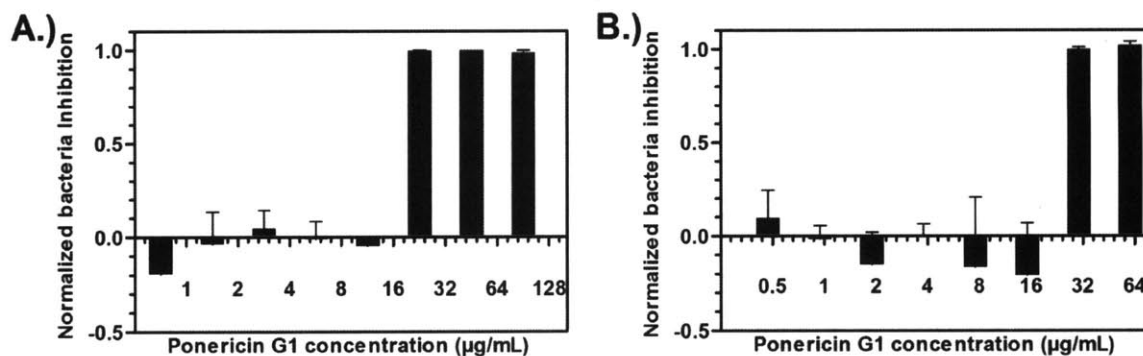
Figure 2-5: Normalized bacteria inhibition versus ponericin G1 concentration. A.) Inhibition of *S. aureus* growth by a standard of non-film-released ponericin G1. B.) Inhibition of *S. aureus* growth by (poly 2/alginate/ponericin G1/alginate)₇₅ film release solution.

We also explored the efficacy of each of the three film constructs against *S. aureus* growth on agar plates. The agar surface was evenly coated with bacteria and the films and controls (uncoated substrates) were placed on this surface. Figure 2-6B-D shows optical microscopy images of the film-agar interface, while Figure 2-6A shows the uncoated substrate-agar interface (negative control). Examining Figure 2-6B for the alginate film, there are no discernable bacteria present and only the small irregularities in the film surface can be seen. In the case of the alginate film, a small inhibition zone surrounding the film (approximately 0.2 cm wide) was also observed; this zone was mostly void of bacteria, characteristic of a leaching antimicrobial system. No clear zone of inhibition was seen surrounding the chondroitin sulfate and dextran sulfate containing films, most likely due to their lower ponericin G1 loading.
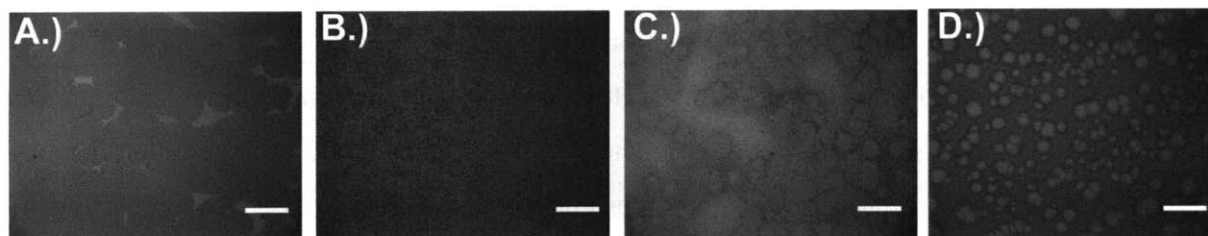
Figure 2-6: *S. aureus* growth inhibition assay for all film constructs and control. A.) Uncoated silicon control. B.) (Poly 2/alginate/ponericin G1/alginate)₇₅ film. C.) (Poly 2/chondroitin sulfate/ponericin G1/chondroitin sulfate)₇₅ film. D.) (Poly 2/dextran sulfate/ponericin G1/dextran sulfate)₇₅ film. Scale bar = 200 μm.

For the case of the alginate system, 100% of the bacteria growth was inhibited, as expected from the results shown in Figure 2-5. The agar assay was also able to capture a

44

decrease in bacteria compared to the negative control for the chondroitin sulfate and dextran sulfate films seen in Figure 2-6C and 2-6D, comparing to Figure 2-6A. The micrograph of the control slide shows large bacteria colonies with very little bare silicon substrate exposed. Digital image analysis showed that the area covered by bacteria colonies for the chondroitin sulfate film treated agar (Figure 2-6C) was 61.5 ± 3.9% less than the area covered by bacteria colonies in the negative control. The dextran sulfate film treated agar (Figure 2-6D) was also found to significantly reduce *S. aureus* growth, with a colony coverage area of 86.8 ± 2.0% less than the negative control. It is noteworthy that although overall ponericin G1 loading in dextran sulfate films was less than loading in chondroitin sulfate films, there was greater inhibition of *S. aureus* growth for the dextran sulfate films. It has previously been established that large biomacromolecules are able to complex with AmPs, reducing antibacterial properties of the peptide [94]. The reduced inhibition of *S. aureus* growth in chondroitin sulfate versus dextran sulfate films is likely also due to a potential complexation of chondroitin sulfate with ponericin G1 which may lower overall ponericin G1 activity.

2.3.4 Bacterial Attachment

To examine the efficacy of these films in preventing biofilm formation, the inhibition of *S. aureus* attachment on substrates coated with film versus negative controls (uncoated substrates) was assessed. All samples were placed in bacteria-media solutions for a predetermined time and subsequently placed on agar plates and allowed to incubate. Figure 2-7B-D shows optical microscopy images of the film-agar interface, while Figure 2-7A shows the negative control which is almost completely covered by *S. aureus*. Figure 2-7B is completely void of bacteria, showing 100% inhibition of *S. aureus* attachment on substrates coated with alginate films. Figure 2-7C and 2-7D are representative images which demonstrate that chondroitin sulfate and dextran sulfate films inhibit bacteria attachment by 80.6 ± 2.7% and 58.9 ± 2.3% compared to an uncoated substrate. Bacteria attachment is the first necessary step of biofilm formation. By coating surfaces with these ponericin G1 films, we can significantly inhibit *S. aureus* attachment, and therefore have the potential to prevent biofilm development.
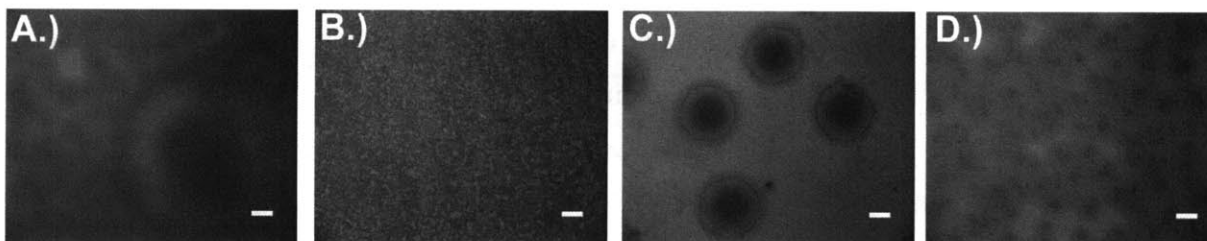
Figure 2-7: *S. aureus* **attachment assay for all film constructs and control. A.) Uncoated silicon control. B.) (Poly 2/alginate/ponericin G1/alginate)₇₅ film. C.) (Poly 2/chondroitin sulfate/ponericin G1/ chondroitin sulfate)₇₅ film. D.) (Poly 2/dextran sulfate/ponericin G1/dextran sulfate)₇₅ film. Scale bar = 200 μm.**

2.3.5 Film Biocompatibility

Finally, it is most important to ensure that film release media is not toxic to healthy wound healing cell lines. As model cells, fibroblasts (NIH 3T3 embryonic murine fibroblasts) and endothelial cells (human umbilical vein endothelial cells) were examined using a standard MTT assay for cell viability. Cells were exposed to media in which films were allowed to erode entirely, as well as standards of amine-terminated ponericin G1 and polyanions dissolved in media. It has previously been shown that poly(β-amino esters) are relatively nontoxic to cell lines such as NIH 3T3; therefore, standards of poly 2 were not directly examined here [61]. Figure 2-8 shows normalized viability of the 3T3 and HUVEC. Figure 2-8A shows cell response to standards of the polyanions and ponericin G1 dissolved in media at a concentration of 25 μg/mL, while Figure 2-8B shows cell response to film release solutions of media. As expected, the biologically friendly polyanions do not elicit any marked negative response on either cell line. However, ponericin G1, at the same tested concentration significantly lowers NIH 3T3 viability. It has been previously suggested that at high concentrations AmPs can prove cytotoxic [81, 95]. Examining Figure 2-8B, release media from each of the three film architectures did not demonstrate any cytotoxic behavior. It appears that the presence of the polyanions is actually beneficial to the health of the cells, particularly in the case of the NIH 3T3 cells, which responded poorly to the ponericin G1 standard. Previously, AmPs have been found to complex with biomacromolecules leading to reduction in cytotoxicity against mammalian cells, by preventing interactions with the membranes of these cells [94]. This may also explain the effect of the polyanions on cell viability which has been noted in this work.

46
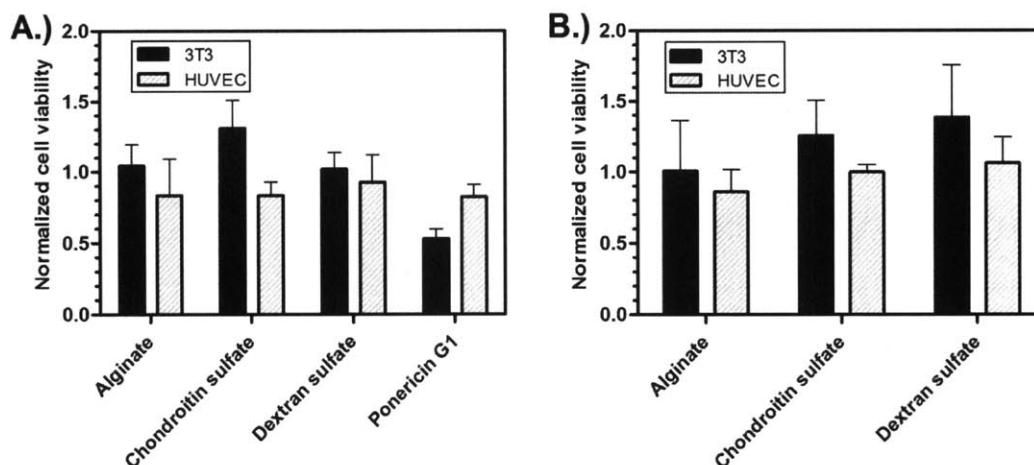
Figure 2-8: Normalized cell viability for all film constructs. A.) Viability of cells exposed to media containing dissolved polyanions or ponericin G1 standards. B.) Viability of cells exposed to release media based on polyanion used in film architecture.

2.4 Conclusions

A recent rise in antimicrobial resistance as well as the prevalence of biofilm related implant failure, has lead to an immediate need for novel means of addressing infection. This is necessary for the treatment of flesh wounds as well as the functionalization of bandages, medical devices, and implant materials. Because AmPs are not susceptible to resistance and have been shown to inhibit biofilm formation, they are a natural choice for use in applications such as these. In this work, we have described the successful incorporation and release of an AmP, ponericin G1, from hydrolytically degradable LbL assembled thin films. We have demonstrated sustained release and control over AmP loading in an LbL thin film, which had previously been unattained. The film composition, in particular the polyanion used, strongly influences the film growth and degradation properties as well as the incorporation and release properties of ponericin G1. Films were shown to be effective in inhibiting *S. aureus* growth, a common cause of infection. Additionally, film coated substrates inhibited *S. aureus* attachment, a necessary step in preventing the formation of biofilms on surfaces. Film release media was also found to be compatible with important wound healing cells, NIH 3T3 fibroblasts and HUVEC. With the findings of this paper, we are significantly further along in using such thin film coatings in medically relevant applications for infection treatment.

Chapter 3

Tunable Vancomycin Releasing Surfaces for Biomedical Applications

3.1 Introduction

Infection is a major complication in a wide range of medical conditions with prevalent causes ranging from common hospital procedures to battlefield trauma [3]. Infection can lead to sepsis, resulting in severe medical device complications, amputations, and even death [96]. The systemic overuse of broad-spectrum antibiotics has led to a great rise in multi-drug resistant bacteria [6]. Prevalence of drug-resistant infections is of grave concern in the face of a slowed discovery, development, and approval of new classes of antibiotics [6, 65]. Although treatments are being explored with novel antimicrobials such as natural and synthetic antimicrobial peptides [97, 98] that may address issues such as systemic toxicity, the fact remains that at this time, few agents are able to compete in efficacy with currently used antibiotics. With a dearth of potentially effective therapeutics for infection treatment, there is an immediate need for controlling the spread of these virulent drug-resistant bacteria. For this, we must engineer novel methods for controlled local delivery of existing and highly effective antibiotics, which both decreases opportunities for the development of resistance and decreases drug toxicity. Here, we report the design of such systems for the local delivery of a well known glycopeptide antibiotic, vancomycin hydrochloride. Vancomycin was the specific focus of this work as it is highly effective against many Gram-positive bacteria; it is also a preferred treatment in battlefield medicine and a first line of defense against resistant forms of *Staphylococcus aureus* (*S. aureus*) such as *methicillin-resistant S. aureus* [99], which has become a hospital epidemic [65]. The rates of *vancomycin resistant S. aureus* occurrence are still low [99], and therefore, developing delivery methods that prevent the formation and spread of such resistant strains is highly desirable.

Local antimicrobial delivery has been examined for numerous applications including orthopedic devices, wound dressings, periodontal devices, and vascular grafts amongst others [8,

100]. Specifically, local delivery of vancomycin has previously been explored in the context of hydroxyapatite coatings [8], calcium phosphate ceramic coatings [101], biodegradable calcium alginate wound dressings [9], hydrogels [11], and sol-gels [102, 103]. When developing antibiotic delivery systems, it is necessary to achieve a variety of release profiles and drug loadings to address specific medical needs. Eradication of an infection is best addressed by bolus antibiotic delivery, whereas the prevention of infection requires lower levels of drug delivery lasting over several days. Combining a bolus release followed by sustained delivery may be preferred to simultaneously eradicate an existing infection and prevent bacteria re-colonization. It is of utmost importance that antibiotic concentrations remain above the lowest antimicrobial concentration at which visible growth of bacteria is inhibited [104]. Prolonged exposure of bacteria to drug concentrations lower than this minimum inhibitory concentration (MIC) is implicated as a major cause of drug resistance [6, 8]. To ensure drug concentrations above the MIC at the site of infection, large drug doses are typically delivered systemically, often causing toxicity. The ability to engineer coatings for local vancomycin delivery from a variety of substrates that can achieve a wide range of drug loadings and release profiles while maintaining concentrations above MIC levels is therefore highly desirable. We have designed such coatings by creating layer-by-layer (LbL) assembled hydrolytically degradable polymer multilayer films containing vancomycin.

The aqueous LbL assembly technique takes advantage of complementary interactions between film components, including electrostatic interactions [22] and hydrogen-bonding [23] to assemble multilayered films. LbL assembly has been used extensively in drug delivery [42-44, 75], tissue engineering applications [47], sensors, and electrochromics [41] amongst other applications. Additionally, by taking advantage of dip [22], spray [25, 26], and spin [29] LbL assembly techniques, these films have been used to coat a wide variety of substrates, including electrospun materials [27], microfluidic devices [105], cells [49], and microparticles [38]. Compared to other drug delivery methods, such as therapeutic incorporation and release from hydrogels or incorporation in bulk polymers, LbL assembly of polymer multilayers allows for encapsulation of temperature and solvent sensitive therapeutics such as proteins [30] and peptides [13], temporal control over drug release [44], and potential for multi-agent delivery [64]. We have extensively examined hydrolytically degradable poly(β-amino esters) [61] as the

cationic component of LbL films for various drug delivery applications to achieve erodible films that release drug with controlled profiles [12, 13, 30, 39, 58, 62, 64, 80].

Herein we demonstrate the direct incorporation and release of vancomycin from a LbL assembled degradable polymer film, a previously unexplored system. The effects of varying film architecture and assembly technique (spray versus dip LbL assembly) on vancomycin loading and release are thoroughly examined. We find that certain architectures and assembly techniques best promote the formation of interactions between film components, which are found to be critical for direct incorporation of a small, weakly charged molecule, such as vancomycin in an LbL construct. We take advantage of both these electrostatic and other secondary interactions to design coatings with a wide range of release profiles and drug loadings that are highly applicable to various medical applications. Additionally, we study the antimicrobial capabilities of these films and their long term storage stability.

3.2 Materials and Methods

3.2.1 Materials

Poly 2 was synthesized as previously described [61, 86, 106] (molecular weight, M_n = 6.7 kDa). All chemicals and reagents were used as purchased without further purification. Alginate (M_n = 120-190 kDa), poly(sodium 4-styrene-sulfonate) (SPS, M_n = 70 kDa), poly(acrylic acid) (PAA, M_n = 100 kDa), and vancomycin hydrochloride from *Streptomyces orientalis* (biotechnology performance certified) were purchased from Sigma-Aldrich (St. Louis, MO). Chondroitin sulfate sodium salt (M_n = 85 kDa) was purchased from TCI International (Tokyo, Japan). Dextran sulfate sodium salt (M_n = 500 kDa), linear polyethyleneimine (LPEI, M_n = 25 kDa), and branched polyethyleneimine (BPEI, M_n = 50-100 kDa) were purchased from Polysciences (Warrington, PA). Silicon substrates (test grade, *n* type) for film deposition were obtained from Silicon Quest International (Santa Clara, CA). Latex-free absorbent sterile pad bandage substrates were obtained from RiteAid Pharmacy (Harrisburg, PA). Sodium acetate buffer (3 M, tissue culture grade) was purchased from Sigma-Aldrich (St. Louis, MO). Dulbecco's phosphate buffered saline (PBS, 0.1 M) was purchased from Invitrogen (Carlsbad, CA). Deionized water (18.2 MΩ, Milli-Q Ultrapure Water System, Millipore) was utilized throughout all experiments. For bacteria growth inhibition tests, *S. aureus* 25923 was obtained

from ATCC (Manassas, VA). Cation-adjusted Mueller Hinton broth (CaMHB) and Bacto agar were obtained from BD Biosciences (San Jose, CA). Vancomycin hydrochloride susceptibility test discs were obtained from BD Biosciences (Sparks, MD). For biocompatibility tests, NIH 3T3 cells and reagents for cell culture were obtained from ATCC (Manassas, VA).

3.2.2 Polyelectrolyte-Drug Interaction Studies

Specific drug-polyelectrolyte interactions were evaluated using high performance liquid chromatography (HPLC). Mixtures of known vancomycin and polyanion (dextran sulfate, chondroitin sulfate, and alginate) concentrations ranging from 5-500 µg/mL were evaluated chromatographically compared to pure vancomycin and pure polyanion standards. Mixtures were formulated at pH 7.4 in either 0.01 M PBS or 1 M sodium chloride solution. A 70:30 0.01 M PBS:methanol mobile phase at a flow rate of 1 mL/min and 500 µL sample injection volume was utilized. All solutions were examined using a C18 reversed phase column (Supelco) on a HPLC (Agilent Technologies, 1100 series) equipped with a fluorescence detector. An excitation wavelength of 280 nm was used and emission was evaluated at 355 nm, at which vancomycin is clearly visible. Peak integration and analysis were performed using Agilent ChemStation software. Retention time of vancomycin in the mixtures was evaluated in comparison to pure vancomycin solutions as an indication of vancomycin-polyanion interactions.

3.2.3 Film Assembly

Films were assembled on silicon substrates, which were cleaned using deionized water and methanol rinses and dried under nitrogen prior to assembly. These substrates were then plasma etched using air in a Harrick PDC-32G plasma cleaner at high RF level for 60 seconds. Following plasma etching, substrates were immediately submerged in a LPEI solution (10 mM with respect to repeat unit, pH 4.25) for a minimum of 20 minutes. For dipped LbL assembly, LPEI and SPS (10 mM with respect to repeat unit, pH 4.75) were used to coat the substrates with (LPEI/SPS)$_{10}$ bilayers and create stable charged base layers for the subsequent deposition of vancomycin containing films. The construction of these dipped layers was carried out using a Carl Zeiss programmable slide stainer with 5 minute alternating deposition steps of LPEI and SPS with 10, 20, and 30 second deionized water wash steps following each polyelectrolyte deposition.

Following base layer deposition, drug containing tetralayer architecture films were constructed with an architecture denoted: (poly 2/polyanion/vancomycin/polyanion)$_n$. All polyelectrolytes, including poly 2, alginate, chondroitin sulfate, and dextran sulfate, as well as vancomycin were dissolved at a concentration of 2 mg/mL (4.6 mM, 5.7 mM, 4.4 mM, 5.0 mM, and 1.3 mM respectively) in 0.1 M sodium acetate buffer at pH 5.0. For these films, all wash steps were carried out in 0.1 M sodium acetate buffer (pH 5.0). Poly 2 was deposited for 10 minutes, followed by three wash steps at 10, 20, and 30 seconds. The polyanion (alginate, chondroitin sulfate, or dextran sulfate) was then deposited for 7.5 minutes, also followed by 10, 20, and 30 second wash steps. Vancomycin was then deposited for 10 minutes followed by 20 and 30 second wash steps. This was followed by a second polyanion deposition and subsequent wash steps. These 4 deposition steps were repeated for n tetralayers. For all non-(LPEI/SPS)$_{10}$ bilayer dipped films described in this work, polycation and polyanion were deposited for 10 and 7.5 minutes, respectively, with 10, 20, and 30 second wash steps following each deposition.

For spray LbL assembly, LPEI and SPS solutions at the concentrations previously mentioned were used to spray (LPEI/SPS)$_{10}$ bilayers on silicon substrates using a programmable spraying apparatus (Svaya Nanotechnologies). For each bilayer, LPEI was sprayed for 2 seconds followed by a 3 second deionized water wash spray, followed by a 2 second SPS spray and 3 second wash. Following base layer deposition, tetralayer films of vancomycin were sprayed upon these charged surfaces. For each tetralayer, poly 2, the polyanion, and vancomycin were sprayed for 2 seconds each with 3 second wash steps (0.1 M sodium acetate buffer, pH 5.0) between each deposition step. Each spray step had a flow rate of approximately 0.25 mL/s. Dipped and sprayed films were dried under nitrogen and stored at 2-8 °C before use in subsequent experiments.

3.2.4 Bandage Coating

A commercially available absorbent bandage was spray coated with (poly 2/alginate/vancomycin/alginate)$_{60}$ using the spray LbL procedure described earlier. The bandage was plasma etched and subsequently soaked in LPEI solution at the conditions described earlier prior to film deposition. A 50 psi vacuum was applied to the back of the bandage during the spray deposition process to assist in complete bandage coating. Following deposition, a gentle vacuum was used to dry the bandage before subsequent experiments.

3.2.5 Film Growth and Morphology Characterization

The thickness of bilayer films was monitored using a spectroscopic ellipsometer (J.A. Woollam Co., Inc. M-2000D). Growth of vancomycin tetralayer films was tracked using a surface profilometer (KLA Tencor P-16). Films were scored with a razor and tracked over a 700 μm scan length to measure film thickness. Final film morphologies were examined using a Dimension 3100 atomic force microscope with Nanoscope 5 controller (Veeco Metrology). Tapping mode AFM was used to monitor film topology over 10 μm by 10 μm areas. Root mean squared roughness values were obtained using Nanoscope Analysis 1.10 software (Veeco). Film cross-sections were examined using a field emission scanning electron microscope (JEOL JSM-6700F). Additionally, bandage coatings were examined by scanning electron microscopy (JEOL JSM-6060).

3.2.6 Drug Release

Vancomycin release experiments were conducted by submerging film coated substrates in 500 μL of 0.01 M PBS at pH 7.4 and 37 °C. At predetermined times the films were removed from the current elution buffer and added to a fresh PBS aliquot; the previous aliquot was frozen at -20 °C. Each drug release sample was evaluated via HPLC with a fluorescence detector, using the column, solvent, and protocol discussed earlier.

3.2.7 Bacterial Growth Inhibition

Inhibition of *S. aureus* 25923 growth by a vancomycin film coated bandage and film release samples was monitored using both a modified Kirby-Bauer and microdilution assay [13, 87]. This particular strain of *S. aureus* was chosen based on recommendations by the Clinical and Laboratory Standards Institute [87]. In all Kirby-Bauer assays, agar plates were formulated from CaMHB and Bacto Agar. These agar plates were evenly coated with *S. aureus* in its exponential growth phase at a concentration of 10^8 CFU/mL. Immediately after coating the agar, a bandage coated with the LbL drug architecture of choice was placed on the substrate, along with an LPEI coated bandage negative control, and a 30 μg vancomycin susceptibility disc positive control. Following 18 hours of incubation at 37 °C, agar plates were digitally imaged and zones of inhibition were measured.

For microdilution assays, release samples were taken as previously described for vancomycin films. Assays were conducted in 96 well clear bottom plates. Release samples in 0.01 M PBS were added in triplicate to the plate and diluted with an equal volume of 2x concentrated CaMHB, reducing the effective concentration to 1x. These samples were subsequently serial diluted in 1x CaMHB. Similarly, pure 0.01 M PBS containing no vancomycin was also diluted. *S. aureus* in its exponential growth phase was isolated and added to diluted release samples at a final concentration of 10^5 CFU/mL, along with positive controls of plain PBS. Negative controls of PBS did not contain any bacteria. Controls of non-film released vancomycin were also examined in a similar manner. These plates were incubated at 37 °C for 18 hours. Following incubation, the optical density at 600 nm of all wells was examined using a BioTek PowerWave XS plate reader. Normalized bacteria inhibition was calculated as follows:

$$Normalized\ Bacteria\ Inhibition = \frac{\left(OD_{600,positive\ control} - OD_{600,sample}\right)}{\left(OD_{600,positive\ control} - OD_{600,negative\ control}\right)}.$$

3.2.8 Biocompatibility

Film biocompatibility was quantified by examining cell viability of NIH 3T3 embryonic murine fibroblasts upon exposure to film eluent, pure vancomycin, and pure polyanion samples. Cells were seeded at 10,000 cells per well in a 96 well polystyrene tissue culture plate and incubated at 37 °C and 5% CO_2 in 100 μL of media for 24 hours. Dipped and sprayed films for each of the three polyanion architectures explored were allowed to completely elute in culture media at 37 °C. Non-film eluted alginate, chondroitin sulfate, dextran sulfate, and vancomycin were also allowed to incubate in culture media at concentrations of 2 mg/mL (and 0.25 mg/mL for alginate which was insoluble in media at greater concentrations) for the same length of time as the films. All samples were filtered through 0.2 μm filters, and the cell culture media was replaced with 100 μL of this test media in the growing cells. Positive controls were cells cultured in untreated media, while negative controls contained no cells and untreated media. After 18 hours of exposure to the test media, a standard MTT assay (Sigma-Aldrich, St. Louis, MO) was performed and cell viability was established following 3 hours of incubation with MTT solution. A BioTek PowerWave XS plate reader was used to detect the absorbance of the wells at 570 nm (proportional to cell viability). Absorbance at 690 nm was subtracted as background and cell viability was calculated as follows:

$$Normalized\ Cell\ Viability = \frac{\left(Abs_{570-690,sample} - Abs_{570-690,negative\ control}\right)}{\left(Abs_{570-690,positive\ control} - Abs_{570-690,negative\ control}\right)}.$$

3.2.9 Long Term Storage Stability

A representative dipped film architecture, (poly 2/dextran sulfate/vancomycin/dextran sulfate)$_{60}$, was used to explore the long term storage stability of vancomycin in these multilayer films. Films were prepared as described earlier and stored dry at three different conditions: 4 °C, 25 °C, and 37 °C. Films at 4 and 25 °C were stored up to 6 months, and those at 37 °C were stored for up to 1 month. Following storage, films were released in 0.01 M PBS at 37 °C and release was quantified via HPLC as described earlier. Some of these stored films were also allowed to release completely into a 1 mL aliquot of 0.01 M PBS. Part of this sample was used for quantification of the total drug loading and the remaining was used to determine the MIC of the vancomycin in the sample against *S. aureus* in a microdilution assay as described earlier.

3.2.10 Statistical Analysis

All experiments reported in this work were conducted in triplicate at minimum. Data is reported as mean ± standard deviation. Film thickness measurements were taken at five different locations for each of the films examined per experimental repeat. Film morphology (AFM and SEM) was characterized at 3 different locations for each of the films examined per experimental repeat.

3.3 Results and Discussion

3.3.1 Choice of Film Architecture

Polymer films containing vancomycin were assembled using the electrostatic LbL assembly method, in which films are constructed by alternate deposition of polymers and molecules of opposite charge. Figure 3-1 shows a schematic of the LbL process and the structure of all agents examined in this study. Poly 2, a polyelectrolyte from the poly(β-amino ester) series of polycations [61, 86, 106], was incorporated into all architectures, rendering the films hydrolytically degradable. Vancomycin is also cationic at the deposition conditions of this study, with a net charge of positive 1 [107]. To electrostatically layer films with the cationic

poly 2 and vancomycin, a counter polyanion was required; we chose to use biological polymers, including dextran sulfate, chondroitin sulfate, and alginate.
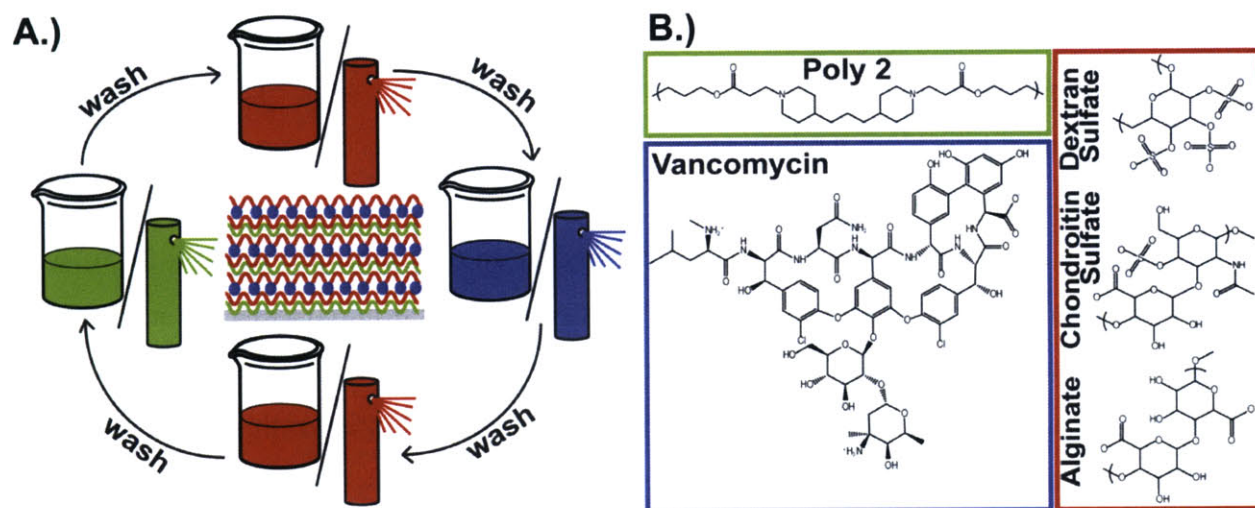
Figure 3-1: Film assembly and components. A.) LbL assembly schematic (dipped and sprayed assembly); tetralayer film architecture. B.) Film component structures (cations highlighted in green and purple, anions in red).

It is well understood that aside from electrostatic interactions, other secondary interactions such as hydrogen bonding, hydrophobic interactions, and dispersion forces between film components play an important role in film assembly [84, 108-111]. The use of HPLC as a tool to study molecular interactions has also been well established [112]. To elucidate secondary interactions that may exist between vancomycin and the polyanions being explored, solutions of vancomycin combined with each of these polyanions were formulated at pH 7.4 in 0.01 M PBS and examined with HPLC. Vancomycin's isoelectric point is reported to exist between pH 7.2 [113] and 8.3 [114], and therefore the pH of these mixtures was intentionally chosen to lie in this range to specifically consider non-electrostatic interactions. As shown in Figure 3-2A-C, for mixtures containing vancomycin and dextran sulfate, chondroitin sulfate, and alginate, respectively, the retention time of vancomycin shifted approximately 2 minutes from 6.5 minutes for pure vancomycin to 8.6 minutes for all mixtures, as measured using a fluorescence detector. This retention time shift is indicative of an interaction between vancomycin and these polyanions [112]. The interaction was visible in dilute solutions with equal vancomycin and polyanion concentrations (as low as 5 µg/mL). At these concentrations, only vancomycin fluorescence is detected with the excitation and emission wavelengths used; the polyanions cannot be detected.

To further elucidate the nature of the particular interaction observed between vancomycin and the polyanions and due to the wide range of the reported vancomycin isoelectric point, it was necessary to determine whether the interaction could be electrostatically driven aggregation. These same vancomycin-polyanion mixtures were formulated in a 100 times more concentrated salt solution of 1 M sodium chloride at pH 7.4 and examined via HPLC. If the interaction was entirely electrostatic, charge shielding in this higher salt concentration would be expected to disrupt the interaction, and no shift in retention time would be observed. As seen in Figure 3-2D-F, the interaction between vancomycin and the polyanions was not disrupted in this increased salinity, providing further evidence for the existence of non-electrostatic interactions between vancomycin and these polyanions. Additionally, it should be noted that peak areas remained consistent for mixtures of vancomycin and the polyanions compared to pure vancomycin solution in the HPLC chromatograms obtained.
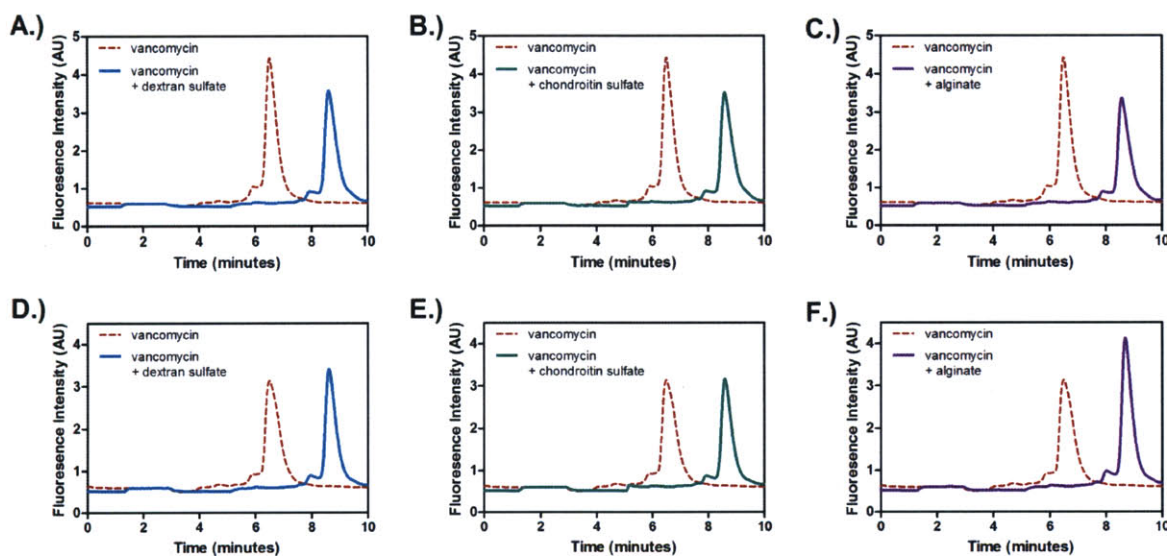
Figure 3-2: Drug-polyelectrolyte interaction studied via HPLC. The dashed red traces in A-C represent pure 5 µg/mL vancomycin solution at pH 7.4 in 0.01 M PBS. The dashed red traces in D-F represent pure 5 µg/mL vancomycin solution at pH 7.4 in 1 M NaCl. The solid traces represent mixtures containing 5 µg/mL vancomycin and 5 µg/mL polyelectrolyte. A.) Vancomycin-dextran sulfate mixture, pH 7.4, 0.01 M PBS. B.) Vancomycin-chondroitin sulfate mixture, pH 7.4, 0.01 M PBS. C.) Vancomycin-alginate mixture, pH 7.4, 0.01 M PBS. D.) Vancomycin-dextran sulfate mixture, pH 7.4, 1 M NaCl. E.) Vancomycin-chondroitin sulfate mixture, pH 7.4, 1 M NaCl. F.) Vancomycin-alginate mixture, pH 7.4, 1 M NaCl.

Vancomycin has a complex structure consisting of a seven membered peptide chain linked to two unique sugar moieties [115]. The drug is known to dimerize with itself [116, 117],

promote protein aggregation [118], act as a Cu^{2+} chelator [119], and bind to peptides and polymer surfaces [120]. These phenomena are a result of hydrogen bonding, hydrophobic interactions, and ionic interactions [121]. Vancomycin dimerization is specifically due to amide-amide hydrogen bonding between the peptide backbones of two vancomycin molecules [116]. Additionally, vancomycin is known to partition preferentially into the hydrophobic polymer phase of a two-phase mixture [121], displaying the importance of hydrophobic interactions with the vancomycin phenolic groups. The secondary interactions encountered in this work are also likely a result of both hydrogen bonding (with phenolic and amido groups in vancomycin and the carboxyl and sulfate groups of the polyanions) and hydrophobic interactions between vancomycin and the polyanions. NMR spectroscopy is currently being employed to further elucidate the nature of these interactions.

Due to the clear existence of interactions between vancomycin and dextran sulfate, chondroitin sulfate, and alginate, these three polyanions were selected for use as the counter polyanions required in multilayer film assembly. It was hypothesized that the secondary interactions between vancomycin and the polyanions investigated would strongly support and promote film assembly at conditions beyond what is attainable due only to electrostatic interaction. Tetralayer film architectures of (poly 2/polyanion/vancomycin/polyanion)$_{60}$ were built using both dip and spray LbL assembly. Sixty tetralayers were found to be sufficient to realize significant differences between film growth and morphology for various film architectures and deposition conditions.

3.3.2 Film Growth and Morphology

Despite the presence of interactions between vancomycin and all of the polyanions used in building these films, the film growth characteristics of each of the three film architectures were found to be quite different. Figure 3-3A-C shows the growth profiles of dip and spray assembled dextran sulfate, chondroitin sulfate, and alginate containing tetralayer films, respectively, for which films were built up to 60 tetralayers in each case. Exploring first the dip assembled films, all three architectures exhibited non-linear growth profiles and large ultimate thicknesses, both of which are signs of interdiffusion of molecules during assembly. Chondroitin sulfate and alginate films have similar growth profiles that can best be described as a two-stage process, with a shallow growth regime up to approximately 15-20 tetralayers, followed by a

rapid increase in slope in the second growth regime lasting through the 60 tetralayer deposition. For the purpose of this discussion, we have used linear fits to each of these two regions, which yield R^2 fit parameters ranging from 0.94 to 0.99 for these film systems. The change in slope is most dramatic in the case of alginate, where the linear fit slope of the initial regime has a value of 5.2 ± 0.5 nm/tetralayer, and that of the second growth regime becomes 80.6 ± 2.6 nm/tetralayer. The chondroitin sulfate growth curve exhibits a change in slope of 12.2 ± 1.2 to 137 ± 11 nm/tetralayer. Super-linear growth profiles such as these have been encountered in LbL systems where polysaccharides and peptides have been used in assembly, and have become increasingly observed in the recent past [13, 46, 47]. This type of multilayer growth can be attributed to the ability of any or all of the components of a particular film architecture to diffuse within the underlying film [89, 90, 122, 123]. The interdiffusion of film components depends on several factors, including charge density, molecular weight, ionic strength, and pH [51, 52, 83, 124]. Many of these factors may contribute to the interdiffusion observed in these vancomycin films, especially the weak charge density of vancomycin and its significantly lower molecular weight compared to the polyelectrolytes being incorporated. Appendix B shows the effect of wash step ionic strength on film growth.
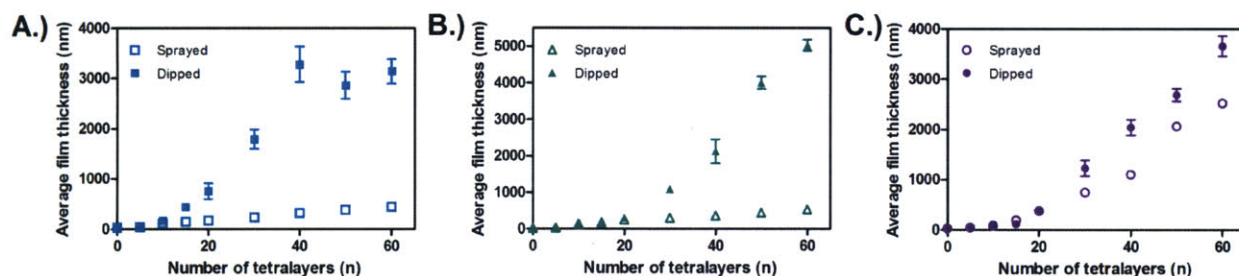
Figure 3-3: Film growth profiles. A.) (Poly 2/dextran sulfate/vancomycin/dextran sulfate)$_n$ sprayed and dipped. B.) (Poly 2/chondroitin sulfate/vancomycin/chondroitin sulfate)$_n$ sprayed and dipped. C.) (Poly 2/alginate/vancomycin/alginate)$_n$ sprayed and dipped.

The dextran sulfate film enters an exponential growth regime early in the growth process, starting at 5 tetralayers, but does not present a second linear growth phase. As in the case of chondroitin sulfate and alginate, this exponential growth is highly indicative of interdiffusion between film components. The film grows in this way until it reaches approximately 40 tetralayers at which point the film no longer increases in thickness. Stagnation in film growth may occur in systems where the surface no longer displays charge reversal upon deposition of

subsequent layers and/or no longer allows for the secondary interactions which assist in film growth (including changes in surface hydrophobicity). To further explore what leads to lack of growth for these films, the construction of five bilayers of branched polyethyleneimine and poly(acrylic acid), at pH 5.1, was attempted on a forty tetralayer dextran sulfate dipped film (the point at which film growth stagnation is encountered). This bilayer architecture was chosen as a well established film system which should grow on any charged surface. Following the attempted bilayer deposition, the assembly of twenty tetralayers of the dextran sulfate dip architecture was attempted on these films. No increase in film thickness compared to the initial forty tetralayers was observed. This is a strong indication that the ceasing dextran sulfate film growth is due to lack of charge reversal at approximately forty tetralayers.

For all architectures examined in this work, sprayed films were found to be significantly thinner when compared to the same dipped film architectures. Specifically, the sprayed films were approximately 7, 9, and 1.5 times thinner than the dipped films for dextran sulfate, chondroitin sulfate, and alginate films, respectively. Final film thicknesses for both the dipped and sprayed films are summarized in Table 3-1. The differences in growth profiles between the sprayed and dipped architectures is perhaps most dramatic in the case of dextran sulfate, where the sprayed film grows linearly with a slope of 7.1 ± 0.2 nm/tetralayer for the 60 tetralayer films explored in this work. Linear growth is characteristic of polyelectrolyte multilayer films where there is little or no interdiffusion of species during the growth process. This is typical of films in which high molecular weight species and/or species with high degrees of ionization are used [52]. The chondroitin sulfate and alginate films also undergo a striking change in growth profile in the sprayed films compared to dipped films, with a significantly more linear growth profile with slope of 7.4 ± 0.4 nm/tetralayer and 52 ± 4 nm/tetralayer following the initial deposition of 5 and 10 tetralayers, respectively. In the rapid cycle times presented in the spray process, each polyelectrolyte and the vancomycin drug is kinetically trapped during the deposition steps, rather than being able to diffuse into or out from the film as would happen when dipping in dilute solutions where significantly longer deposition times are required. This data suggests that the spray LbL process can lead to kinetic inhibition of the super-linear growth processes described earlier, as evidenced by the linear growth profiles of the sprayed films and the significantly thinner final film thicknesses, as compared to dipped films. We have also observed this behavior with other LbL systems using synthetic polymers, which will be reported separately.

The degree of suppression of interdiffusion in the sprayed films was much less significant for the alginate film. This system is the only one for which the polyanion is a completely carboxylated carbohydrate and lacks sulfate functionality, and it is possible that it may exhibit lower effective charge densities at the LbL deposition conditions; this could affect critical factors such as the diffusion coefficient of the polyanion into the LbL film and thus the adsorption times needed for interdiffusion. The acid groups may also undergo significant hydrogen bonding compared to the sulfate groups, and thus the driving force for interdiffusion and exchange within the film may also be greater, leading to faster rates of transport into the film. The net result is that the spray and diffusion times in alginate films are of the same magnitude, thus enabling time for interdiffusion in these films.

Table 3-1: Film morphology and drug loading properties at sixty tetralayers.

	Dip Assembly			Spray Assembly		
	Film Thickness (nm)	RMS Roughness (nm)	Drug Loading ($\mu g/mm^3$)	Film Thickness (nm)	RMS Roughness (nm)	Drug Loading ($\mu g/mm^3$)
Alginate	3660 ± 200	18.7 ± 2.2	20.8 ± 2.0	2520 ± 44	1.78 ± 0.26	156 ± 21
Chondroitin Sulfate	5030 ± 155	9.93 ± 1.09	17.8 ± 2.2	532 ± 27	0.839 ± 0.180	106 ± 10
Dextran Sulfate	3140 ± 243	18.3 ± 1.4	69.2 ± 6.7	443 ± 3	0.607 ± 0.086	219 ± 22

The clear differences between dipped and sprayed films are also evident when examining final film morphology of 60 tetralayer dipped versus sprayed films. Atomic force microscopy images reveal that the sprayed films have much lower roughness values compared to the dipped films as seen in Figure 3-4A and exemplified by the root mean squared roughness values summarized in Table 3-1. Cross-sectional scanning electron microscope images for each film architecture were also taken, and the dense internal structure appears very similar for all of the films explored, with the only clear difference between images being the final thickness of the films. An example of the cross-sectional SEM images taken for a dipped and sprayed dextran sulfate film is shown in Figure 3-4B.
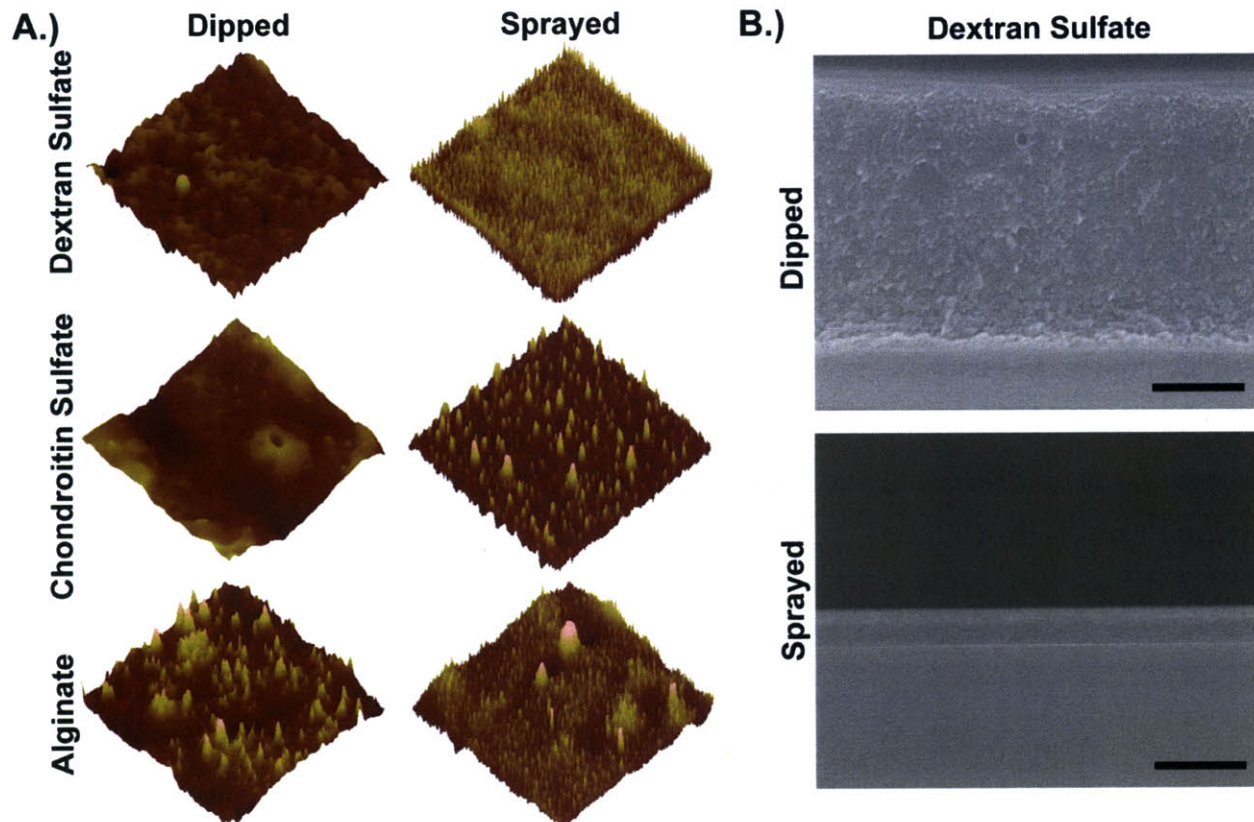
Figure 3-4: Final film morphology. A.) Atomic force microscope images (10 μm x 10 μm) for sprayed and dipped films of architecture (poly 2/polyanion/vancomycin/polyanion)$_{60}$. The maximum z-scale for each of the polyanions is as follows: dextran sulfate (dipped, z_{max} = 250 nm; sprayed, z_{max} = 4 nm), chondroitin sulfate (dipped, z_{max} = 150 nm; sprayed, z_{max} = 7 nm), and alginate (dipped, z_{max} = 200 nm; sprayed, z_{max} = 15 nm). B.) Scanning electron microscope cross-section images for (poly 2/dextran sulfate/vancomycin/dextran sulfate)$_{60}$ dipped and sprayed films (scale bar = 1 μm).

3.3.3 Drug Incorporation and Release

After examining film growth properties, the vancomycin release profile for each 60 tetralayer architecture was determined. Films were released in physiologic conditions in 37 °C at pH 7.4 (0.01 M PBS). Periodically, film eluent was removed and the phosphate buffer bath was completely refreshed. This eluent was examined using HPLC with a fluorescence detector to quantify the vancomycin released. The results from vancomycin release quantification can be seen in Figure 3-5A-B for both dipped and sprayed films. Figure 3-5C-D shows normalized release data. Appendix B shows the effect of wash step ionic strength on drug release profiles.
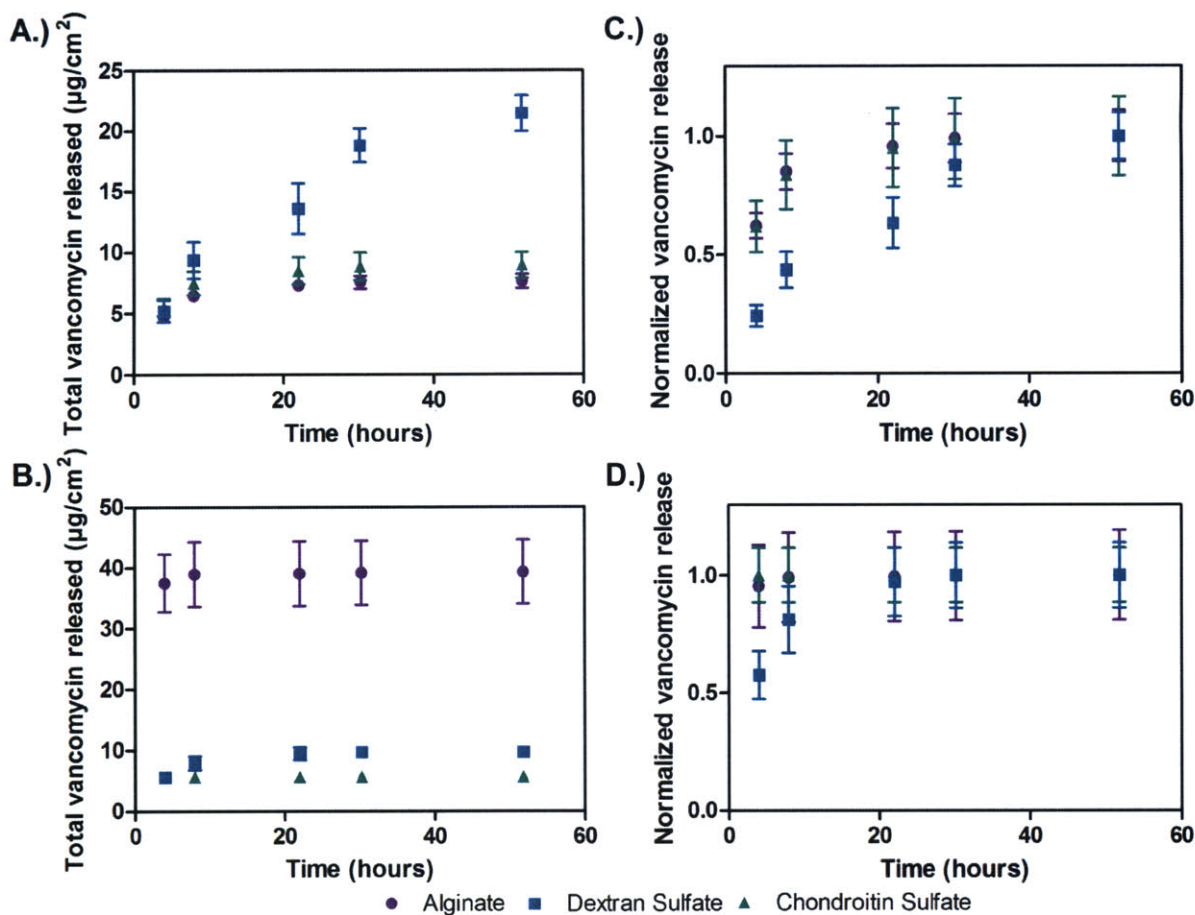
Figure 3-5: Vancomycin release from (poly 2/polyanion/vancomycin/polyanion)$_{60}$ films. A.) Total vancomycin release over time from dipped films. B.) Total vancomycin release over time from sprayed films. C.) Normalized vancomycin release over time from dipped films. D.) Normalized vancomycin release over time from sprayed films.

Examining first the dipped architecture release profiles in Figures 3-5A and 3-5C, the dextran sulfate films appear to have a linear release over approximately 40 hours, particularly following the first 4 hours of release. During the linear release period, approximately 88% of the incorporated drug is released. Drug release lasts for a total of 52 hours. Neglecting the first 4 hours of release, the half-life of the remaining vancomycin release is approximately 22 hours. For a theoretical film which releases drug with a completely linear profile from 0 to 52 hours, the half life for release is 26 hours, which is comparable to the film developed here. In the case of both alginate and chondroitin sulfate, there is a bolus release of 88% of the total incorporated vancomycin in the first 8 hours, with total drug release lasting over approximately 24 hours. Bolus release is characteristic of films in which a large amount of the released component is

populating the top layers of the film, which can be the case for films growing with a super-linear or exponential growth profile [13]. Additionally, it is important to note the conditions in which film release was conducted, namely body pH, which lies near the vancomycin isoelectric point. Therefore, vancomycin is close to or completely uncharged at this pH as compared to its positive charge at the film deposition conditions. The large bolus release that is seen in alginate and chondroitin sulfate dipped films may be attributed to the difference between film deposition and release pH and ejection of vancomycin from these films. This phenomenon has been observed in other LbL systems where polyelectrolytes were ejected due to pH induced charge imbalance and the requirement for charge neutrality in these multilayer films; the kinetics of the ejection process are more rapid for lower molecular weight polyelectrolytes [125], and should be rapid for small molecular species such as vancomycin.

Despite its exponential growth profile and identical release conditions, the dextran sulfate dipped film maintains a linear release of vancomycin over a longer period of time than the other polyanion films. It was observed that dextran sulfate dipped film eluent examined via HPLC frequently displayed a vancomycin peak at 8.6 minutes as seen in Figure 3-6A as compared to 6 minutes for non-film released vancomycin standards. This shift in retention time was not reproducibly observed in the alginate and chondroitin sulfate film release samples. The peak shift is analogous to the shift that was observed in HPLC analysis of solutions containing mixtures of vancomycin and the polyanions at pH 7.4. It appears that this drug-polyelectrolyte interaction which was observed in solution was maintained in the dipped dextran sulfate films only. The appearance of this interaction only for dextran sulfate may be attributed to the differing growth kinetics of these films compared to the other polyanions. The highly interdiffusing film may allow for vancomycin to appropriately form secondary interactions with dextran sulfate during film growth in a manner that is not supported during the growth of other dipped films. Additionally, the fact that there is some level of interdiffusion in dipped alginate and chondroitin sulfate films (evidenced by their non-linear growth) which is unable to promote significant vancomycin release stabilization suggests that the dextran sulfate-vancomycin interaction is stronger than vancomycin's interaction with the other polyanions.

To confirm the hypothesis regarding interaction strengths, construction of bilayer film architectures of (vancomycin/polyanion)$_{120}$ at pH 7.4 was attempted utilizing the same conditions used in tetralayer film assembly. Construction of tetralayer architecture films was not examined

at this pH due to the rapid degradation of poly 2 that has been reported at pH 7.4 [61]. At these conditions, the only bilayer film that formed was (vancomycin/dextran sulfate)$_{120}$ with a film thickness of 157 ± 16 nm. The lack of film formation for the other polyanions was confirmed using spectroscopic ellipsometry (data not shown). This finding supports the notion that the interaction of vancomycin and dextran sulfate is stronger than the interaction of vancomycin with the other polyanions. Additionally, it should be noted that bilayer film construction at the original deposition pH of this study (pH 5.0) was also attempted. At these conditions none of the polyanions were able to build films, as confirmed by spectroscopic ellipsometry (data not shown). This provides further justification for the need to layer with a polycation such as the poly(β-amino esters) to promote film growth and allow favorable polymer chain conformations allowing for the formation of drug-polyelectrolyte interactions. The higher charge density of these polycations assists in forming the bulk of the film. The high degree of interdiffusion in dextran sulfate dipped films which promotes secondary interaction formation, and the stronger interaction of vancomycin with dextran sulfate compared to the other polyanions, contributes to the more linear and lengthy release profile of vancomycin from dextran sulfate dipped films compared to other dipped architectures.
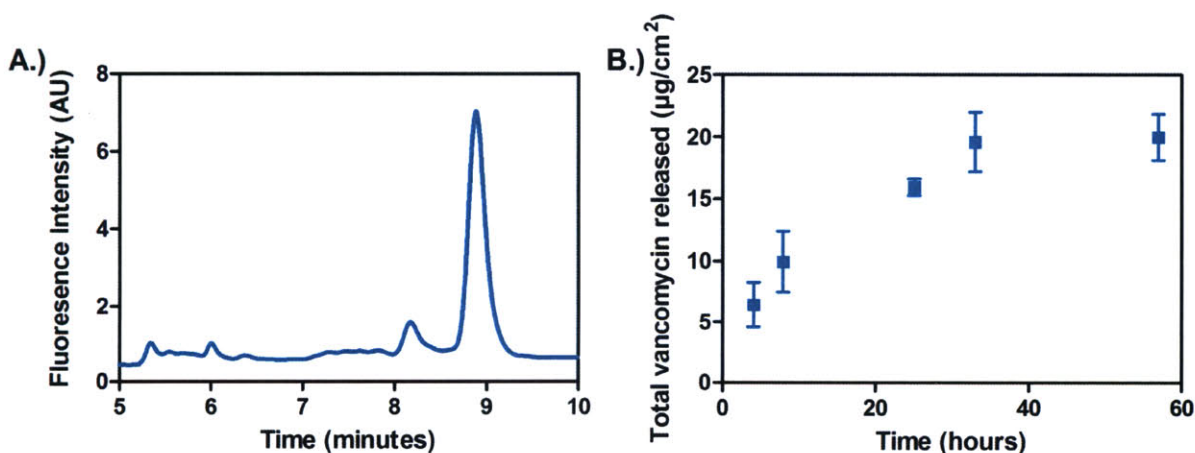
Figure 3-6: Interdiffusion in vancomycin dipped and sprayed films. A.) HPLC spectra of film release eluent from a representative dipped (poly 2/dextran sulfate/vancomycin/dextran sulfate)$_{60}$ film. B.) Vancomycin release from sprayed film of architecture (poly 2/dextran sulfate/vancomycin/dextran sulfate)$_{120}$.

Vancomycin release from sprayed films differs greatly compared to release from dipped films. Specifically, release times for all three polyanions are greatly accelerated. The alginate and chondroitin sulfate films release approximately 97% and 100% of their vancomycin content

in 4 hours as seen in Figures 3-5B and 3-5D. The dextran sulfate sprayed films release approximately 60% of the incorporated vancomycin in 4 hours, and continue to release vancomycin up to 24 hours. The linear growth observed in these sixty tetralayer sprayed films, indicating low interdiffusion, does not support the formation of secondary interactions which are critical in stabilizing vancomycin release from these constructs, as witnessed for the dextran sulfate dipped film. Although the lack of interdiffusion occurring in the case of the sprayed films may be the primary factor leading to faster drug release, the dextran sulfate sprayed film is the most stable of the three sprayed architectures examined. The dextran sulfate films released vancomycin over a longer timescale than the other sprayed architectures, implying that the dextran sulfate interaction with vancomycin is stronger than the vancomycin interaction with alginate and chondroitin sulfate, as previously seen with dipped films.

To determine whether interdiffusion could be induced in these sprayed films and prolong vancomycin release, a 120 tetralayer sprayed dextran sulfate film was assembled. Final film thickness was found to be 2250 ± 86.3 nm, approximately 2.5 times greater than the thickness expected if the film continued to grow linearly after depositing the first 60 tetralayers. This non-linear growth behavior indicates that increasing the number of sprayed layers can eventually lead to significant film interdiffusion. Examining release from this 120 tetralayer construct, shown in Figure 3-6B, the film is found to release with a profile similar to a sixty tetralayer dipped dextran sulfate film. Specifically, 20.0 ± 1.9 $\mu g/cm^2$ is released over 45 hours, where following 4 hours, there is a linear release of nearly 70% of the incorporated drug. This increased release linearity and timescale highly supports the importance of the effect of film interdiffusion on promoting favorable interactions within the film and stabilizing vancomycin release from LbL constructs.

An important consideration in designing these vancomycin releasing films is the potential for efficacy against bacterial growth and usefulness in clinical situations. The most important parameter for assessing effectiveness against bacteria is drug loading and release above the MIC of vancomycin. Releasing sub-MIC antibiotic concentrations [8] and unnecessary prolonged exposure [100] to an antibiotic can lead to a rise in drug resistant organisms. All architectures explored in this work lead to release above MIC values for vancomycin against *S. aureus*, namely 0.5-2 $\mu g/mL$. The drug loadings and release timescales observed in the films designed in this study are highly therapeutic. Table 3-1 shows the vancomycin loading density for each of the dipped and sprayed architectures examined. These drug densities are comparable to other

techniques of drug loading not involving self-assembly and in some cases exceed what is achievable by other means. In both the sprayed and dipped cases, the dextran sulfate films have the highest drug density although they are overall the thinnest films. This is likely due to the strong interaction of vancomycin and dextran sulfate. Interestingly, in all cases sprayed films have a 3-8 times higher drug density than the dipped films. This can be attributed to the same phenomena that lead to the sprayed films growing with increased linearity as compared to the dipped films. There is a much smaller sink and less time for vancomycin to diffuse out of the growing film during spray assembly. Instead of a large bath in which films are submerged for significant lengths of time as in dip assembly, the only sink for drug out-diffusion from the film during spray assembly is the existence of a small boundary layer of solution from each short spray. Therefore, little vancomycin is lost during non-vancomycin spray steps as compared to the amount of vancomycin which may be lost during dipped assembly.

3.3.4   Combining Dip and Spray LbL Assembly for Practical Application

The bolus release and large drug loads in the sprayed films assembled in this work are useful for immediate eradication of bacteria. The longer and more linear release of the dextran sulfate dipped films is appropriate for preventing infection or re-colonization of a wound. To create an architecture that has both a large drug release initially followed by a linear release above the antibiotic MIC, a composite spray and dipped architecture was examined. Dipped dextran sulfate films were first constructed per the standard protocol. After construction, these films were used as the substrate for spray LbL of an alginate vancomycin film. The release profile of the composite film architecture of (poly 2/dextran sulfate/vancomycin/dextran sulfate)$_{60, dip}$ + (poly 2/alginate/vancomycin/alginate)$_{60, spray}$ is seen in Figure 3-7. As expected, there is a large therapeutic dose of vancomycin released in the first 8 hours from the alginate sprayed film which comprises the top layers of the composite film and amounts to 50% of the total drug incorporated. The absolute amount ($20.7 \pm 4.2 \ \mu g/cm^2$) released in these first 8 hours is approximately 50% less than the amount of vancomycin incorporated into an alginate sprayed film on a treated silicon substrate. This lower incorporation of vancomycin during spraying upon the dextran sulfate dipped film is likely due to the highly differing nature of this substrate compared to the substrates the films were typically sprayed on. The rest of the drug releases linearly with the release leveling off at around 52 hours. There is approximately 20.0 ± 4.8

$\mu g/cm^2$ of drug released during the linear release period, which is comparable to the 21.5 ± 1.5 $\mu g/cm^2$ vancomycin released from a dextran sulfate dipped film over a similar timescale. This provides further support to the lack of out-diffusion that occurs during the spray process as no significant drug is lost during spray LbL on the dipped films. This composite architecture is able to address both an existing infection via its bolus release and prevent bacteria re-colonization of a wound over time with above-MIC levels of sustained vancomycin release.
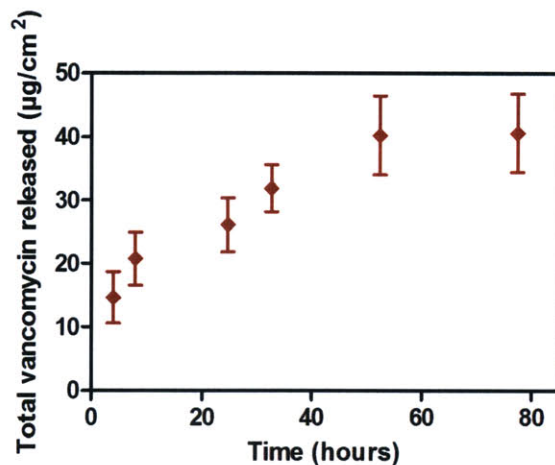
Figure 3-7: Vancomycin release from composite dip and spray film of architecture: (poly 2/dextran sulfate/vancomycin/dextran sulfate)$_{60,dip}$ + (poly 2/alginate/vancomycin/alginate)$_{60, spray}$.

For sprayed films, the practical applicability to a medically relevant substrate was investigated. Films were sprayed on commercially available bandages. These drugstore bandages were not functionalized with any antimicrobials prior to the spray LbL deposition that was performed. Films were sprayed as previously described and a vacuum was applied to the back of the substrate at 50 psi to assist in better coating the entire bandage. Prior to spraying the films, the bandage was soaked in linear polyethyleneimine (LPEI) and dried to create a uniform positively charged functionality to promote film deposition. Figure 3-8A shows SEM images of the bandage before and after coating with an alginate film. The thick coating appears to bridge many of the bandage fibers. Release from these coated bandages was examined; an example for the case of alginate is shown in Figure 3-8B. As expected, with a higher surface area substrate, there is a 2 times greater drug loading for the sprayed bandage material compared to a planar substrate while the release kinetics are similar. Had conformal coating of all bandage fibers been achieved, drug loading would be expected to be even greater. The rapid release of vancomycin from this sixty tetralayer sprayed film at concentrations above the drug MIC is applicable to the

direct eradication of an existing infection. To mitigate the burst and obtain a longer release of drug from these bandages, a sprayed architecture similar to the 120 tetralayer dextran sulfate film (whose release from a planar substrate was shown previously in Figure 3-6B) would be appropriate.
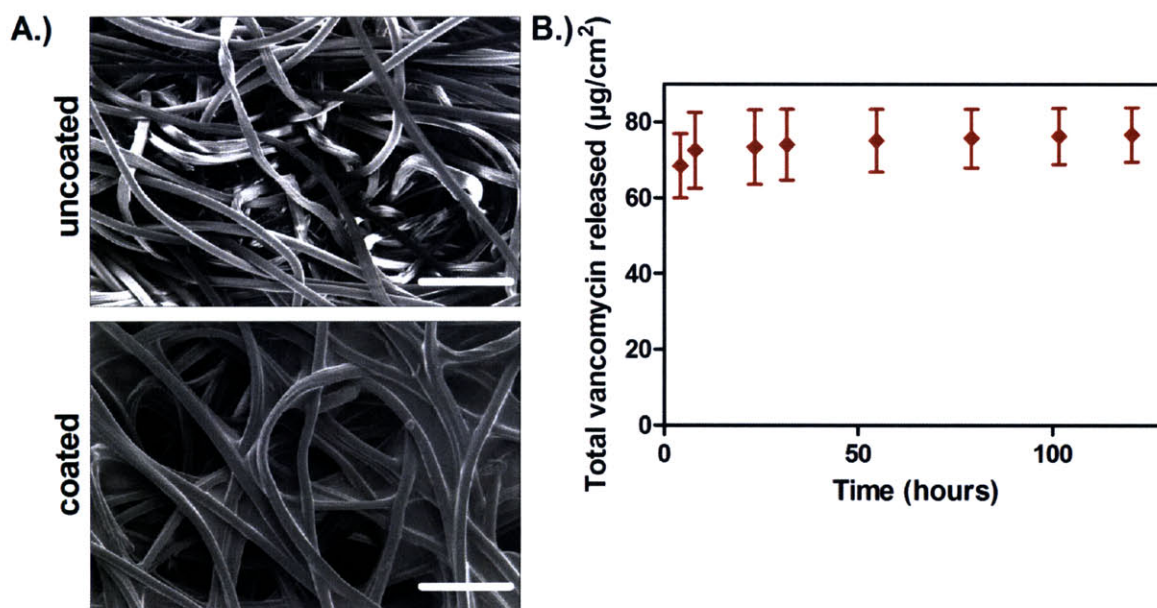
Figure 3-8: Spray coating of a commercial bandage with film architecture (poly 2/alginate/vancomycin/ alginate)$_{60}$. A,) Aerial view scanning electron microscope images of an uncoated and coated bandage (scale bar = 100 μm). B.) Total vancomycin release from spray coated bandage.

3.3.5 Film Efficacy

To further examine practical applicability of films, the effect of both sprayed and dipped films on *S. aureus* growth was explored. *S. aureus* in particular was examined due to its common occurrence in hospital acquired infections. Additionally, vancomycin is active against *S. aureus* and resistant *S. aureus* strains [65]. The effect of a coated bandage along with drug released from a dipped dextran sulfate film on *S. aureus* was investigated. For the bandage, a piece of (poly 2/alginate/vancomycin/alginate)$_{60}$ coated bandage was applied to an agar plate coated with *S. aureus*. Figure 3-9A shows the results of this assay. A positive control of a commercially available vancomycin loaded disc (30 μg) and a negative control of an LPEI soaked bandage were also tested, as seen in Figure 3-9A. There is a clear zone of inhibition surrounding both the vancomycin positive control and the alginate film coated bandage as compared to no zone surrounding the negative control. The coated bandage inhibitory zone

diameter is comparable to the 1.8 cm zone diameter of the positive control. Film eluent from dipped 60 tetralayer dextran sulfate films were also applied to *S. aureus* suspensions in a liquid growth inhibition assay. Figure 3-9B shows the response of the bacteria to dilutions of the eluent from the first 10 hours of film release as well as the response to the drug released in the remaining time. For both of the eluent samples, the MIC of the released vancomycin was found to lie between 0.5 to 2 µg/mL. Controls of non-film incorporated vancomycin were also examined (data not shown) which as expected from reported MIC values of native vancomycin against *S. aureus* was found to lie between 0.5 to 2 µg/mL [87]. The similarity of the MIC values of film released vancomycin and native vancomycin confirm that the film assembly and release process do not affect vancomycin activity against its bacterial target.
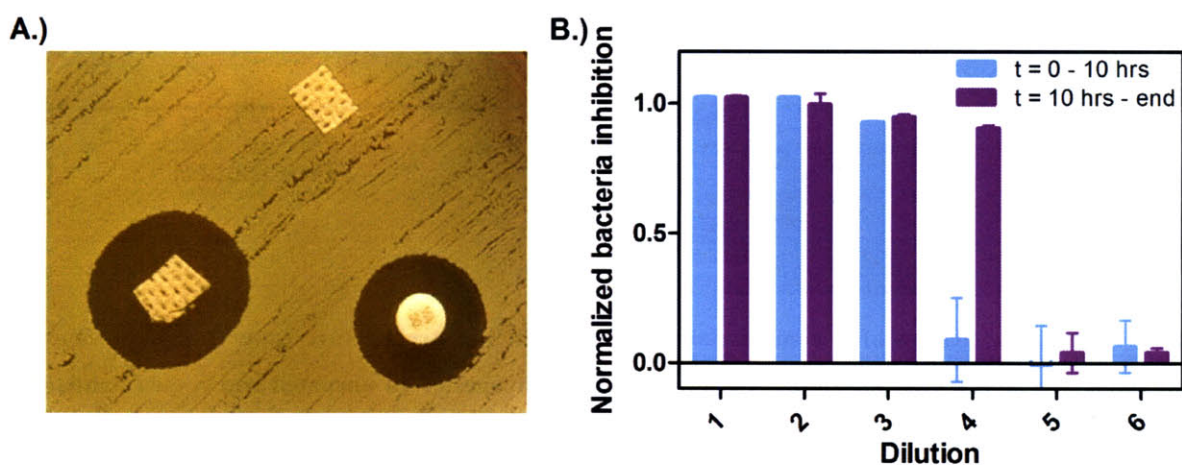
Figure 3-9: *Staphylococcus aureus* **growth inhibition.** **A.)** *S. aureus* **growth inhibition by (poly 2/alginate/vancomycin/alginate)$_{60}$ coated bandage. Zone of inhibition surrounding coated bandage and circular 30 µg vancomycin disc control (diameter of control zone = 1.8 cm); no inhibitory zone surrounding uncoated bandage. B.)** *S. aureus* **growth inhibition by film released eluent from a dipped (poly 2/dextran sulfate/vancomycin/dextran sulfate)$_{60}$ film. For release from 0 – 10 hours, dilution 1 contains 7 µg/mL of vancomycin and subsequent dilutions correspond to 50% reduction in concentration of the previous dilution. For the remaining release, dilution 1 contains 16 µg/mL vancomycin and subsequent dilutions correspond to 50% reduction in concentration of the previous dilution.**

It was necessary to ensure that film eluent was nontoxic to healthy mammalian cells. Therefore, the response of NIH 3T3 embryonic murine fibroblasts (a representative wound healing cell line) upon exposure to culture media samples in which vancomycin films were eluted was examined. Additionally, vancomycin and all polyanions utilized in film architectures were also dissolved in culture media and incubated with cells in their native non-film released

form. Poly(β-amino esters) have previously been shown to have no effect on NIH 3T3 fibroblast viability [61]; the effect of poly 2 on these cells was therefore not directly examined here. Figure 3-10A shows the normalized viability of cells exposed to film release media for both dipped and sprayed films. Cell viability is not affected by the film release media as compared to untreated cell controls. Figure 3-10B shows cell viability in response to non-film incorporated components, which also do not affect cell viability. Therefore, it was concluded that film released media is non-toxic to healthy mammalian cells, while maintaining complete efficacy against *S. aureus*.
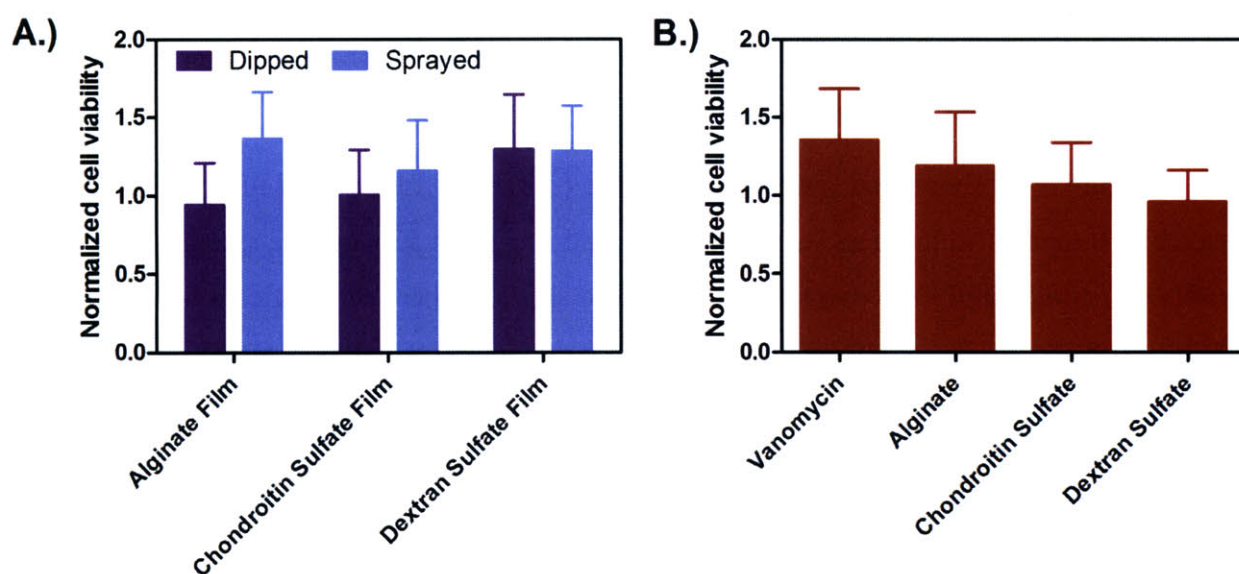
Figure 3-10: Normalized cell viability for vancomycin films. A.) Viability of cells in response to film release media for all film architectures. B.) Viability of cells in response to non-film incorporated drug and polyanions.

3.3.6 *Vancomycin Storage Stability in LbL Films for On-Demand Care*

To examine the practical use of this LbL vancomycin coating technology, the effects of long term storage on the drug release kinetics as well as bacteria growth inhibition characteristics must be assessed. This is especially critical as vancomycin is known to undergo degradation via asparagine deamidation [126]. Vancomycin is typically administered via intravenous injection of water, 5% dextrose, or 0.9% sodium chloride solutions [127]. One particular study found that vancomycin in these intravenous formulations stored in ready to administer syringes lost activity when stored at 25 °C over 29 to 55 days depending on the solution composition and syringe used

when compared to 4 °C where activity was maintained over at least 84 days [128]. Other studies have shown that vancomycin in aqueous dextrose solutions stored at 37 °C suffered increasing degradation starting at only 7 days of storage [129]. It is apparent that ready-to-use formulations of vancomycin cannot be easily stored for long periods of time in environments were refrigeration may not be available but rapid use of the drug is desirable. Here, we examined the storage stability of vancomycin containing LbL films spanning a range of conditions in which they may commonly be stored, transported, and/or used, namely standard refrigerator temperature (4 °C), room temperature (25 °C), and an elevated temperature (37 °C) representing harsher climates which are commonly encountered in emergency medicine [130]. As a representative film we chose to examine properties of dipped (poly 2/dextran sulfate/vancomycin/dextran sulfate)$_{60}$ films only.

Figure 3-11 shows the vancomycin release profiles of films released immediately upon assembly (0 months storage) and after 3 and 6 months of room temperature storage. The release profile of a film stored for 6 months at 4 °C is also shown. There is significant overlap in these release profiles and seemingly no effect on release due to storage at both refrigerator and room temperature over a minimum of 6 months. Following the first 4 hours, there is a linear release of vancomycin for 40 hours, with release lasting up to approximately 55 hours for all of the films tested. A slight variation in final drug release quantity (equal to the total drug loading) in each stored film is an artifact of the film assembly process.
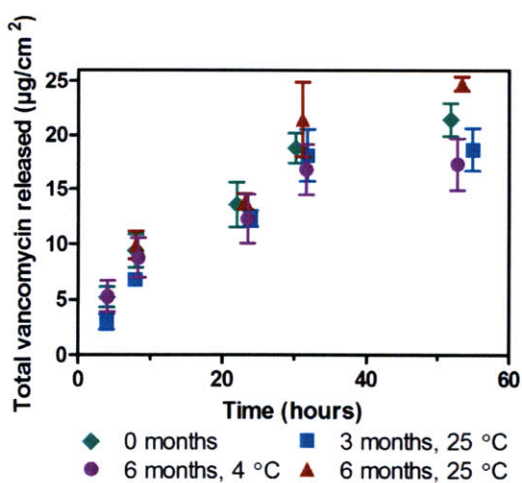
Figure 3-11: Vancomycin release profiles upon storage. Profiles shown here correspond to storage for 0 months, 3 months at 25 °C, 6 months at 25 °C, and 6 months at 4 °C.

The MIC of vancomycin against *S. aureus* released from films stored at room temperature over 6 months was also assessed to ensure that vancomycin activity was maintained. Figure 3-12 shows the normalized *S. aureus* density upon exposure to film-released solution at 0, 3, and 6 months of room temperature storage. As seen in Figure 3-12, all tested film samples maintained MIC values between 0.5 to 2 µg/mL, as expected for non-film released vancomycin against *S. aureus*. Overall, the drug release profiles and vancomycin activity remain unaltered over at least 6 months of room temperature storage. These films maintain stability at temperature conditions and timescales well beyond what is possible for ready-to-use intravenous solutions of vancomycin.
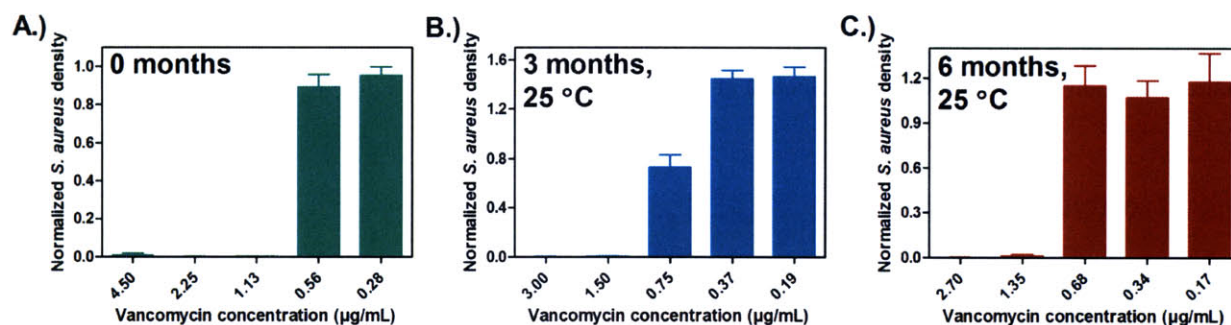
Figure 3-12: Normalized *S. aureus* density upon exposure to vancomycin film release solution. Films stored for A.) 0 months, B.) 3 months at 25 °C, and C.) 6 months at 25 °C.

In many situations, temperature control in the 4 to 25 °C range may not be possible, especially in harsh climates where military personnel may operate. To simulate such conditions, we stored vancomycin LbL films at elevated temperatures of 37 °C for up to 1 month (conditions in which aqueous formulations of vancomycin are known to degrade rapidly). Fig. 3-13A shows vancomycin release profiles for films stored for 0 and 1 month at 37 °C, demonstrating that both films have the same release kinetics and drug loading. Additionally, Fig. 3-13B shows normalized *S. aureus* density upon exposure to film-released vancomycin from films stored for 1 month at 37 °C. Similar to the samples stored at room temperature, no loss in vancomycin activity is detected, and the MIC against *S. aureus* is completely maintained.
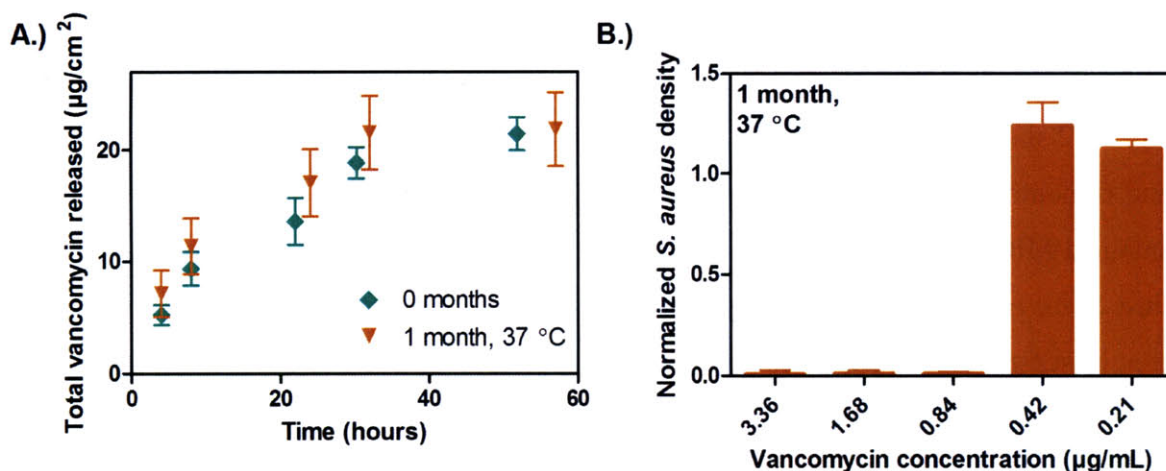
Figure 3-13: Vancomycin film behavior after 1 month storage at 37 °C. A.) Vancomycin release profiles of films stored for 0 and 1 month at 37 °C. B.) Normalized *S. aureus* density upon exposure to vancomycin film release solution for films stored for 1 month at 37 °C.

3.4 Conclusions

In this work, we have developed drug release coatings for the delivery of a potent antibiotic, vancomycin. The versatile LbL assembly technique was utilized to engineer sprayed and dipped coatings to achieve a variety of drug release profiles. Secondary-interactions between film components were found to play a critical role in the assembly of these films and provide control over drug density and release profile. Formation of these interactions was sustained in film architectures experiencing significant interdiffusion. The drug loadings and release profiles attained in this work were highly therapeutic and able to address a variety of infection needs. Film released vancomycin maintained complete activity against *S. aureus* for the duration of film release. Films were benign to healthy mammalian wound healing fibroblasts. A representative film architecture was tested for long term storage stability of the encapsulated vancomycin and found to be highly stable. In fact, these vancomycin films are significantly more stable than the commonly used intravenous solutions of vancomycin stored in similar conditions. These drug release coatings are an important advance in preventing the spread of drug resistant bacteria while maintaining efficacy of current therapeutics. Moreover, this film technology provides a new therapeutic option for infection treatment in environments where rapid care is desired but refrigeration of ready-to-use intravenous formulations of vancomycin is not possible. Most significantly, this work provides insight on how to control the

direct incorporation and release of small weakly charged agents from multilayer assemblies; by focusing on promoting favorable interactions between film components, films with high drug densities and controlled release profiles can be attained.

Chapter 4

Design of Multi-Drug Release Coatings Targeting Infection and Inflammation

4.1 Introduction

Infection and inflammation are debilitating medical conditions that commonly coexist [131]. The treatment requirements for each of these co-morbidities can vary significantly. A bolus antibiotic administration may be required to immediately eradicate infection versus a prolonged preventative treatment. In the case of inflammation, short term pain management or long term inflammation mitigation may be needed. There are severe consequences to antibiotic or non-steroidal anti-inflammatory drug (NSAID) administration at inappropriate or excessive concentrations, including the development of antibiotic resistant bacteria [6, 8, 65], gastrointestinal ulcers [132], congestive heart failure [133, 134], and interference with normal wound healing processes. Controlled local delivery of therapeutics, rather than systemic delivery, can help prevent undesirable outcomes of infection and inflammation treatment. Currently, there are no effective modalities for controlled local co-delivery of both antibiotics and NSAIDs. In this work, we have shown how to design polymer multilayer coatings that simultaneously target infection and inflammation.

Layer-by-layer (LbL) assembly of polymer films is a versatile technique that has shown great promise in drug delivery [31, 34, 44, 45, 55, 62]. LbL films are assembled by the repetitive direct adsorption of components with complementary functionality [22]. Therapeutics can be incorporated into these multilayer assemblies either directly [14] or within a carrier [58, 135, 136]. Vancomycin is a glycopeptide antibiotic that is highly effective in treating drug resistant forms of Gram-positive bacteria, such as methicillin-resistant *Staphylococcus aureus* (*S. aureus*). We have previously created tunable vancomycin releasing films as described in Chapter 3 using both dip and spray LbL assembly by incorporating vancomycin directly via its net positive charge into a tetralayer architecture utilizing hydrolytically degradable cationic poly(β-amino esters) (PBAEs) in alternation with biocompatible polyanions, including alginate, chondroitin

sulfate, and dextran sulfate [61, 86, 106]. This work highlighted the power of using the LbL spray assembly technique, in particular, to increase drug loading and control interdiffusion, a key factor promoting interactions between film components. Films were engineered to exhibit release profiles ranging from 4 hours to 2.5 days with maximum drug loadings of approximately 20 weight percent [14]. This is a significant drug loading for vancomycin delivery devices, which typically are limited to containing just a few weight percent of the drug in order to preserve the structure of the delivery system. Hydrolytically degradable LbL films have also been designed for the delivery of hydrophobic small molecules, including NSAIDs such as diclofenac. These films were constructed by alternating deposition of PBAEs and diclofenac encapsulated in an anionic polymer carrier, poly(carboxymethyl-β-cyclodextrin) (polyCD), to release therapeutic drug concentrations over a sustained period of approximately 17 days via a controlled surface erosion based release [58, 136]. These films showed efficacy against production of prostaglandins by A549 human lung carcinoma cells by inhibiting cyclooxygenase (COX) activity over the duration of drug release.

Herein, we demonstrate the concurrent release of two small molecule therapeutics, vancomycin and diclofenac, from degradable polymer multilayer films, to combat both infection and inflammation. The construction of a dual release film is complicated by the fact that each new component introduced into the film can significantly impact film stability, drug loading, and drug release rate. Additionally, the release of macromolecular species from LbL films is well understood and characterized [34, 62], while we are still trying to gain control and understanding over the incorporation of small molecule therapeutics into these films. For example, here we discover that for small molecule films, there can be stark differences in drug loading and release behavior when films are dipped versus sprayed. In this work, we show that a thorough understanding of the relevant interactions between therapeutic agents and drug carriers and the effects of these interactions on film assembly can be used to appropriately take advantage of previously developed single-therapeutic films and predict *a priori* the behavior of composite films, in which either the antibiotic or NSAID film is deposited first, followed by the film containing the complementary therapeutic as shown in Figure 4-1. The findings of this study provide significant insight on the specific considerations needed to design and optimize multi-drug releasing systems relevant to a variety of conditions, ranging from common hospital procedures to battlefield trauma.

A.) Single-therapeutic film architectures

Antibiotic film | NSAID film

B.) Composite film architectures

Antibiotic + NSAID film | NSAID + Antibiotic film
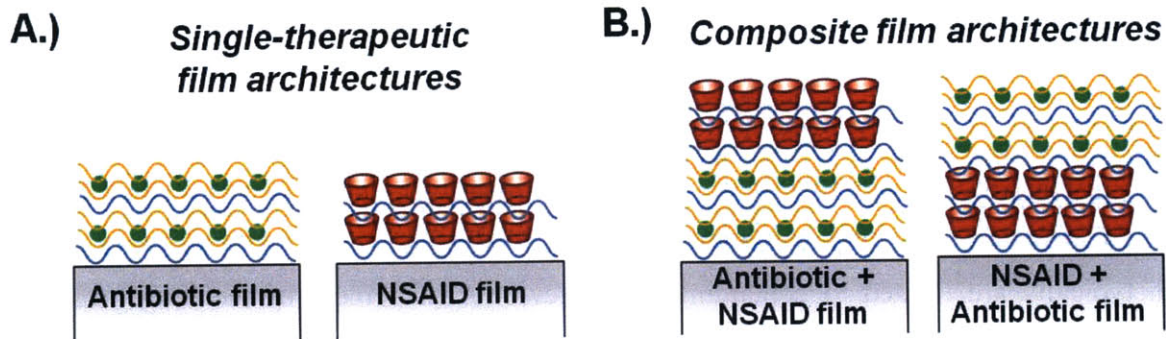
Figure 4-1: Layer-by-layer film architectures. A.) Antibiotic-only and NSAID-only LbL film architectures. B.) Composite antibiotic and NSAID LbL film architectures. Note: orange = polyanion, blue = poly(β-amino ester), green = vancomycin, red = diclofenac encapsulated within poly(carboxymethyl-β-cyclodextrin).

4.2 Materials and Methods

4.2.1 Materials

Poly 2 was synthesized as previously described [61, 86, 106]. Vancomycin, alginate (M_n = 120 – 190 kDa), poly(sodium 4-styrene-sulfonate) (SPS, M_n = 70 kDa), and sodium acetate buffer (3 M) were purchased from Sigma-Aldrich (St. Louis, MO). Diclofenac and polyCD (2.8% substituted) were purchased from TCI America (Portland, OR) and CTD, Inc. (Gainesville, FL), respectively. Chondroitin sulfate sodium salt (M_n = 85 kDa) was purchased from TCI International (Tokyo, Japan). Dextran sulfate sodium salt (M_n = 500 kDa) and linear polyethyleneimine (LPEI, M_n = 25 kDa) were purchased from Polysciences (Warrington, PA). Silicon and glass substrates were obtained from Silicon Quest International (Santa Clara, CA) and VWR Scientific (Edison, NJ), respectively. Intraocular lenses were generously donated by Aurolab (Aravind Eye Care System, Madurai, India). Vicryl sutures and latex-free absorbent sterile pad bandages were obtained from the Department of Comparative Medicine (Massachusetts Institute of Technology) and RiteAid Pharmacy (Harrisburg, PA), respectively. Dulbecco's phosphate buffered saline (PBS, 0.1 M) was purchased from Invitrogen (Carlsbad, CA). Deionized water (18.2 MΩ, Milli-Q Ultrapure Water System, Millipore) was utilized in all experiments. *S. aureus* 25923 was obtained from ATCC (Manassas, VA). Cation-adjusted Mueller Hinton broth (CaMHB), Bacto agar, and vancomycin susceptibility test discs were obtained from BD Biosciences (San Jose, CA). Cyclooxygenase fluorescence inhibitor screening assay kit was purchased from Cayman Chemical (Charlotte, NC).

4.2.2 Film Assembly

Prior to assembly, substrates (approximately 1 cm^2) were cleaned, plasma etched, and coated with (LPEI/SPS)$_{10}$ base layers as previously described [14]. Composite films containing both diclofenac and vancomycin were created by combining single-therapeutic film architectures whose assembly has been previously described in Chapter 3 [14, 58, 136]. Briefly, antibiotic-only films were built with a tetralayer architecture, denoted: (poly 2/polyanion/vancomycin/polyanion)$_{60}$, where the polyanion was alginate, chondroitin sulfate, or dextran sulfate and sixty represents the number of tetralayers deposited. All deposition solutions for the antibiotic films were formulated at 2 mg/mL in 0.1 M sodium acetate buffer (pH 5). In dipped LbL films, poly 2 and vancomycin were deposited for 10 minutes, and the polyanions for 7.5 minutes, with 10, 20, and 30 second rinses following each step. For alginate and chondroitin sulfate films, deionized water (pH 5) was used for the rinse steps, and for dextran sulfate films, 0.1 M sodium acetate buffer (pH 5) was used. NSAID-only films were built with bilayer architecture, (poly 2/polyCD-diclofenac)$_{20}$. NSAID film poly 2 deposition solution was formulated at 2 mg/mL in 0.1 M sodium acetate buffer (pH 6), while polyCD-diclofenac solution was prepared at 20 mg/mL polyCD and 1.4 mg/mL diclofenac in 0.1 M sodium acetate buffer (pH 6). In short, dipped NSAID film deposition steps lasted 10 minutes, followed by 10, 20, and 30 second rinses in deionized water (pH 6).

Spray LbL films were created using a programmable spray apparatus (Svaya Nanotechnologies) as previously described in Chapter 3 [14]. All drug and polyelectrolyte spray deposition steps were 2 seconds, while a single 3 second rinse step was used following each deposition with a flow rate of 0.25 mL/s. All solution formulations used for spray LbL were the same as those used in dipping.

For composite dipped and sprayed films, the NSAID film was either layered directly on a preformed antibiotic film or the NSAID film coated substrate was used for subsequent deposition of antibiotic films. Composite films were also created on intraocular lenses (using dipped LbL), sutures, and bandages (using spray LbL and applying a 50 psi vacuum to the back of the substrate). These materials were pre-treated in the same way as the silicon and glass substrates prior to film assembly.

For all optimal film architectures constructed in this study, film thickness on glass or silicon substrates was monitored using either a spectroscopic ellipsometer (J.A. Woollam Co.,

Inc. M-2000D) or a surface profilometer (KLA Tencor P-16). For profilometer measurements, films were scored with a razor, tracked over a 700 μm length, and average film thickness was obtained. Device coatings were also examined using a scanning electron microscope (JEOL JSM-6060).

4.2.3 Drug Release

Films were dried under nitrogen after assembly and released in 500 μL of 0.01 M PBS at 37 °C. At predetermined time points films were removed and added to fresh PBS aliquots. Vancomycin and diclofenac presence in each of the release samples was quantified with high performance liquid chromatography (Agilent Technologies HPLC, 1100 series) using a C18 reverse phase column (Supelco) equipped with a fluorescence detector. An excitation wavelength of 280 nm and emission wavelength of 355 nm was utilized. Vancomycin fluorescence was monitored with a 70/30 0.01 M PBS/methanol mobile phase, while diclofenac fluorescence was monitored with a 70/30 0.01 M PBS/acetonitrile mobile phase. A flow rate of 1 mL/min and injection volume of 500 μL and 100 μL was used for vancomycin and diclofenac, respectively.

4.2.4 Studying Film Component Interactions

Molecular interactions between film components were examined chromatographically. Interactions between polyCD and vancomycin were studied by dissolving vancomycin at a concentration of 41 μM in polyCD (0, 2, 4, 8, and 16 mM) at pH 5 and 6 in sodium acetate buffer (0.1 M) and sodium chloride (1 M) and examining vancomycin fluorescence with HPLC as described under *Drug Release*. Interactions between diclofenac and vancomycin were studied by suspending excess diclofenac (34 mM) in vancomycin solutions (1.3 mM, 0.65 mM, and 1.3 μM) in the same four solution conditions and exploring diclofenac solubility (proportional to diclofenac fluorescence) via HPLC after filtering these solutions through 0.2 μm filters.

To quantify diffusion and exchange capabilities of single-therapeutic films, the NSAID-only or antibiotic-only film architectures were introduced to film deposition and wash solutions (described under *Film Assembly*) for the complementary film for 10 minutes (the maximum deposition time). Following this, each film was rinsed briefly in deionized water to remove non-specifically bound material. It was chromatographically determined how much of the deposition component diffused into the film (by taking these films after treatment and allowing them to

80

release completely in 0.01 M PBS solution and examining these with HPLC) as well as how much of the film therapeutic was displaced in this process (by examining the test solutions with HPLC). A representative antibiotic film architecture containing chondroitin sulfate was used in all of these experiments. A twenty bilayer film assembled analogous to the NSAID-only film but containing no diclofenac, denoted (PolyCD$_{20}$), was also included in these studies.

4.2.5 Measuring Drug Activity

Vancomycin activity was assessed using both a modified Kirby-Bauer and microdilution assay. For these assays, *S. aureus* 25923 in its exponential growth phase was utilized. In the Kirby-Bauer assay, *S. aureus* at 10^8 CFU/mL concentration was applied evenly to an agar plate. Film coated bandages, an uncoated control, and a 30 µg vancomycin susceptibility disc were each applied to the coated agar and incubated for 16-18 hours at 37 °C, after which the zone of inhibition surrounding the test materials was examined. In the microdilution assay, film released solutions and controls of 0.01 M PBS were serial diluted in CaMHB in a 96 well clear bottom plate. *S. aureus* was added to each of the film release dilutions and positive controls at a final concentration of 10^5 CFU/mL, with no bacteria added to the negative controls. After 16-18 hours of incubation with shaking at 37 °C, the optical density of each well at 600 nm (proportional to bacteria concentration) was read on a BioTek PowerWave XS plate reader. Normalized bacteria density was calculated as previously reported in Chapter 3 [14].

To quantify diclofenac activity, a COX inhibition assay was utilized. When uninhibited, COX leads to the production of hydroperoxy endoperoxide (PGG2) from arachadonic acid. PGG2 reacts with 10-acetyl-3,7-dihydroxyphenoxazine (ADHP) to produce fluorescent resorufin. Resorufin fluorescence upon exposure to film release solution and controls of polyCD, polyCD-diclofenac, and vancomycin solution, was quantified.

4.2.6 Statistical Analysis

All experiments conducted in this work were done in triplicate at minimum. Data is reported as mean ± standard deviation. All thickness measurements were taken at a minimum of three locations per sample.

4.3 Results and Discussion

4.3.1 Film Component Interactions

Having previously developed optimal antibiotic [14] and NSAID [58] LbL assembled films, we sought to combine these film architectures to formulate dual drug-release films as shown in Figure 4-1. However, this process introduces many complexities, including the large parameter space for combining single-therapeutic films (i.e. choice of LbL assembly technique – dip or spray, film architecture – polyanion choice, etc.), which influences potential film component interactions that ultimately affect drug loading and release characteristics. To predict composite LbL film behavior *a priori* and reduce the complexity of film assembly, the potential for solution based interactions of film components was investigated by examining mixtures of varying film components using liquid chromatography coupled with fluorescence detection. In this study, changes in fluorescence intensity of vancomycin and diclofenac in these mixtures compared to pure drug solutions indicated the formation of complexes between interacting species. Interactions between film components were probed at four different conditions, 0.1 M sodium acetate buffer and 1 M sodium chloride at pH 5 and 6. The 0.1 M pH 5 and 6 solvents represent the previously determined optimal deposition conditions for the vancomycin and diclofenac films, respectively [14, 58, 136]. Two critical interactions were discovered to exist, namely the interaction of polyCD with vancomycin and the interaction of vancomycin with diclofenac.

Figure 4-2A shows vancomycin fluorescence for a constant vancomycin concentration (34.5 μM) dissolved in varying polyCD concentrations at each solvent condition tested normalized by its fluorescence in pure vancomycin solution (absent any polyCD). Normalized vancomycin fluorescence increased with increasing polyCD concentrations only in the pH 5 (0.1 M) solvent, an indication of an interaction occurring between vancomycin and polyCD at these conditions [112]. At pH 5, vancomycin has a net positive charge of 1 [107], and the cationic vancomycin can interact electrostatically with the anionic polyCD. At pH 6, vancomycin charge is greatly reduced with its isoelectric point near neutral pH [113, 114], and therefore, this interaction is not promoted at these conditions. Further evidence that this interaction is primarily electrostatic was obtained from results of solutions formulated at the higher ionic strength of 1 M (pH 5). At these conditions, charge screening inhibits the electrostatic polyCD-vancomycin

interaction and these solutions no longer show increased normalized vancomycin fluorescence in the presence of polyCD.

Next, we examined mixtures of diclofenac and vancomycin. The hydrophobic diclofenac was suspended in excess in the same four solvent conditions described earlier containing three separate vancomycin concentrations (1.3 μM, 0.65 mM, and 1.3 mM). Note that the 1.3 mM vancomycin concentration represents the concentration of vancomycin used in antibiotic-only film construction [14]. These solutions were filtered to remove non-soluble diclofenac and normalized diclofenac fluorescence was determined by comparing diclofenac fluorescence in these filtered solutions to those of pure filtered diclofenac (absent any vancomycin). The results of this interaction study are summarized in Figure 4-2B. At pH 5 in 0.1 M buffer, increasing vancomycin concentration led to increased diclofenac solubilization (directly proportional to diclofenac fluorescence). This effect was nonlinear with no increase in diclofenac solubilization at the lowest vancomycin concentration tested, and an approximate 14 times increase in diclofenac solubility at the highest vancomycin concentration equal to that used in antibiotic-only film assembly. This interaction does not occur at pH 6 conditions (due to reduced vancomycin charge) and at high salt concentration (due to charge screening) suggesting that like the interaction of polyCD and vancomycin, the interaction of diclofenac and vancomycin is primarily electrostatic between the positively charged vancomycin (at pH 5) and the negative charge of the diclofenac carboxyl group.
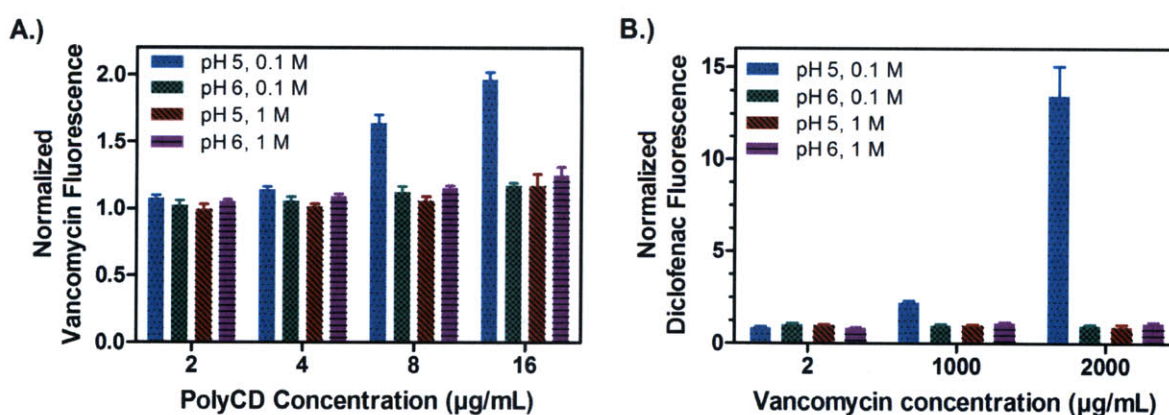
Figure 4-2: Solution based film component interactions. A.) Vancomycin-polyCD interaction. B.) Vancomycin-diclofenac interaction. All interactions were studied at four conditions: 0.1 M sodium acetate buffer and 1 M NaCl, pH 5 and 6.

Based on the discovery of these two interactions, namely the interaction of polyCD and vancomycin as well as the interaction of diclofenac and vancomycin, one can anticipate the behavior of composite films in which the antibiotic component would be deposited upon a preformed NSAID film. We predicted that these films would experience increased vancomycin loading compared to antibiotic-only films, due to electrostatic attraction between polyCD and vancomycin. Additionally, submerging an NSAID film into the vancomycin deposition solution should lead to diclofenac stripping from the existing NSAID film, due to electrostatic attraction of vancomycin and diclofenac.

To translate these solution-based observations to films, a series of experiments was conducted to quantify the ability of components to diffuse into and out of single-therapeutic films upon exposure to LbL assembly deposition and wash conditions for the complementary drug containing film. The observed phenomena is related to commonly observed diffusion and exchange behavior in LbL films and found to be strongly dependent on charge density, molecular weight, and ionic strength of the species involved [51, 52, 87]. A schematic of these studies is shown in Figure 4-3, while the results of this study are summarized in Table 4-1. As expected based on the solution interaction studies, NSAID films incorporated large amounts of vancomycin. Additionally, films assembled with polyCD containing no NSAID incorporated larger amounts of vancomycin than those films in which diclofenac was encapsulated in the polyCD, suggesting that the interaction of polyCD and vancomycin is more likely to occur when there is nothing populating the hydrophobic core of the cyclodextrins. Although vancomycin is too large and hydrophilic to completely fit within the polyCD core, the hydrophobic phenolic groups of vancomycin may partially associate with empty cores. An unexpected finding was adsorption of significant diclofenac quantities (approximately 6 times the final loading of an NSAID film) into antibiotic films at the pH 6 deposition conditions of polyCD-diclofenac. This interaction at pH 6 was not visible in solution, although a strong interaction of polyCD and vancomycin as well as diclofenac and vancomycin was observed at pH 5. At pH 6, vancomycin is slightly charged [107, 113, 114]; due to the localized concentration of vancomycin in the antibiotic film versus a dilute solution, it is likely that interactions observed strongly at pH 5 in solution are also visible at pH 6 in the case of the film. Based on these findings, we predicted that films in which the NSAID component is deposited on the antibiotic film would experience increased diclofenac loading.
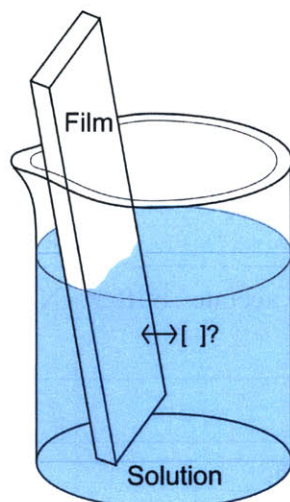
Figure 4-3: Study of diffusion and exchange behavior in single-therapeutic films.

Each single-therapeutic film was stable in its own wash condition. However, at the pH 6 NSAID film wash conditions, 11 ± 3 µg of vancomycin was lost in the duration of a single deposition step; 64% less vancomycin was lost in the polyCD-diclofenac solution at pH 6. It could be expected that the antibiotic film would be severely destabilized at the pH 6 conditions necessary for NSAID film construction. The level of destabilization should be strongly dependent on the initial stability of the antibiotic-only film, which is heavily dependent on the polyanion choice and deposition technique (spray versus dip LbL) which was demonstrated in Chapter 3 [14]. NSAID films were found to be stable at the pH 5 wash conditions of the antibiotic film, retaining all diclofenac. However, as expected from solution interaction studies, in the presence of vancomycin, diclofenac was stripped from these films at significant amounts (comparable to the total loading of an NSAID film). These findings strongly indicated that deposition of antibiotic films upon preformed NSAID films may lead to severely depleted diclofenac loadings and increased vancomycin loadings in these films. The solution based interaction studies appropriately predicted the behavior of single-therapeutic films, while the single-therapeutic film studies helped formulate further predictions on the behavior of composite films.

Film	Deposition/ wash solution	Vancomycin (µg)		Diclofenac (µg)	
		In	Out	In	Out
(NSAID film)$_{20}$	Vancomycin	5 ± 3	NA	NA	4 ± 1
	0.1 M sodium acetate buffer (pH 5)	NA			0
(PolyCD film)$_{20}$	Vancomycin	13 ± 6	NA	NA	NA
(Antibiotic film)$_{60}$	PolyCD-diclofenac	NA	4 ±1	28 ± 10	NA
	PolyCD		8 ±1	NA	
	0.1 M sodium acetate buffer (pH 6)		11 ±3		

[a]NA = not applicable.

4.3.2 Film Assembly and Drug Release Characteristics

Following extensive interaction studies, we designed composite films using both dip and spray assembly to test our findings and create several optimal multi-drug release film architectures. Table 4-2 summarizes the relevant drug loading and release characteristics of these composite films as well as single-therapeutic films (corresponding co-release profiles are either exhibited in Figure 4-4 or in Figure 4-7). In films where the NSAID component was deposited first followed by the antibiotic component, there was increased vancomycin loading as compared to antibiotic-only films. The difference in loading (approximately 1.2 to 1.5 times) is not strongly dependent on the polyanion used in the antibiotic film tetralayer. The spray assembled composite architecture incorporated approximately 1.7 times more vancomycin than a sprayed antibiotic-only film. In addition, diclofenac had been completely stripped from these films. These findings for the composite architecture formulated from an antibiotic film deposited upon an existing NSAID film were all in agreement with the pre-construction interaction studies.
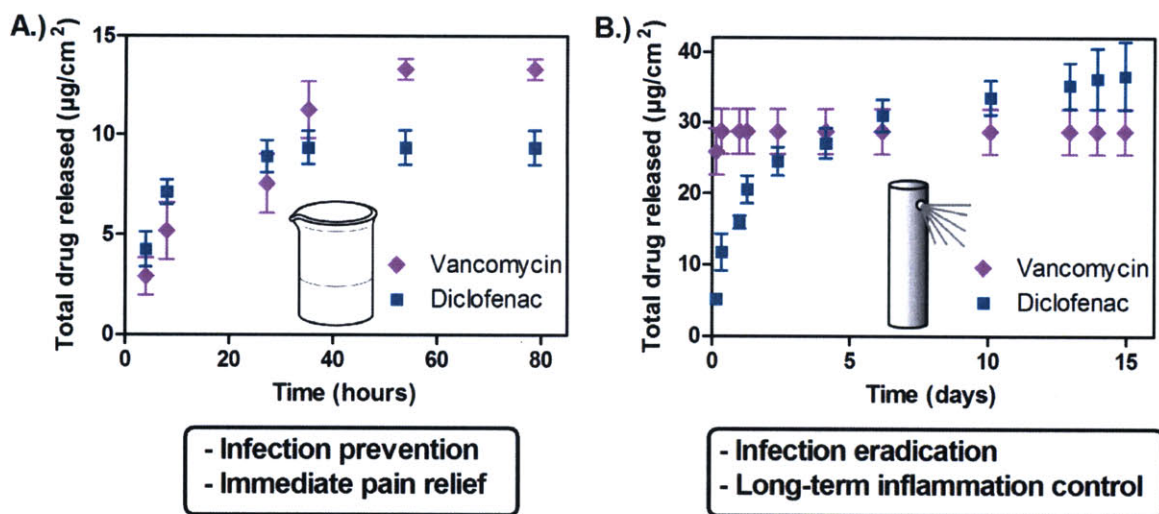
Figure 4-4: Composite film drug release profiles. A.) Drug release from dipped LbL film: (poly 2/dextran sulfate/vancomycin/dextran sulfate)$_{60}$ + (poly 2/polyCD-diclofenac)$_{20}$. B.) Drug release from sprayed LbL film: (poly 2/chondroitin sulfate/vancomycin/chondroitin sulfate)$_{60}$ + (poly 2/polyCD-diclofenac)$_{20}$.

It was clear that it would be necessary to deposit NSAID films on top of preformed antibiotic films to ensure retention of diclofenac in composite films. However, in the case of alginate and chondroitin sulfate dipped films with this architecture, there was little vancomycin retained after NSAID deposition (as predicted by the pH 6 destabilization of vancomycin films). Figure 4-4A shows the release profile of the NSAID film built on the more stable dextran sulfate containing vancomycin architecture. This composite film was found to have a thickness of 4.36 ± 0.28 μm, greater than a dextran sulfate dipped antibiotic-only film (thickness of 3.14 ± 0.24 μm [14]). The increased affinity for polyCD-diclofenac in the pre-deposited antibiotic film is expected to lead to interdiffusion and higher loading of polyCD-diclofenac, thereby increasing film thickness (note that dipped NSAID-only films have a thickness of approximately 20 nm). There was an approximate 38% reduction in the incorporated vancomycin in these films during NSAID film deposition. However, the remaining 13.3 ± 0.5 μg/cm^2 of vancomycin in this film remains highly therapeutic, able to meet and exceed the minimum inhibitory concentration of vancomycin against *S. aureus* (0.5-2 μg/mL) [87]. Additionally, the timescale of vancomycin release from this film architecture was comparable to the antibiotic-only film, approximately 2.3 days, with a linear release profile following the first 4 hours ($R^2 = 0.95$). This architecture also incorporated approximately 1.9 times more diclofenac than an NSAID-only film (9.4 ± 0.9 μg/cm^2 versus 5.0 ± 1.0 μg/cm^2), also predicted by the interaction studies; release timescale was

reduced from 20 to 1.7 days, dictated by the underlying antibiotic film architecture. Approximately 50% of diclofenac was released in the first 4 hours. This architecture led to moderate release times for both drugs at therapeutic doses, appropriate for infection prevention and immediate pain management following injury or surgery, avoiding the complications of prolonged therapeutic exposure.

Spray LbL assembly was explored as a method for preventing the pH 6 destabilization of the underlying antibiotic film during assembly of the NSAID film due to the rapid kinetics and short time frame of the spray process. A representative chondroitin sulfate antibiotic-only film was used in these studies. The fast LbL spray process allows for the kinetic trapping of film components and does not allow significant film component interdiffusion for the systems studied here [14]. This composite architecture was found to have a film thickness of 3.00 ± 0.16 μm, compared to 2.54 ± 0.06 μm for a chondroitin sulfate spray antibiotic-only film (note that sprayed NSAID-only films have a thickness of 0.20 ± 0.01 μm). Due to the short spray times of the NSAID architecture upon the antibiotic film, there was indeed no significant decrease in vancomycin loading in composite films compared to antibiotic-only sprayed films. In Chapter 3, spray LbL of antibiotic-only films was shown to lead to short (4 hr) burst release of drug [14], which was also observed here. This composite architecture was found to best address the potential need for immediate bacteria eradication and allow long term inflammation control, as seen in Figure 4-4B. There was an NSAID release time of 13.9 days (twice as long as an NSAID-only film) with 36.2 ± 4.4 μg/cm^2 diclofenac (5 times increased loading compared to an NSAID- only sprayed film) released in a nonlinear manner; 80% of the incorporated drug was released in the first 6 days. It is interesting that there was such a large increase in diclofenac loading during the spray process, which has previously been shown to lack the level of film component interdiffusion that is often visible in dip assembled films [14]. However, the level of interpenetration of layers in the thin NSAID film may be enough to promote polyCD-vancomycin interactions, which are not as visible with thicker films. For all of the composite architectures explored in this work, drug loading characteristics were consistent with the interaction studies completed prior to film assembly.

4.3.3   Therapeutic Potential of Optimal Film Architectures

The therapeutic potential of the optimal dip and spray LbL architectures (whose release profiles are shown in Figure 4-4) was assessed by applying these films to several medical device surfaces, including intraocular lenses (IOLs), bandages, and sutures. Scanning electron microscopy confirmed the successful coating of these devices, as seen in Figure 4-5. The IOL was coated using dip LbL film assembly, while both the bandages and sutures were coated using spray assembly. In the uncoated IOL SEM image in Figure 4-5, we see both the smooth lens region and the haptic. In the coated IOL image, a scratch was intentionally imaged to elucidate the existence of a smooth film on the IOL. Both the bandage and suture images clearly show the existence of film coating after the spray process on the substrates. Coating of these substrates demonstrates the versatility of these composite films in their ability to coat various medical device surfaces.
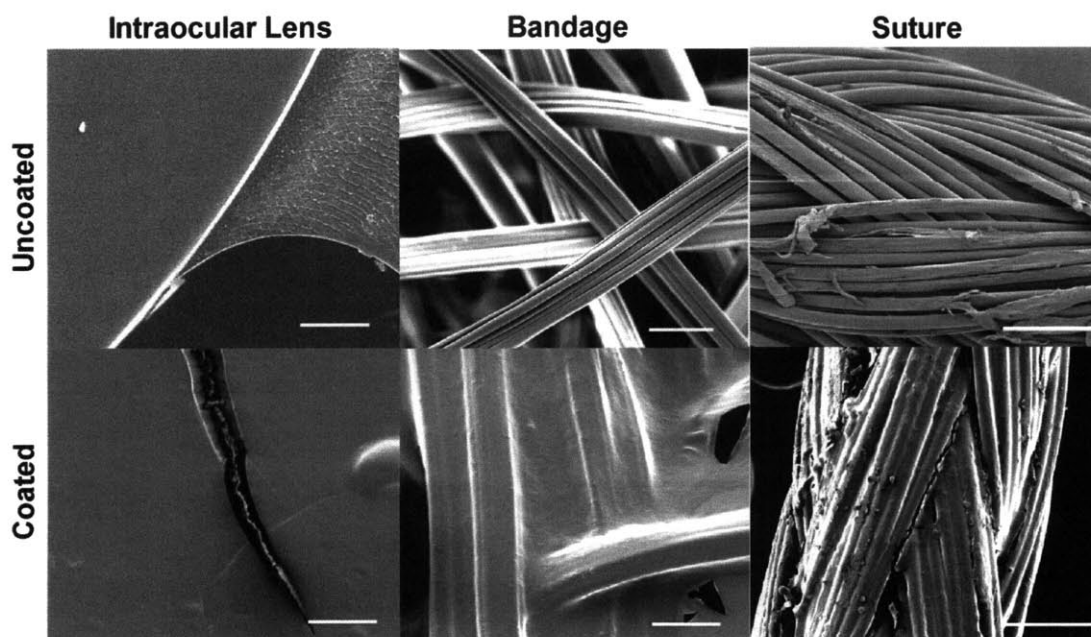
Figure 4-5: Multi-drug release device coatings. Scanning electron microscopy images of coated medical devices (scale bar = 20 μm for IOL and bandage; 100 μm for suture). The uncoated IOL image shows both the lens and haptic regions. The visible crack on the coated IOL is a scratch on the film showing the existence of a smooth film on the lens.

Therapeutic efficacy of bandages spray coated with the LbL film architecture whose release is shown in Figure 4-4B was examined by challenging with specific infectious and

inflammatory targets, namely *S. aureus* and COX. Figure 4-6A shows the COX activity in response to diclofenac released from these coated bandages, along with several negative and positive controls. Film-released diclofenac was highly effective in inhibiting COX activity over the duration of its release. Vancomycin released from this coated bandage was also completely effective in inhibiting *S. aureus* growth *in vitro*, shown in Figure 4-6B.
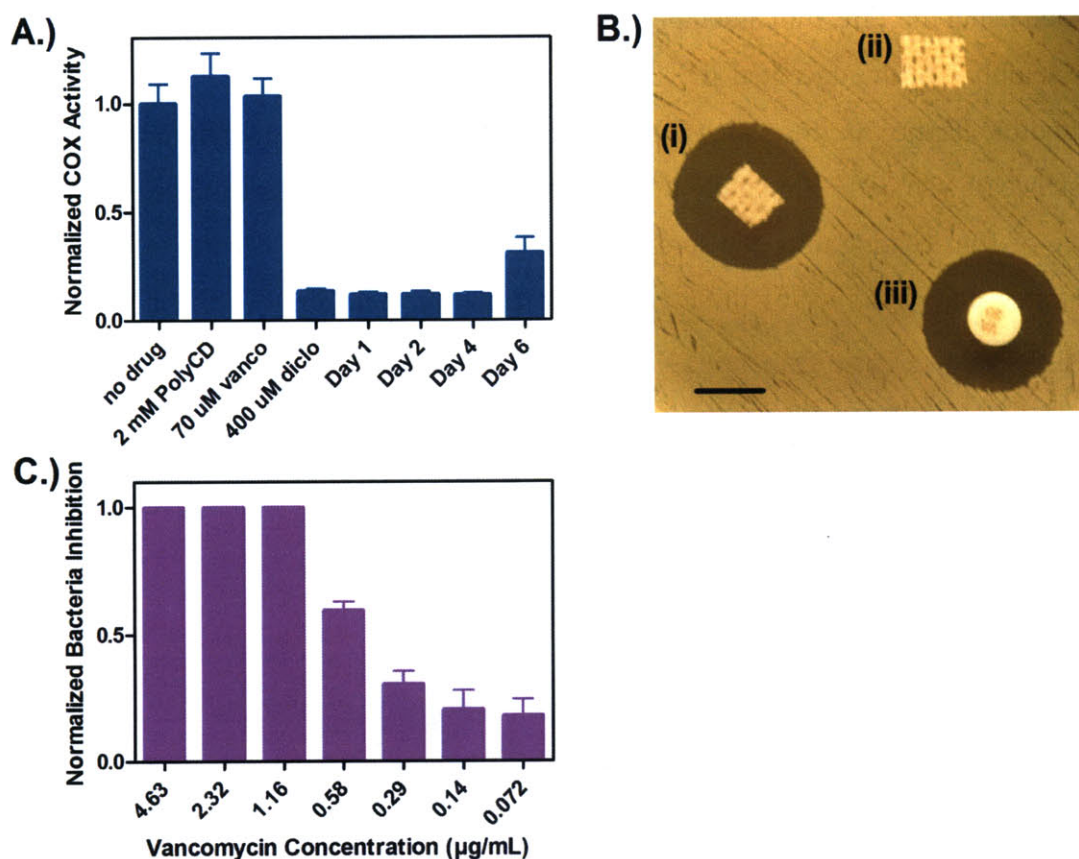
Figure 4-6: Composite film-released drug efficacy. A.) COX activity of diclofenac released from LbL bandage coating at Day 1, 2, 4, and 6 of release. Controls of pure polyCD, pure vancomycin, and pure diclofenac were also included. B.) Vancomycin activity against agar coated *S. aureus* of (i) LbL coated bandage, (ii) uncoated bandage, and (iii) vancomycin control (30 μg) (scale bar = 9 mm). C.) Normalized *S. aureus* inhibition by vancomycin released from dipped LbL film architecture: (poly 2/dextran sulfate/vancomycin/dextran sulfate)$_{60}$ + (poly 2/polyCD-diclofenac)$_{20}$.

The coated bandage has a surrounding zone of inhibition (ZOI) similar to a vancomycin control disc (30 μg); the ZOI is absent for the uncoated control bandage. Vancomycin released from a coated intraocular lens was also shown to completely maintain its native MIC against *S. aureus* (0.5-2 μg/mL) as shown in Figure 4-6C; here the coating architecture was that of the dipped film

release shown in Figure 4-4A. Overall, the antibiotic and anti-inflammatory properties of the incorporated therapeutics were not affected by the composite film deposition and release process. These dual drug releasing films have great potential to be used in a variety of medical scenarios which would benefit from the localized delivery of both an antibiotic and an NSAID.

4.3.4 Composite Film Summary

Table 4-2 summarizes the total drug loading and timescales for drug release for all composite film architectures explored in this work along with single therapeutic films.

Table 4-2: Total drug loading and release timescale of single-therapeutic and composite films.

Film			Vancomycin		Diclofenac	
Architecture[a]	Polyanion[b]	LbL	Loading [$\mu g/cm^2$]	Release time [days]	Loading [$\mu g/cm^2$]	Release time [days]
AB_{60}	A	Dip	89.6 ± 0.3	0.3	NA	NA
AB_{60}	CS	Dip	107.6 ± 0.2	2.1	NA	NA
AB_{60}	DS	Dip	21.5 ± 1.5	2.2	NA	NA
AB_{60}	CS	Spray	28.5 ± 3.0	0.3	NA	NA
$NSAID_{20}$	NA	Dip	NA	NA	5.0 ± 1.0	20.0
$NSAID_{20}$	NA	Spray	NA	NA	7.0 ± 0.2	7.0
$AB_{60} + NSAID_{20}$	A	Dip	0.5 ± 0.2	1.1	54.1 ± 1.9	4.4
$AB_{60} + NSAID_{20}$	CS	Dip	0.5 ± 0.3	9.3	50.3 ± 3.6	9.3
$AB_{60} + NSAID_{20}$	DS	Dip	13.3 ± 0.5	2.3	9.4 ± 0.9	1.7
$AB_{60} + NSAID_{20}$	CS	Spray	28.7 ± 3.2	0.4	36.2 ± 4.4	13.9
$NSAID_{20} + AB_{60}$	A	Dip	106.1 ± 4.0	1.0	0	0
$NSAID_{20} + AB_{60}$	CS	Dip	158.6 ± 44.8	1.4	0	0
$NSAID_{20} + AB_{60}$	DS	Dip	26.1 ± 2.9	2.2	0	0
$NSAID_{20} + AB_{60}$	CS	Spray	48.5 ± 7.9	0.4	0	0

[a]AB_{60} = vancomycin film; $NSAID_{20}$ = diclofenac film
[b]A = alginate; CS = chondroitin sulfate; DS = dextran sulfate; NA = not applicable

The release profiles from these architectures are shown in Figure 4-4 and Figure 4-7. As discussed earlier, all architectures in which the NSAID film was deposited first, followed by the antibiotic film, had no diclofenac remaining in the film.
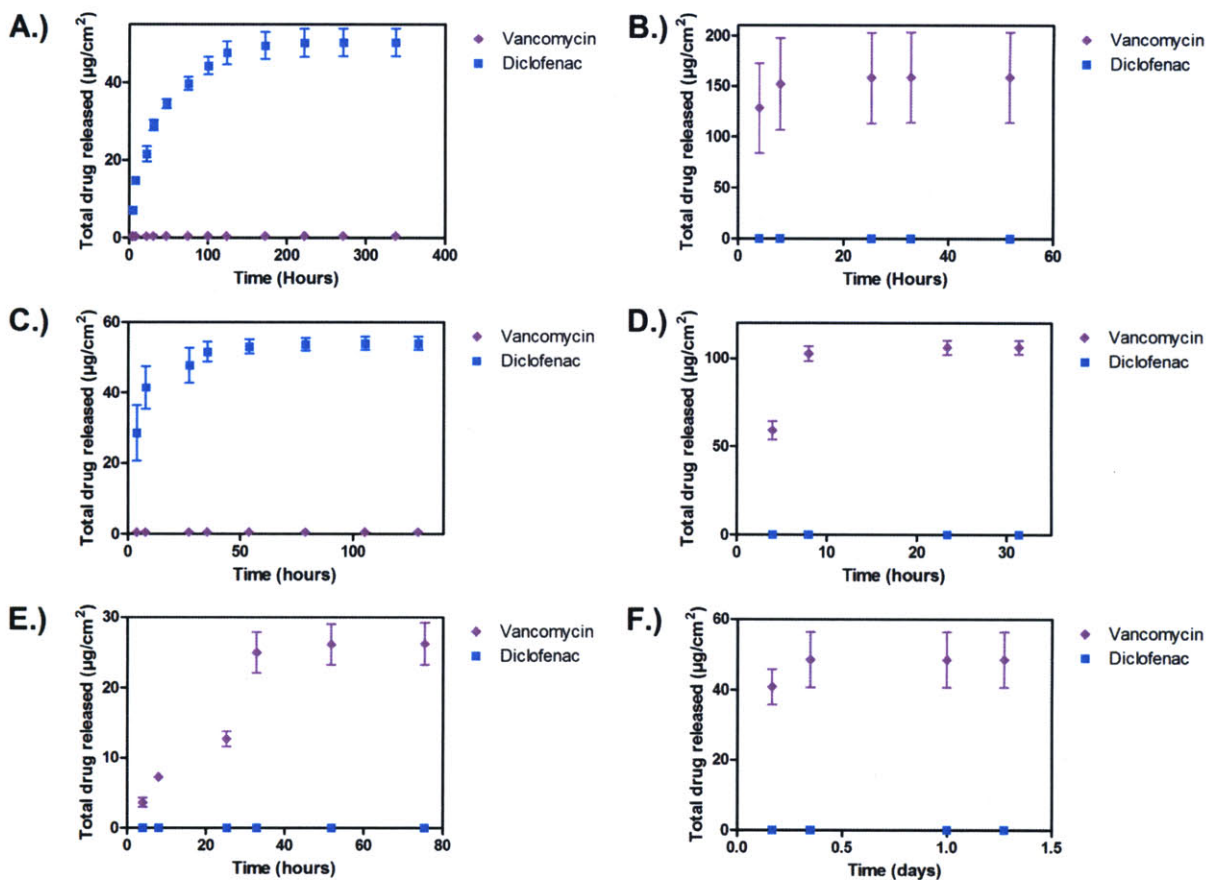
Figure 4-7: Total drug release from composite film architectures. A.) (Poly 2/chondroitin sulfate/vancomycin/chondroitin sulfate)$_{60}$ + (poly 2/polyCD-diclofenac)$_{20}$ dipped. B.) (Poly 2/polyCD-diclofenac)$_{20}$ + (poly 2/chondroitin sulfate/vancomycin/chondroitin sulfate)$_{60}$ dipped. C.) (Poly 2/alginate/vancomycin/alginate)$_{60}$ + (poly 2/polyCD-diclofenac)$_{20}$ dipped. D.) (Poly 2/polyCD-diclofenac)$_{20}$ + (poly 2/alginate/vancomycin/alginate)$_{60}$ dipped. E.) (Poly 2/polyCD-diclofenac)$_{20}$ + (poly 2/dextran sulfate/vancomycin/dextran sulfate)$_{60}$ dipped. F.) (Poly 2/polyCD-diclofenac)$_{20}$ + (poly 2/chondroitin sulfate/vancomycin/chondroitin sulfate)$_{60}$ sprayed.

4.4 Conclusions

In this work, we have developed a method to simultaneously deliver an antibiotic, vancomycin, and an NSAID, diclofenac, from composite LbL films, over relevant timescales and concentrations. The coating technology developed here is an important progression in the

engineering and design of multi-drug releasing devices. The therapeutics incorporated in this LbL drug delivery system are complementary in that they address two critical and often simultaneous medical conditions, infection and inflammation. However, their differing chemical nature makes their direct incorporation into a single therapeutic technology a difficult task. Our study of film component interactions proved to be a valuable way of designing and understanding the behavior of these multi-drug releasing LbL films. The interaction studies along with the versatility of spray and dip LbL assembly have both been used in this work to manipulate the kinetics of diffusion and exchange processes to design dual-functionality coatings. The films developed here exhibit release profiles and drug loadings which specifically address differing medical needs, ranging from rapid to more prolonged delivery of either therapeutic incorporated. The design principles utilized in this study can be applied to the efficient development of other clinically relevant device coatings.

Chapter 5

Release of Vancomycin from Multilayer Coated Absorbent Gelatin Sponges

5.1 Introduction

The use of local techniques to controllably deliver effective concentrations of antibiotics at a site of interest has the potential to prevent drug resistance, a growing problem with frequent systemic antibiotic exposure [65]. Typical broad spectrum antibiotics are delivered intravenously or orally, often eliminating healthy bacteria and allowing resistant strains to flourish. By delivering therapeutics locally, unnecessary systemic administration can be avoided. Several approaches for local antimicrobial delivery have been explored, including antibiotic-infiltrated wound dressings [8, 9], polymer scaffolds [10], sol-gels [103], and hydrogels [11], amongst others. Typical polymeric scaffolds have limited capacity for small molecule drugs, and are not able to effectively coat the complex geometries and small scale features of wound dressings, thus making it difficult to find means of incorporating the drug while maintaining function. Layer-by-layer (LbL) assembly of polymer multilayer films can be used to address these issues via the direct surface functionalization and coating of complex structures for local antimicrobial applications.

The LbL technique, which involves the alternate deposition of positively and negatively charged species [22], is extremely versatile and has been applied in coating a variety of biomedically relevant substrates, including stents [37], red blood cells [48], electrospun materials [27], and microparticles [31], to name a few [43, 44, 47]. Because the method is water-based, a variety of sensitive molecules and macromolecules have been successfully assembled in LbL films while preserving biological efficacy, including proteins [30-33], peptides [13, 55], and small molecules [55, 58]. Bactericidal LbL films have previously been developed, including non-degradable coatings containing antimicrobial polymers [15, 137] and films designed to release antimicrobial agents [13, 14, 54, 55]. We have shown that small molecule antibiotics can be directly incorporated into LbL films without prior encapsulation [14, 54]. A large advantage

of using LbL systems is the ability to generate high drug loadings within the film and conformally coating complex geometries such as implant surfaces and structures with micro- to nanometer scale features.

In our previous work described in Chapter 3, we demonstrated that vancomycin, a potent glycopeptide antibiotic used primarily in the treatment of resistant Gram-positive bacterial infections, can be controllably released from hydrolytically degradable multilayer films [14]. Both traditional dip LbL, as well as spray LbL assembly, in which each solution is aerosolized and sprayed at the substrate, can be used to assemble these films. The rapid kinetics of the spray process ensure large vancomycin loading in these films (up to 20 weight percent); interdiffusion of species in these sprayed films leads to formation of favorable non-electrostatic secondary interactions between film components, promoting drug release up to 45 hours [14]. Spray LbL assembly provides a means of manipulating the deposition of LbL films on porous media and scaffolds with regard to the resulting degree of pore coverage and film morphology [27].

In this work, we show that spray LbL assembly enables the coating of vancomycin containing LbL films on a clinically relevant biomaterials scaffold without modifying its underlying structure, even when the substrate is water sorbable. The substrate we used is a highly porous and absorbent gelatin sponge, Surgifoam®, manufactured by Ferrosan and distributed by Johnson and Johnson. Surgifoam® can be soaked in solutions of clotting factors, such as thrombin, to promote rapid hemostasis [138]; it has been used in a variety of medical procedures [138, 139]. It is of significant interest to coat these gelatin scaffolds with antibiotics that can release directly to the wound as a means of concurrently addressing infection and hemostasis for urgent care. Here, we functionalize Surgifoam® with vancomycin containing LbL films and examine the effects of substrate morphology on drug release while simultaneously monitoring substrate properties before and after LbL film coating.

5.2 Materials and Methods

5.2.1 Materials

Poly 2 was synthesized as previously described [86, 106]. Vancomycin and sodium acetate buffer (3 M) were purchased from Sigma-Aldrich (St. Louis, MO). Dextran sulfate sodium salt (M_n = 500 kDa) was purchased from Polysciences (Warrington, PA). Dulbecco's

phosphate buffered saline (PBS, 0.1 M) was purchased from Invitrogen (Carlsbad, CA). Deionized water (18.2 MΩ, Milli-Q Ultrapure Water System, Millipore) was utilized in all experiments. *S. aureus* 25923 was obtained from ATCC (Manassas, VA). Cation-adjusted Mueller Hinton broth (CaMHB), Bacto agar, and vancomycin susceptibility test discs were obtained from BD Biosciences (San Jose, CA). Surgifoam® absorbent gelatin sponges were generously donated by Ferrosan (Soeborg, Denmark).

5.2.2 Film Assembly on Surgifoam®

Vancomycin containing films were assembled using spray LbL assembly as previously described in Chapter 3 [14]. Briefly, these films were constructed using a tetralayer architecture, denoted: (poly 2/dextran sulfate/vancomycin/dextran sulfate)$_n$, where n represents the number of tetralayers deposited (films with n = 60 and 120 were assembled in this work). All deposition solutions were formulated at a concentration of 2 mg/mL in 0.1 M sodium acetate buffer (pH 5). Films were assembled using a programmable spraying apparatus (Svaya Nanotechnologies). The Surgifoam® substrate was used as received with no pretreatment. A 50 psi vacuum was applied to the back of Surgifoam® substrates (with dimensions of 1 cm x 5.5 cm x 4.5 cm) during the LbL deposition process. For each tetralayer, each deposition step lasted 2 seconds, followed by a 3 second rinse with 0.1 M sodium acetate buffer (pH 5) at a flow rate of 0.25 mL/s. Following film deposition, the Surgifoam® was allowed to dry using gentle house vacuum and then stored at 4 °C prior to subsequent analysis. For contact angle and swelling measurements, films were coated on silicon substrates without vacuum application.

5.2.3 Characterization of Film and Surgifoam® Properties

Advancing water contact angle of 60 and 120 tetralayer films coated on silicon wafers was obtained using a standard sessile drop technique with a VCA 2000 video contact angle system and the accompanying VCA OptimaXE software (AST Products, Inc.). Additionally, film swelling was monitored for the 60 tetralayer film using a MultiMode 8 scanning probe microscope with a Nanoscope V controller (Veeco Metrology) operated in tapping mode. Dry film thickness measurements were made by scanning over a region containing both the film and a deliberate scratch. Change in film thickness was monitored upon introducing 0.01 M PBS into a liquid chamber.

Surgifoam® morphology before and after LbL spray coating was examined using scanning electron microscopy (JEOL JSM-6060). The surface area of uncoated Surgifoam® was evaluated using an accelerated surface area and porosimetry analyzer (Micromeritics ASAP 2020). Additionally, the ability of Surgifoam® to absorb 0.01 M PBS before and after LbL coating was examined. Pieces of coated and uncoated Surgifoam® were weighed and subsequently submerged in 10 mL of 0.01 M PBS for 10 minutes. Following this, the foam was removed from the solution and weighed again. The difference is mass before and after soaking corresponded to the mass of PBS absorbed by the sponge. This value was normalized by the initial mass of the sponge, to give a measure of absorbency in milligrams of PBS per milligram of sponge. An absorbency ratio of LbL coated to uncoated Surgifoam® was calculated using the following equation:

$$\text{Absorbency ratio} = \frac{(mg\ PBS\ absorbed/mg\ sponge)_{LbL\ coated}}{(mg\ PBS\ absorbed/mg\ sponge)_{uncoated}}.$$

5.2.4 Vancomycin Release from Surgifoam®

After LbL spray deposition, the coated Surgifoam® was cut into smaller pieces using a razor blade (with dimensions of approximately 0.7 cm x 0.8 cm x 1 cm). Each piece of sponge was released in 1 mL of 0.01 M PBS at 37 °C. At predetermined times, the PBS was removed and frozen at -20 °C before subsequent analysis; a fresh 1 mL of PBS was added to continue film release. These film release solutions were monitored with high performance liquid chromatography (Agilent Technologies HPLC, 1100 series) using a C18 reverse phase column (Supelco) coupled with fluorescence detection, as previously described in Chapter 3 [14]. Briefly, each sample was run for 10 minutes using a 70/30 0.01 M PBS/methanol mobile phase, 1 mL/min flow rate, 500 µL injection volume, and an excitation wavelength of 280 nm and emission wavelength of 355 nm for vancomycin detection. Fluorescence peak height was correlated with standards of known vancomycin concentrations and used to determine drug concentrations in coated Surgifoam® release samples. A piece of uncoated Surgifoam® was also released similarly to the coated sponges and examined with the same HPLC protocol, to ensure that potential peaks from sponge degradation did not interfere with vancomycin peaks (no interference was noted).

Release of vancomycin from Surgifoam® pieces containing drug but no LbL coating was also examined. After determining the total vancomycin loading in the 60 and 120 tetralayer LbL

film coated sponges, these quantities of vancomycin were dissolved in deionized water and allowed to soak completely into pieces of non-film coated sponge. Immediately after soaking, these sponge pieces were released in PBS in the same way that LbL film-coated Surgifoam® was released; release was quantified using HPLC as described above.

5.2.5 Bacterial Growth Inhibition

The ability of LbL coated Surgifoam® to inhibit the growth of *S. aureus* 25293 was examined by exploring the activity of the LbL coated sponge directly as well as drug release solutions using previously described methods [14]. Briefly, coated Surgifoam® activity was assessed directly using a modified Kirby-Bauer test on a bacteria coated agar plate. Here, pieces of coated sponge, along with controls of uncoated sponge and vancomycin susceptibility discs (30 μg), were applied to CaMHB-agar plates which were evenly coated with *S. aureus* in its exponential growth phase at a concentration of 10^8 CFU/mL. These plates were incubated at 37 °C for 16-18 hours and observed for zones of inhibition surrounding the test samples following incubation.

A quantitative determination of vancomycin activity from a coated Surgifoam® sample was obtained by first completely releasing the coated sponge into a 1 mL, 0.01 M PBS bath, at 37 °C. The exact concentration of vancomycin in this release solution was determined using HPLC methods described earlier. Subsequently, *S. aureus* in its exponential growth phase was added to dilutions of this release solution in CaMHB at a final concentration of 10^5 CFU/mL. Non-film released vancomycin was also tested. Additionally, controls of 0.01 M PBS dilutions in media containing no drug exposed to *S. aureus* (positive control) and not exposed to *S. aureus* (negative control) were included. These dilutions were incubated at 37 °C for 16-18 hours with agitation, following which, optical density at 600 nm was read using a BioTek PowerWave XS plate reader. Normalized bacteria density was calculated as follows:

$$\text{Normalized } S.\, aureus \text{ density} = \frac{\left(OD_{600,sample} - OD_{600,negative\ control}\right)}{\left(OD_{600,positive\ control} - OD_{600,negative\ control}\right)}.$$

5.2.6 Statistical Analysis

All experiments performed in this work were done in triplicate at minimum. Data is reported as mean ± standard deviation. Surgifoam® morphology via SEM was examined for a

minimum of three separate samples per test condition at a minimum of three locations per sample.

5.3 Results and Discussion

5.3.1 Surgifoam® Coating Characterization

In the LbL self-assembly process, substrates are coated with materials that have complementary functionality (i.e. charge, hydrogen bonding interactions, etc.) one layer at a time. Rinsing between deposition steps removes non-specifically bound material [22]. We used this technique to coat Surgifoam® gelatin sponges with antibiotic releasing LbL films. Due to the fact that Surgifoam® is highly water absorbent, these sponges were coated with spray LbL assembly rather than the traditional dip assembly technique. In spray LbL assembly, each film component and rinse solution is aerosolized and propelled at the substrate being coated as shown in Figure 5-1 [25, 26]. Due to the fact that the process is not diffusion limited, spray LbL significantly reduces the overall assembly time compared to the dip LbL technique, from approximately 40 minutes per tetralayer to 20 seconds per tetralayer. As shown in Figure 5-1, a vacuum was applied to the back of the porous Surgifoam® substrate to take advantage of the large surface area available for coating while sweeping liquid through the substrate at a fast rate during the spray process. For the 60 and 120 tetralayer films deposited in this work, it takes 20 and 40 minutes to complete film spray assembly compared to 40 and 80 hours for dipping. Soaking Surgifoam® in the buffer solution used in film assembly for the same 20 and 40 minute time period, 8.2 ± 1.4 and 11.5 ± 1.5 milligrams of buffer per milligram of sponge, were absorbed without any significant change in sponge dimensions. Spray assembly does not require complete immersion of the Surgifoam® in liquid for lengthy times, which avoids this significant absorption that may lead to inadequate coating and contamination from carryover of deposition solutions [26]. Vacuum application further eliminates these complications. Overall, the short and significantly drier spray process, allows for effective coating of the porous and absorbent Surgifoam®.
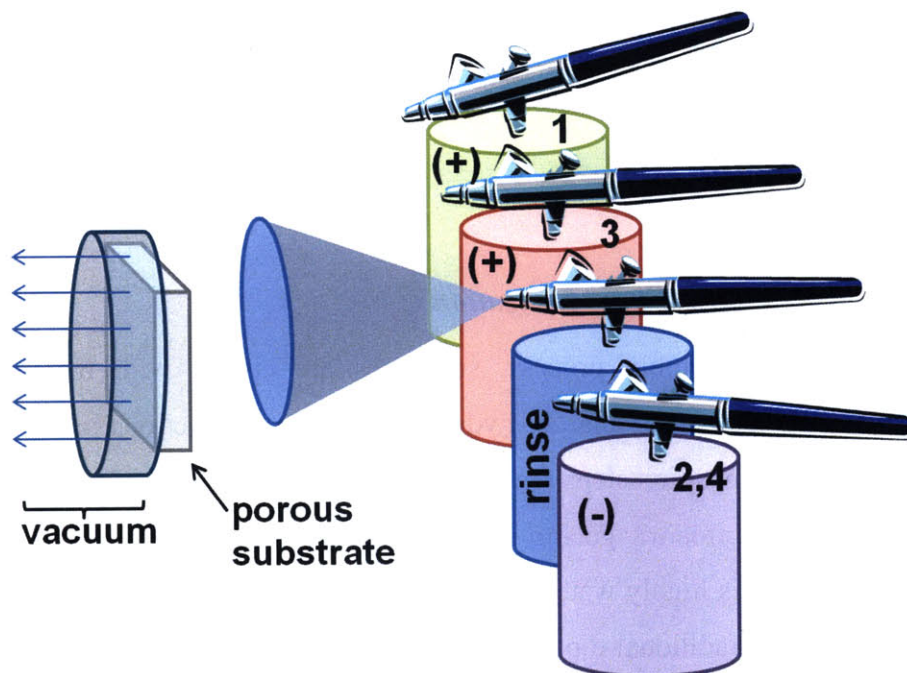
Figure 5-1: Spray layer-by-layer assembly for porous substrates. Each airbrush aerosolizes and sprays film components or the rinse solution at the substrate; a vacuum is applied to pull solutions through the substrate. For the vancomycin LbL films, 1 = poly 2, 2 and 4 = dextran sulfate, and 3 = vancomycin.

Prior to and after spray coating with antibiotic LbL films, scanning electron microscopy was used to examine dry sponge morphology. Figure 5-2 shows both plan-view and cross-sectional SEM micrographs of uncoated sponges and sponges coated with both 60 and 120 tetralayers of (poly 2/dextran sulfate/vancomycin/dextran sulfate)$_n$ films. Poly 2 is a cationic and hydrolytically degradable poly (β-amino ester) [11, 106], vancomycin is the cationic antibiotic, dextran sulfate is a counter polyanion, and n is the number of tetralayers deposited. The properties of these films on flat, non-porous, and non-absorbent substrates have previously been described in Chapter 3 [14]. Figure 5-2 shows the highly porous nature of Surgifoam®; the surface area was found to be approximately 5.3 m^2/g. As evidenced in Figure 5-2, the underlying Surgifoam® morphology is maintained following the spray LbL process; there is no evidence of collapse, expansion, or degradation of the sponge microstructure. The only visible difference between the coated and uncoated samples is the presence of the coating itself, which, as expected, appears thicker for the 120 tetralayer films compared to the 60 tetralayer films. As the coating grows, it lines the pore surfaces and eventually begins to partially fill gaps between pores.
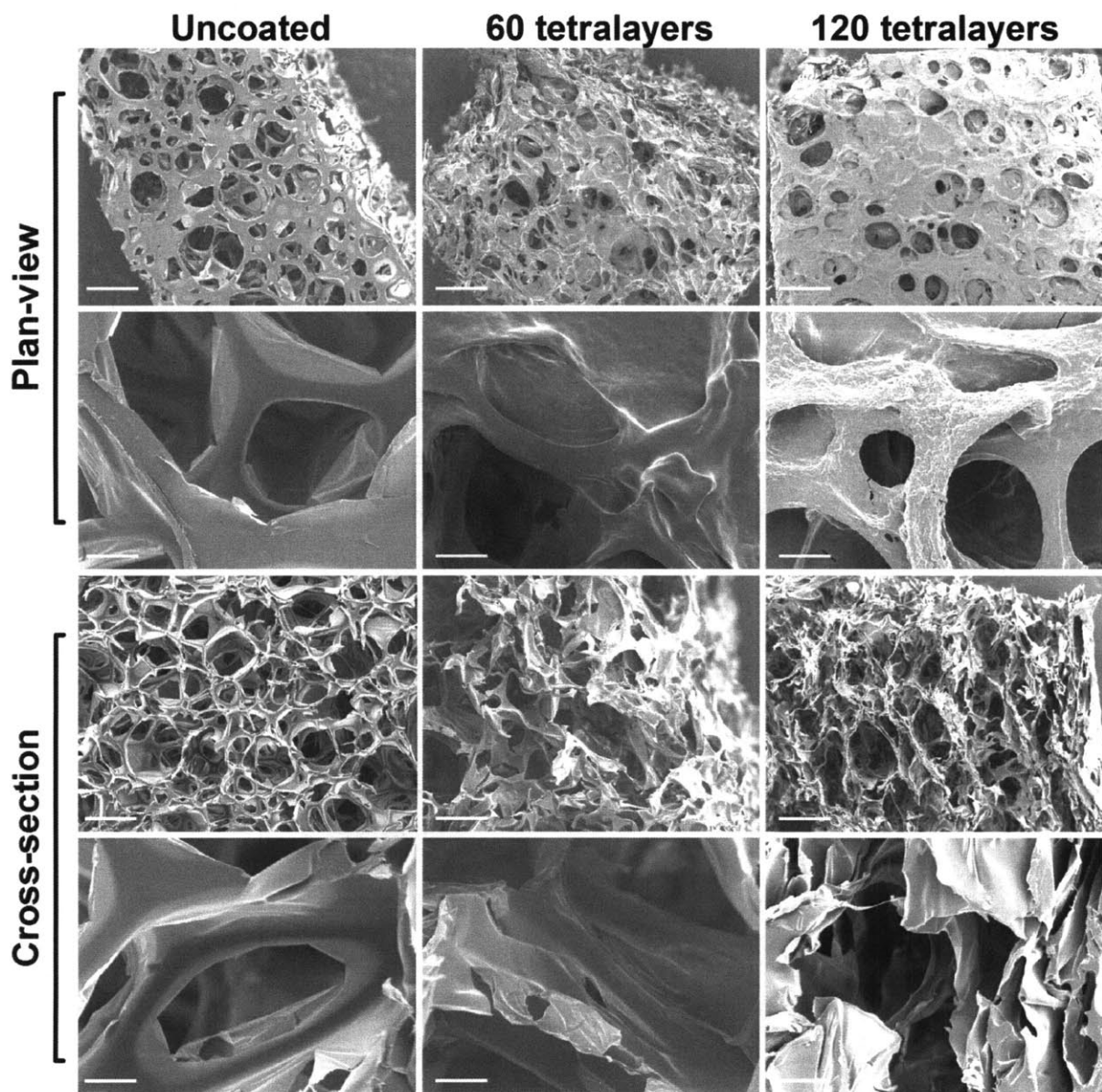
Figure 5-2: SEM micrographs of uncoated and (poly 2/dextran sulfate/vancomycin/dextran sulfate)$_n$ spray LbL coated Surgifoam®. Scale bar = 500 µm and 50 µm for top and bottom row micrographs, respectively, for both plan-view and cross-section images (except 60 tetralayer cross-section top row, where scale bar = 200 µm), respectively.

To ensure that the coated Surgifoam® maintains its primary function, the absorption of aqueous phosphate buffered saline (PBS) by LbL coated versus uncoated sponges was examined. The ratio of mass of PBS absorbed by LbL coated versus uncoated Surgifoam® is shown in Figure 5-3. The LbL coating greatly enhances the absorption of PBS per milligram of sponge. The 60 tetralayer LbL coating increased liquid absorption by approximately 80%, while the 120

tetralayer coating increased sponge absorption by 170% compared to uncoated Surgifoam®. It is generally known that polyelectrolyte multilayers can swell and take up significant amounts of water when hydrated. In fact, the 60 tetralayer vancomycin containing LbL films instantaneously swell to approximately 180% of their dry film thickness in PBS when assembled on a flat substrate. Additionally, the advancing water contact angle on flat substrates coated with 60 and 120 tetralayer vancomycin LbL films, was measured to be $109.6 \pm 6.2°$ and $53.1 \pm 9.2°$, respectively, further demonstrating the hydrophilicity of these films, especially at 120 tetralayers. Gelatin hydrogels have been reported to have high advancing contact angles of approximately 130°, depending on gelatin concentration, despite their large water absorption capabilities [140]. It is clear from this data that the LbL film within the coated sponge is able to enhance Surgifoam® water uptake, likely through increased wetability and capillarity of the sponge pores and the increased thickness of the coating itself, which can add to the total amount of water absorptive material. Overall, the LbL coating lacks any detrimental effect on the functions of Surgifoam® and actually enhances the sponge absorbency by a factor greater than approximately 2.
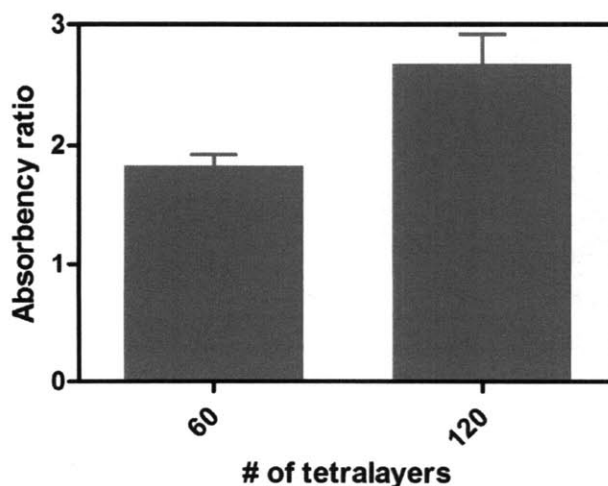
Figure 5-3: Absorbency ratio of phosphate buffered saline by film coated compared to uncoated Surgifoam®.

5.3.2 *Vancomycin Release and Therapeutic Potential*

The effects of the micro and nanoscale structure of drug releasing devices on dictating drug release kinetics have been thoroughly explored [141-143]. The ability to generate uniform conformal coatings within complex porous scaffolds allows us to use the pore morphology of the underlying substrate as a means of modulating the release behavior of our LbL films; here we

have explored the impact of the gelatin sponge morphology on vancomycin loading and release kinetics. Figure 5-4 shows the release profiles of vancomycin from 60 and 120 tetralayer spray LbL coated Surgifoam® at physiologic conditions (PBS, pH 7.4, 37 °C). Two different representations of the data are shown; Figure 5-4A shows total vancomycin released per milligram of the Surgifoam® substrate, while Figure 5-4B shows the total vancomycin released per square centimeter of projected in-plane Surgifoam® surface. Both of these methods of data representation provide valuable information about the final drug loading capabilities of these LbL films. Compared to flat substrates which were previously sprayed with the same vancomycin containing LbL film and found to contain 9.7 ± 1.0 $\mu g/cm^2$ and 20.0 ± 1.9 $\mu g/cm^2$ for $n = 60$ and 120, respectively [14], films sprayed on Surgifoam® showed an $880 \pm 140\%$ and $710 \pm 85\%$ greater vancomycin loading for $n = 60$ and 120, respectively. This significant increase in drug loading comes from the increased overall surface area of the Surgifoam® substrate. From Figure 5-2 it is clear that there is significant bridging of the Surgifoam® pores by the multilayer film coating. The LbL film is observed to penetrate across the 1.0 cm thickness of the Surgifoam® substrate, but with less deposition in regions furthest from the front surface during the spray LbL process. It is conceivable that if complete conformal coverage of all available surface area were achieved, the loadings and release times could be increased even further.
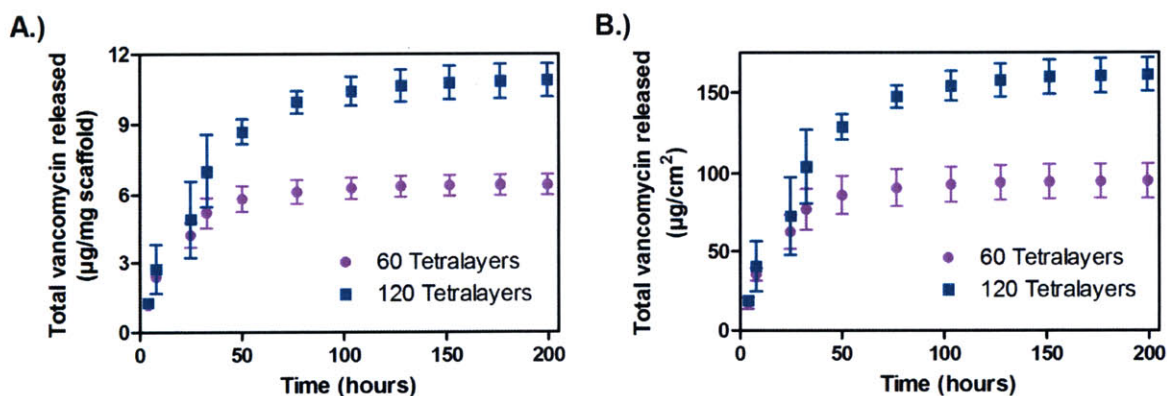
Figure 5-4: Vancomycin release profiles from Surgifoam® coated with (poly 2/dextran sulfate/vancomycin/ dextran sulfate)$_n$ where $n = 60$ and 120. A.) Drug release expressed in µg of vancomycin per mg of Surgifoam®. B.) Drug release expressed in µg of vancomycin per Surgifoam® projected in-plane area (cm^2).

Figure 5-5 shows normalized release profiles for both Surgifoam® and flat substrates coated with (poly 2/dextran sulfate/vancomycin/dextran sulfate)$_n$ where $n = 60$ and 120. The

release at each time point is normalized to the final vancomycin loading in the film. Figure 5-5A and 5-5B show full and partial release data for 60 tetralayer films, while Figure 5-5C and 5-5D show full and partial release data for 120 tetralayer films. These figures also show release profiles from Surgifoam® that was soaked with vancomycin and released immediately into PBS (no LbL film). This condition was used to simulate an option that might be commonly employed by a surgeon, reconstituting a lyophilized formulation of vancomycin in solution and soaking up the solution with the Surgifoam® immediately prior to using the sponge to absorb blood during an invasive procedure.
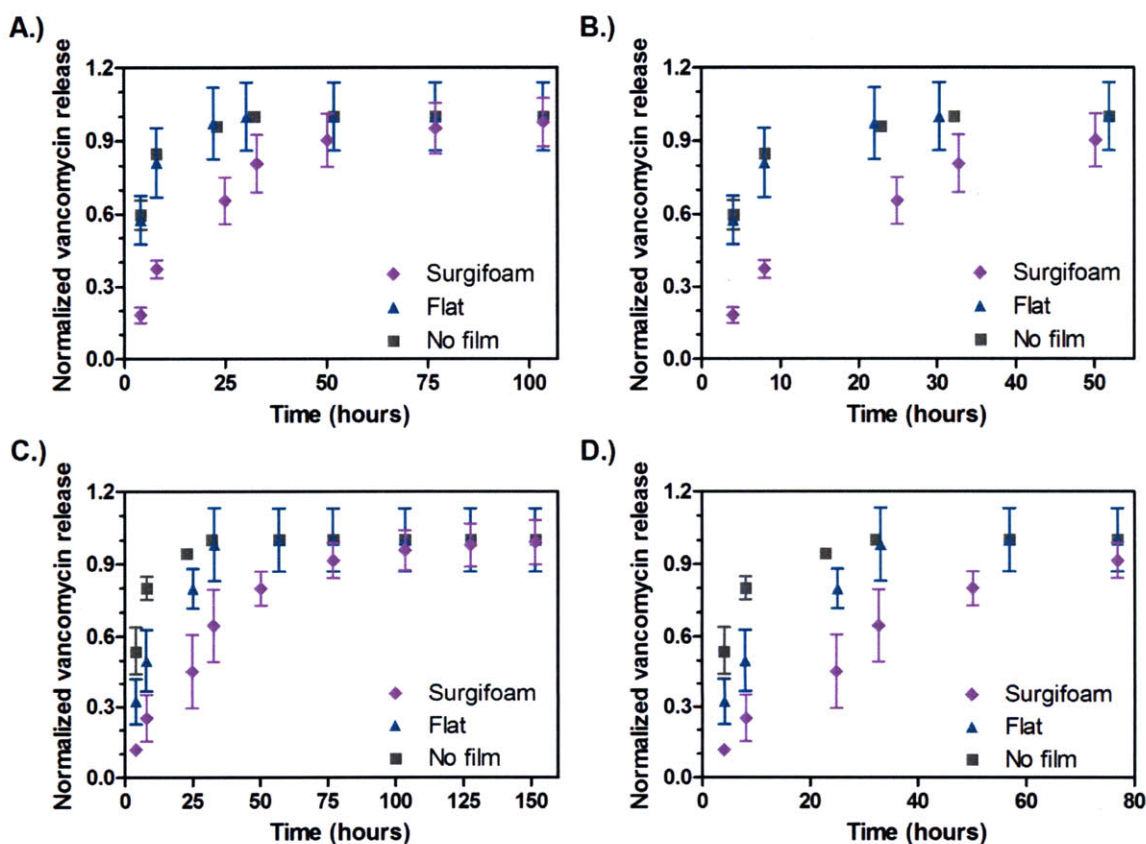
Figure 5-5: Normalized vancomycin release profiles. A.) Complete release from Surgifoam® and flat substrates coated with (poly 2/dextran sulfate/vancomycin/dextran sulfate)$_{60}$ spray LbL films and vancomycin-soaked Surgifoam® (no film). B.) Data shown in (A.) up to 52 hours of release. C.) Complete release from Surgifoam® and flat substrates coated with (poly 2/dextran sulfate/vancomycin/dextran sulfate)$_{120}$ spray LbL films and vancomycin-soaked Surgifoam® (no film). D.) Data shown in (C.) up to 77 hours of release.

Table 1 summarizes several relevant release timescales that can be obtained from the graphs in Figure 5-5, namely, the time for 50, 85, and 99% of the drug to be released ($t_{50\%}$, $t_{85\%}$, $t_{99\%}$) from LbL coated flat and Surgifoam® substrates along with non-LbL coated Surgifoam®. The relevant release timescales were determined by examining each sample that contributed to the averages and standard deviations plotted in Figure 5-5, separately. Figure 5-6 shows an example of three separate 120 tetralayer LbL film coated Surgifoam® samples that were released (Figures 5-5C and 5-5D show the averaged release and standard deviations of these three samples). From Figure 5-6A and 5-6B we can see that although the averages of these individual samples may overlap for consecutive time points (especially towards later time points), the vancomycin quantity in each individual release sample increases significantly. Once significant increase in vancomycin quantities between one or more samples for consecutive time points was not visible, release was considered to be complete.

Table 5-1: Vancomycin release kinetics.

	Substrate	$t_{50\%}$ (hours)	$t_{85\%}$ (hours)	$t_{99\%}$ (hours)
No film[a]	Surgifoam®	<4	8	24
$n = 60$[b]	Surgifoam®	16	40	104
	Flat	<4	10	24
$n = 120$[b]	Surgifoam®	28	63	150
	Flat	8	27	45

[a] Surgifoam® soaked in vancomycin (no LbL coating).
[b] Film architecture: (poly 2/dextran sulfate/vancomycin/dextran sulfate)$_n$.

Together Figure 5-5 and Table 5-1 show that similar to drug loading, there are significant differences in vancomycin release kinetics for both the 60 and 120 tetralayer LbL film coatings on Surgifoam® compared to flat substrates. For both the 60 and 120 tetralayer Surgifoam® films, there is an approximate 4-fold increase in $t_{50\%}$. Final Surgifoam® LbL drug release lasts over approximately 104 and 150 hours versus 24 and 45 hours for the same 60 and 120 tetralayer films, respectively, on flat substrates. On flat substrates, the 120 tetralayer film was previously shown to have a period of linear release lasting from 4 to 33 hours, compared to a rapid bolus release of vancomycin from a 60 tetralayer film [14]. These differences were attributed to an increased level of interdiffusion between film components at 120 tetralayers compared to 60 tetralayers, which appeared to promote non-electrostatic secondary interactions between

vancomycin and dextran sulfate, stabilizing these films [14]. Similar to what was seen on flat substrates, the 120 tetralayer Surgifoam® coatings have a much more linear release profile than the 60 tetralayer Surgifoam® films and release vancomycin over a longer period of time; the linear release period lasts from 4 to approximately 60 hours ($R^2 = 0.97$) at which point approximately 90% of the vancomycin has been released from the films. Overall, the increased porosity and surface area of Surgifoam® appear to greatly increase the vancomycin release timescales from these previously developed LbL spray coatings from 1 to 2 days on non-porous substrates [14] to 4 to 6 days on this clinically relevant substrate.
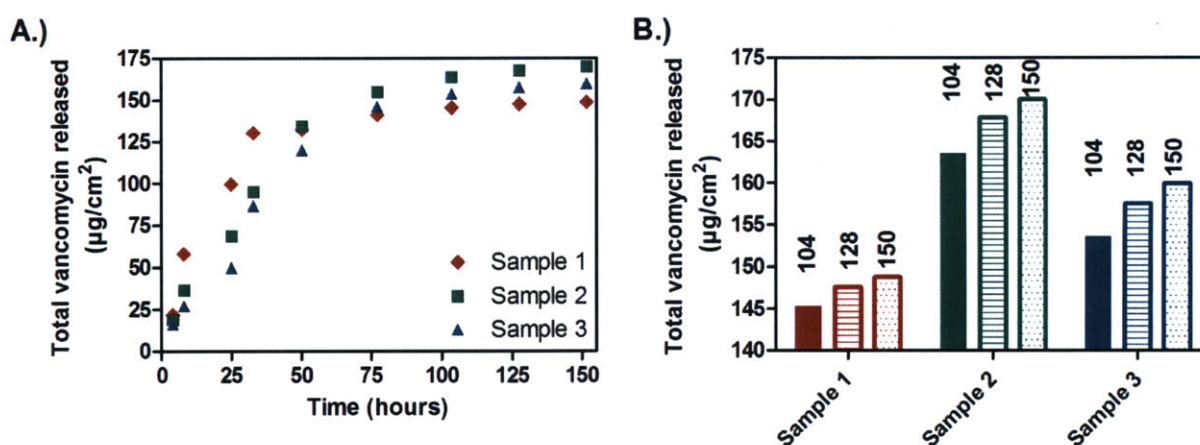
Figure 5-6: Vancomycin release from (poly 2/dextran sulfate/vancomycin/dextran sulfate)$_{120}$ coated Surgifoam®. A.) Release from three individual samples is shown; the average of these three samples leads to the results shown in Figure 5-5C and 5-5D. B.) The total vancomycin released for the last three time points of significant release showing that each individual sample releases a significant quantity of vancomycin through 150 hours.

Additionally, Figure 5-5 and Table 5-1 show comparisons between drug release from Surgifoam® soaked in vancomycin compared to those in which the LbL film was used to encapsulate drug and coat the sponge. Both the 60 and 120 tetralayer films show a significant improvement in controlling drug release from Surgifoam® compared to simply soaking the sponge in vancomycin and releasing. For Surgifoam® soaked in drug, 60% of the loaded vancomycin is released in 4 hours and all of the drug is completely released at 24 hours. The $t_{50\%}$ value is 4 and 7-fold greater for the 60 and 120 tetralayer LbL Surgifoam® coatings, respectively, compared to the soaked sponge. This provides strong support for the use of these LbL films for controlling drug release from coated substrates.

The release profiles and drug loadings of 60 and 120 tetralayer LbL film coated Surgifoam® shown in this work have the potential to be highly therapeutic. Two of the primary causes for development of antibiotic resistance and difficulty in treating infection are drug concentrations below the minimum inhibitory concentration (MIC) of the drug against a particular pathogen and inappropriate delivery timescales [6, 8]. With the Surgifoam® coatings developed here, we obtain tunable drug release over multiple days which can be suitable for both eradicating and preventing infection from occurring at a wound site. Additionally, the large drug loadings of these films can lead to local vancomycin concentrations well above the MIC of vancomycin against common bacteria, including *S. aureus*.

5.3.3 Drug Activity

Upon LbL coating of Surgifoam® and quantifying the release kinetics of vancomycin from these sponges, we established the therapeutic activity of these coatings *in vitro*. First, we released samples of 60 and 120 tetralayer coated Surgifoam® in PBS and examined the efficacy of those release solutions in inhibiting *S. aureus* growth. Figure 5-7A shows the normalized density of *S. aureus* exposed to dilutions of vancomycin released from these coatings, along with a standard solution of vancomycin. Vancomycin released from coated Surgifoam® completely maintains its activity against *S. aureus*, with an MIC between 0.5 to 2 µg/mL as expected for non-film released vancomycin [87].

Activity was also assessed directly upon exposing pieces of coated Surgifoam® to *S. aureus* coated agar for a modified Kirby-Bauer test. Figure 5-7B shows the results of testing a 60 tetralayer film coated Surgifoam® (i and ii) along with an uncoated control (iii) and a vancomycin control disc (30 µg, iv). Sample (i) and (ii) come from the same piece of film coated sponge, which was 1 cm thick. Upon coating, the sponge was sliced into two pieces, such that sample (i) represents the 0.67 cm thick slice of sponge containing the face that was directly exposed to the aerosolized spray from the LbL apparatus. Sample (ii) is the remaining foam from underneath this portion (0.33 cm thick). A clear zone of inhibition (ZOI) surrounds the vancomycin control (iv) along with both coated sponge pieces (i) and (ii), visually showing the inhibition of *S. aureus* growth by these samples. The presence of a ZOI surrounding sample (ii) confirms that vacuum application during LbL deposition allows penetration of the film components throughout the thickness of the Surgifoam® sample. The irregular shape of this

ZOI indicates that although the LbL coating penetrates the entire sponge, the coverage is uneven. As expected, there is no ZOI surrounding the uncoated Surgifoam®. Based on the results of these *in vitro* assays, it is clear that the vancomycin LbL coating of Surgifoam® renders the sponge highly antimicrobial and effective against a common source of infection, *S. aureus*.
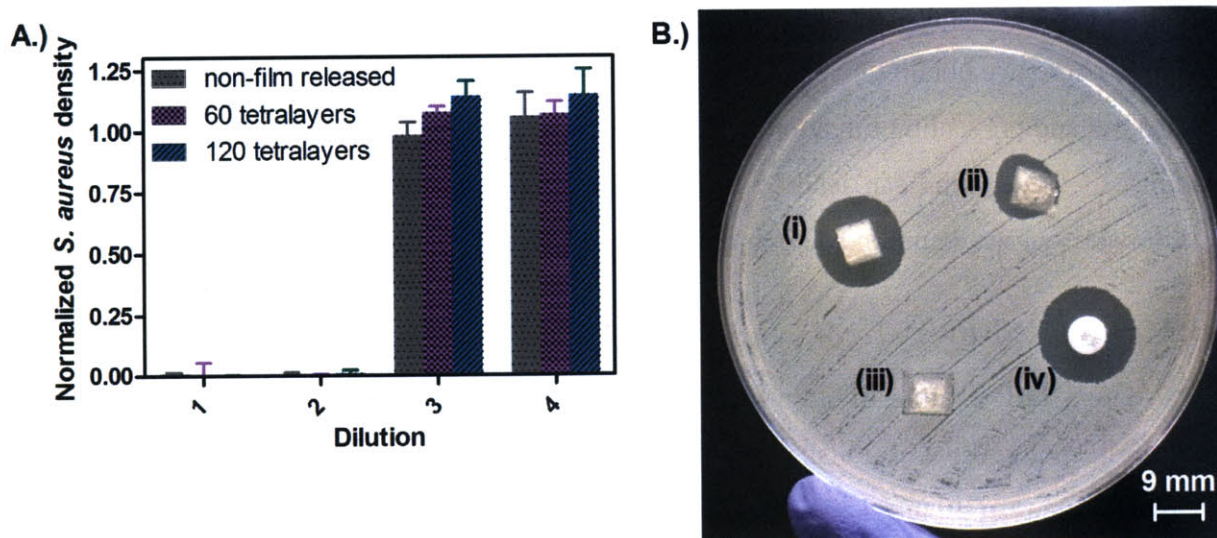
Figure 5-7: Staphylococcus aureus growth inhibition. A.) Normalized *S. aureus* density upon exposure to dilutions of film release solutions from LbL coated Surgifoam® and a standard of non-film released vancomycin (dilution 1 = 2.3, 2.3, and 1.9 μg/mL for non-film released vancomycin, *n* = 60, and *n* = 120, respectively; each subsequent dilution is half the concentration of the previous dilution). B.) Agar coated with *S. aureus* exposed to 60 tetralayer LbL film coated pieces of Surgifoam® (i and ii), an uncoated piece of Surgifoam® (iii), and a 30 μg vancomycin control disc (iv). Sample (i) is the top two-thirds of the coated sponge, while sample (ii) is the bottom one-third.

5.4 Conclusions

In this work, we have demonstrated the application of a vancomycin releasing multilayer film to a clinically relevant, highly absorbent and porous gelatin sponge, Surgifoam®. In the past, the kinetics of vancomycin release from these LbL films and drug loading properties were examined for flat substrates only. Here, we have used spray LbL assembly to coat Surgifoam® and shown that the substrate has a tremendous impact on increasing vancomycin loading and also extending release times compared to a flat substrate. Additionally, we have shown that the LbL films significantly increase the ability of the sponge to absorb liquid. This work has demonstrated that spray LbL assembly is indeed a versatile tool that can be applied to a variety of substrates, even

in the case of water-absorbable biomaterials. Using this technique, we have enhanced the therapeutic properties of Surgifoam®, rendering it antimicrobial while increasing its absorption capabilities. In a similar fashion, multiple substrates such as sutures, bandages, and nanofiber matrices can be coated with therapeutics rapidly and effectively to generate sustained drug release biomedical coatings.

Chapter 6

Layer-by-Layer Assembled Hemostatic Coating

6.1 Introduction

Uncontrolled hemorrhage is the leading cause of death in military trauma and a significant cause of patient mortality in civilian injuries [1, 144]. Traditional mechanical methods of bleeding control include the use of tourniquets, compressive bandages, and ligation. In many cases, these methods fail or cannot be used, including sites where compression is not practical, such as a neck or groin injury [1, 4]. Recently, there has been much research examining the use of hemostatic dressings that typically function by enhancing the clotting cascade [1, 5]. Examples include fibrin dressings and glues, a chitosan based bandage (HemCon, Inc.), and a zeolite based powder dressing (QuikClot, Z-Medica). Although several have shown efficacy in animal studies [1, 2] and human use [4], there are many drawbacks to using these hemostatic dressings. For example, fibrin products pose the risk of transferring infectious agents and activating an adverse immune response, have low shelf-life, and are expensive [1, 5]. The zeolite based powder is often impractical for use in windy environments and some formulations are known to cause severe burns upon skin contact [1, 5]. Chitosan bandages are arguably the most promising of the hemostatic dressings mentioned here, and have been adopted for use by the Department of Defense [1]. The primary drawbacks of this dressing are that the mechanism of action is not entirely understood and the bandage appears to be suitable only for noncomplex wounds [1]. The bandage needs to make good contact with the skin surrounding the wound and if this is not possible as may be the case with non-planar wound configurations, the bandage is often unsuccessful in promoting hemostasis. As an alternative that addresses these drawbacks, we have designed a versatile hemostatic coating that can be applied to existing clinically relevant scaffolds to provide fast bleeding relief for a variety of wound conformations.

We have used the layer-by-layer (LbL) assembly technique to develop this hemostatic coating. LbL assembly is based on the repetitive adsorption of materials with complementary functionality to build a multilayer film [22], and has shown great promise for biological

applications as previously discussed in Chapters 1 through 5 [44, 45, 47]. Here, we sought to incorporate a large density of clotting factor IIa, also known as thrombin, into an LbL assembled film. Thrombin is a serine protease downstream in the clotting cascade, cleaving fibrinogen to form fibrin monomers and allowing its polymerization to form a clot. It serves numerous other functions in the clotting cascade and in wound healing, including recruitment and proliferation of inflammatory and mesenchymal cells and endothelial cell activation [145, 146]. We have specifically used bovine thrombin in our studies, which is approved by the United States Food and Drug Administration (FDA) for promoting hemostasis. Many studies, including our own work described in Chapters 3 through 5, have shown that spray LbL assembly, in which film components are aerosolized and sprayed at a substrate, further increases the practicality and versatility of the LbL technique [14, 26, 27], allowing coating of complex substrates, including porous and absorbent materials. Therefore, our primary focus was on creating a spray assembled thrombin containing LbL film.

The use of hydrogen bonding interactions to assemble multilayer films has been studied extensively [23, 57, 79, 147], and proteins have also previously been successfully incorporated into LbL assembled films [30-34]. In this work, we explored the use of hydrogen bonding interactions to assemble thrombin into thin coatings while preserving the efficacy of this protein. To demonstrate a practical application of the films developed here, we applied them to an absorbent gelatin sponge, Surgifoam®. As discussed in Chapter 5, typically Surgifoam® is soaked in thrombin prior to use in order to promote hemostasis where traditional mechanical methods of bleeding control are unsuitable [138, 139]. By applying hemostatic films to these sponges, we eliminate the need to prepare thrombin solutions and soak the sponge immediately prior to use, which can save valuable time in a critical care situation. Here, we show the development and characterization of these novel coatings, as well as their application to Surgifoam®, and their efficacy in promoting hemostasis in a porcine spleen bleeding model.

6.2 Materials and Methods

6.2.1 Materials

Branched polyethyleneimine (BPEI, M_n = 50-100 kDa) was obtained from Polysciences (Warrington, PA). Tannic acid and mannitol were obtained from Sigma-Aldrich (St. Louis,

MO). Dulbecco's phosphate buffered saline (PBS, 0.1 M) was purchased from Invitrogen (Carlsbad, CA). TCNB buffer (pH 7.5) was formulated in deionized water containing 50 mM Trizma, 1.1 mM calcium chloride, 150 mM sodium chloride, 0.05% Brij® 35, and 0.2 g/L bovine serum albumin each obtained from Sigma-Aldrich (St. Louis, MO). Silicon substrates (test grade, n type) were obtained from Silicon Quest International (Santa Clara, CA). Quartz crystal microbalance sensors (silicon dioxide coated, 50 nm) were purchased from Q-Sense (Biolin Scientific, Linthicum, MD). High purity bovine thrombin powder (12.6% protein, 87.4% mannitol and sodium chloride, BioPharm Laboratories, Bluffdale, UT) and Surgifoam® absorbent gelatin sponges were generously donated by Ferrosan (Soeborg, Denmark). Deionized water (18.2 MΩ, Milli-Q Ultrapure Water System, Millipore) was utilized in all experiments.

6.2.2 Film Preparation

Films were prepared using spray LbL assembly with a programmable spray apparatus (Svaya Nanotechnologies) as previously described in Chapter 3 [14]. The film architecture was denoted (thrombin/tannic acid)$_n$, where n represents the number of bilayers deposited. Films were assembled on silicon to characterize film growth and morphology and on Surgifoam® to examine efficacy. Prior to assembly on silicon, substrates were cleaned with deionized water, methanol, and water again, and dried under nitrogen. The substrates were then plasma etched with air in a Harrick PDC-32G plasma cleaner at high RF level for 60 seconds. Immediately following plasma etching, the substrates were submerged in BPEI solution (2 mg/mL, pH 7.4, in 0.01 M PBS) for 20 minutes. Following this, substrates were rinsed with 0.01 M PBS (pH 7.4) and dried under nitrogen. The bilayer film was then deposited, by spraying thrombin (1 mg/mL, pH 7.4, in 0.01 M PBS) followed by tannic acid (2 mg/mL, pH 7.4, in 0.01 M PBS) each for 20 seconds at a flow rate of 0.25 mL/s. Following each deposition step, a 5 second rinse with 0.01 M PBS (pH 7.4) was sprayed at a flow rate of 0.25 mL/s. For depositing films on Surgifoam®, a vacuum spray setup was used as described in Chapter 5 in which a 50 psi vacuum was applied to the back of the sponge during the spray process. The sponge (approximately 1 cm x 5.5 cm x 4.5 cm) was first sprayed with BPEI for 20 seconds, followed by a 5 second PBS rinse. The bilayer film was then deposited on the sponge with the same spray timings as the flat substrate. Films on silicon were dried under nitrogen, while Surgifoam® films were allowed to dry completely on gentle house vacuum. All films were stored dry at 4 °C prior to subsequent analysis.

6.2.3 Characterization of Film Properties

Initially, film growth was characterized by using quartz crystal microbalance with dissipation monitoring (QCM-D, Q-Sense E4). Silicon dioxide coated sensors (with fundamental frequency of 4.95 MHz ± 50 kHz) were rinsed with deionized water, methanol, and water again, and dried with nitrogen before use. Prior to deposition, the sensors were UV-ozone treated for 20 minutes using a UV-Ozone ProCleaner (Bioforce). The sensor was placed in a flow cell and changes in frequency and dissipation were monitored while flowing in film deposition solution at 150 μL/min. The same solution concentrations and order of deposition steps was used in QCM-D film growth studies as for spray film deposition. Total flow time was 5 minutes for the initial BPEI deposition, 15 minutes for thrombin, and 10 minutes for tannic acid, with 5 minute PBS rinse steps between each deposition; a 5 bilayer film was deposited. To determine if mannitol (which makes up approximately 90% of the thrombin powder as supplied) contributed to film growth, assembly of a control film with architecture (mannitol/tannic acid)$_5$ was attempted. The mannitol (1 mg/mL, pH 7.4, in 0.01 M PBS) deposition step was 15 minutes long.

Spray film growth was monitored via profilometer (Dektak 150 Stylus Profiler, Bruker AXS). Following spray film deposition on silicon substrates at varying bilayer numbers, films were scored with a razor and tracked over a 700 μm scan length to measure film thickness. The surface morphology of these films was monitored using a Dimension 3100 atomic force microscope with Nanoscope 5 controller (Veeco Metrology) operated in tapping mode over 10 μm by 10 μm areas. Root mean squared (RMS) roughness values were obtained using Nanoscope Analysis 1.10 software (Veeco). Morphology of films sprayed on Surgifoam® were examined with scanning electron microscopy (JEOL JSM-6060).

Dissolution of films assembled on silicon substrates with n = 10, 25, and 50, was also monitored. These films (approximately 1 cm^2) were soaked in 500 μL of 0.01 M PBS at 37 °C. At predetermined times, the films were removed from solution, dried under nitrogen, and film thickness was determined using a profilometer as described earlier. This study was carried out over 240 hours.

The absorption of 0.01 M PBS by Surgifoam® was characterized before and after film coating for n = 10, 25, and 50. Sponges were weighed and then submerged in 10 mL of 0.01 M PBS for 10 minutes. Subsequently the sponge was removed from the solution and weighed

again. The difference in mass before and after soaking corresponded to the mass of PBS absorbed by the sponge.

6.2.4 Film Activity

All activity testing was conducted by Ferrosan (Soeborg, Denmark). Film activity was assessed both *in vitro* and *in vivo* for Surgifoam® coated with bilayer films (*n* = 10, 25, and 50). *In vitro*, coated sponges were soaked in 10 mL of TCNB buffer at room temperature under agitation for 10 minutes. Following this, these release solutions, along with standards of thrombin, were tested using an automated coagulation analyzer (START 4, Diagnostica Stago) in which the time for clot formation is measured once fibrinogen (10 mg/mL) solution is added to a sample by monitoring the movement of a metal ball in solution between an applied magnetic field.

In vivo activity of film coated Surgifoam® (*n* = 10, 25, and 50) was determined in a porcine spleen bleeding model. Controls of untreated gauze and Surgifoam® coated with a single monolayer of BPEI, were also tested. All animal tests were performed in accordance with protocols approved by the Committee on Animal Care (Massachusetts Institute of Technology). Danish country breed pigs were used in these studies which were conducted at Københavns Institute for Experimental Medicine (Denmark). Prior to surgery, pigs (approximately 40 kg) were sedated and provided preoperative analgesia via intramuscular injection of a Zoletil® mixture (0.1 mL/kg). This mixture was formulated from a vial of Zoletil 50® (125 mg Tiletamine and 125 mg Zolazepam) dissolved in 2.5 mL Turbogesic® (Butorphanol, 10 mg/mL), 1.25 mL Ketaminol® (Ketamin, 100 mg/mL), and 6.25 mL Rompun® (xylazinhydrochloride, 20 mg/mL). Intraoperative anesthesia was maintained by intravenous administration of Propofol (10 mg/mL, 1 mL/kg/hour) and Fentanyl (0.05 mg/mL, 0.5 mL/kg/hour). The anesthesia and analgesia regimen used here is known not to affect hemostasis. Following anesthesia, pigs were intubated and ventilated with a mixture of 0.5 L oxygen/2.5 L air/min. Pigs were kept fully hydrated with infusion of lactated Ringer's solution (125 mL/hr).

Following anesthesia, the porcine spleen injury model was prepared. A midline abdominal incision was made to expose the spleen. The spleen injury was induced with a punch incision (8 mm wide and 3 mm deep). The bleeding intensity was evaluated on a 0 to 5 scale, where: level 0 indicates no bleeding (for at least 30 seconds), level 1 indicates no bleeding

initially followed by bleeding (within the first 30 seconds post injury), level 2 indicates bleeding (site filling in approximately 30 seconds), level 3 indicates bleeding (site filling in approximately 3 seconds), level 4 indicates bleeding (site filling immediately with no arterial or pulsating bleeding), and level 5 indicates bleeding (site filling immediately with arterial or pulsating bleeding). Only wounds classified as level 4 or 5 were utilized in this study. A new incision was created for each test sample (up to 16 samples were evaluated per pig). Immediately following bleeding intensity evaluation, the test sample (2 cm x 2 cm piece of film coated Surgifoam®, BPEI coated Surgifoam®, or untreated gauze, wet with 0.8 mL of 0.9% saline solution) was placed directly on the injury and even digital pressure was applied for 60 seconds. The site was monitored for up to 120 seconds. If bleeding was not observed in this time following compression, hemostasis was achieved. However, if bleeding occurred within the 120 seconds following compression, digital compression was applied again for 30 seconds, and the injury was monitored. Digital compression and observation were repeated until hemostasis was achieved (classified as 120 seconds free of bleeding) or until the test period reached 12 minutes (classified as an ineffective sample). The final result of time to hemostasis was defined as the total testing time to achieve hemostasis minus the final hemostasis evaluation period. Pigs were euthanized with intravenous pentobarbital (300 mg/mL, 0.1 mL/kg) at the completion of the study.

6.2.5 Statistical Analysis

Film properties on silicon substrates and Surgifoam® coating morphology and absorption capabilities were evaluated for a minimum of three samples per each bilayer number. *In vitro* activity testing was conducted for a minimum of three samples per bilayer number. *In vivo* activity was monitored for 9 samples per each bilayer number and 9 controls. All data presented here is represented as mean ± standard deviation of these multiple trials. Data fitting and analysis were conducted using GraphPad Prism 5 software.

6.3 Results and Discussion

6.3.1 Determining Film Architecture

To create thin hemostatic coatings, we sought to incorporate an essential clotting factor, thrombin, into a layer-by-layer assembled thin film. Thrombin is a large protein with molecular

weight of approximately 36 kDa [146] and an isoelectric point reported to lie between 7.0 and 7.6 [148, 149]. Additionally, thrombin has been shown to degrade rapidly at conditions far from physiologic pH [149]. Therefore, deposition of thrombin in an LbL film is limited to physiologic pH conditions, where thrombin is relatively neutral. Several amino acids in the thrombin protein along with peptide bonds are capable of forming hydrogen bonds. As electrostatic interactions would be unlikely to promote thrombin incorporation into a multilayer film at physiologic pH, we explored hydrogen bonding interactions as an alternative. Additionally, hydrogen bonding has been shown to contribute in the growth of films containing globular proteins and weak polyacids depending on deposition pH [32]. Tannic acid is a polyphenol found in a variety of food products and stains, and approved by the US FDA. It is also known to have many beneficial biological properties, including antitumor, antibacterial, and antioxidant activity [147], as well as reported interactions with proteins [150]. For its relatively small size (1.7 kDa), tannic acid has an abundance of hydrogen bond donating phenolic groups, and a reported pKa near 8.5 [147]. It has recently been incorporated successfully in many hydrogen bonded LbL architectures and importantly for our application here, was shown to assemble successfully at physiologic pH [57, 147].

To test whether potential interactions between thrombin and tannic acid could be used to assemble multilayer films at physiologic pH where thrombin is stable, QCM-D was employed to monitor film growth. Two film architectures were attempted following an initial layer of BPEI deposition, namely: (thrombin/tannic acid)$_n$ and (mannitol/tannic acid)$_n$, up to $n = 5$. Both of these architectures were attempted due to the fact that the bovine thrombin powder used in these studies contains approximately 90% mannitol and 10% thrombin. The resulting frequency shift for a single harmonic is shown in Figure 6-1 for each of these attempted film architectures. Decreased frequency represents mass deposition. For the (thrombin/tannic acid)$_n$ architectures, there is a significant deposition of thrombin and tannic acid at each respective deposition step, with some desorption of material (increased frequency) during each wash step, signifying removal of a small amount of non-specifically bound material. The overall decrease in frequency at each step supports the formation of favorable hydrogen bonding interactions between tannic acid and thrombin at this deposition condition. In contrast, the (mannitol/tannic acid)$_n$ film does not appear to build. Although there is a small overall decrease in frequency for this particular architecture, at each mannitol deposition step, there is no change in frequency,

116

indicating no mass deposited. In fact, following the first tannic acid deposition step, every mannitol step acts like a wash step, removing some of the bound tannic acid. This result was expected, as mannitol consists of hydroxyl functional groups bound to an alkane backbone, which are strong hydrogen bond donors; tannic acid also consists primarily of strong hydrogen bond donors. This finding confirms that a (thrombin/tannic acid)$_n$ LbL film can be constructed successfully at pH 7.4, lacking interference from or incorporation of the mannitol excipient.
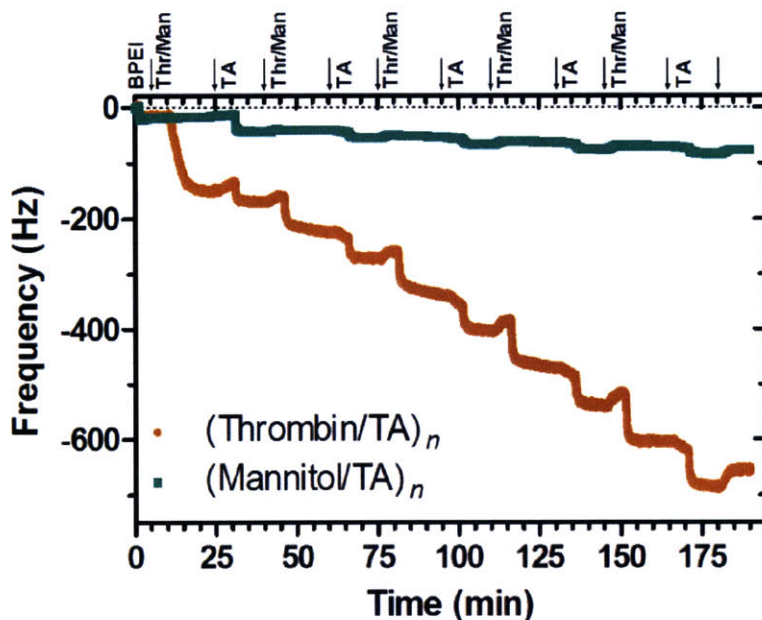
Figure 6-1: Film growth monitored by quartz crystal microbalance. The growth of two different architectures on a monolayer of BPEI are shown: (thrombin/tannic acid)$_n$ and (mannitol/tannic acid)$_n$. The start of BPEI, thrombin or mannitol, and tannic acid flow is indicated by labels above the graph, along with each PBS wash step indicated by an arrow.

6.3.2 Spray Film Assembly and Characterization

After confirming that thrombin and tannic acid indeed interact and are able to formulate a multilayer film, these films were constructed on flat substrates using the spray LbL assembly technique. Figure 6-2 shows the growth profiles of films sprayed upon a monolayer of BPEI with the architecture (thrombin/tannic acid)$_n$, for n = 10, 25, and 50. Additionally, the film thickness per bilayer for each growth region (0 to 10 bilayers, 10 to 25 bilayers, and 25 to 50 bilayers) is also shown in Figure 6-2. With increasing film growth, the change in thickness per bilayer decreases significantly, transitioning from approximately 11 nm/bilayer to 5 nm/bilayer from 10 to 25 bilayers, and from 5 nm/bilayer to 2 nm/bilayer from 25 to 50 bilayers. This

decrease in film thickness per bilayer number may result from the fact that tannic acid is a significantly smaller molecule compared to the large thrombin protein; with an increasing number of deposition steps, the tannic acid has a chance to interdiffuse significantly into the underlying film architecture [14, 52]. This interdiffusion can alter film architecture, promoting less thrombin adsorption at increasing bilayer numbers, translating directly to a lower increase in dry film thickness. Additionally, this decrease in thickness per bilayer with increasing number of bilayers may be due to incomplete reversal of hydrogen bonding functionality with each deposition step.
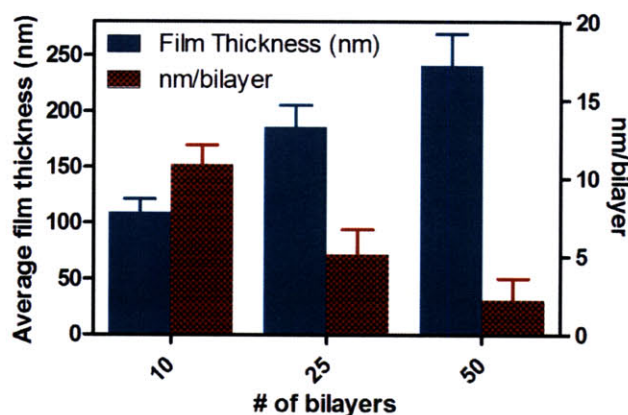
Figure 6-2: Thickness of sprayed (thrombin/tannic acid)$_n$ films for n = 10, 25, and 50. Both average film thickness and the change in thickness per bilayer are shown for each growth region (0 to 10 bilayers, 10 to 25 bilayers, and 25 to 50 bilayers).

This same decrease in thrombin adsorption at increasing n occurred at just 5 bilayers in the QCM-D growth of the same film architecture shown in Figure 6-1. The initial bilayer leads to a frequency drop of approximately 140 Hz, corresponding directly to the total mass of thrombin and tannic acid adsorbed in the first bilayer deposition. If this same drop in frequency were seen for the following 4 bilayers, a final change in frequency (following the BPEI deposition and wash step) of approximately 700 Hz would be expected. However, a total frequency drop of only approximately 630 Hz was observed. QCM-D film deposition is more representative of a dipped LbL film in which significantly longer deposition steps are needed to promote film growth compared to spray assembly, which often leads to a greater degree of interdiffusion in dipped films containing small molecules [14]. Therefore, dipped (thrombin/tannic acid)$_n$ films, might be expected to show a more dramatic decrease in film growth than what was observed for sprayed films and may even stop growing at a certain number of layers. Additionally, to confirm

the lack of mannitol involvement in thrombin film growth, a film with architecture (mannitol/tannic acid)$_{50}$ was sprayed using the same spray timings and conditions as the thrombin films. The result was highly non-uniform and patchy substrate coverage, with maximum thickness of approximately 18 nm in some areas, further confirming that mannitol does not interfere with thrombin film growth.

Figure 6-3 shows the morphology of these films measured via atomic force microscopy. In general, the RMS roughness values, shown in Table 1, which also summarizes the final film thicknesses, are found to increase with increasing film thickness. The RMS roughness values are approximately 28% to 40% of the final film thickness depending on bilayer number. In general, these films are quite rough in comparison to typical spray assembled films that contain small molecules and a variety of polymers, which are seen to have low roughness values in the range of just a few nanometers for films greater than 100 bilayers [14]. In previously assembled hydrogen bonded films formulated with block copolymer micelles and tannic acid, RMS roughness values of approximately 40% of the final film thickness were noted [57], which is comparable to the films developed here. These large roughness values may result from the fact that these films are comprised solely of a protein and a small molecule, which is in contrast to typical protein LbL assembly which usually contains several polymeric components [31, 34].
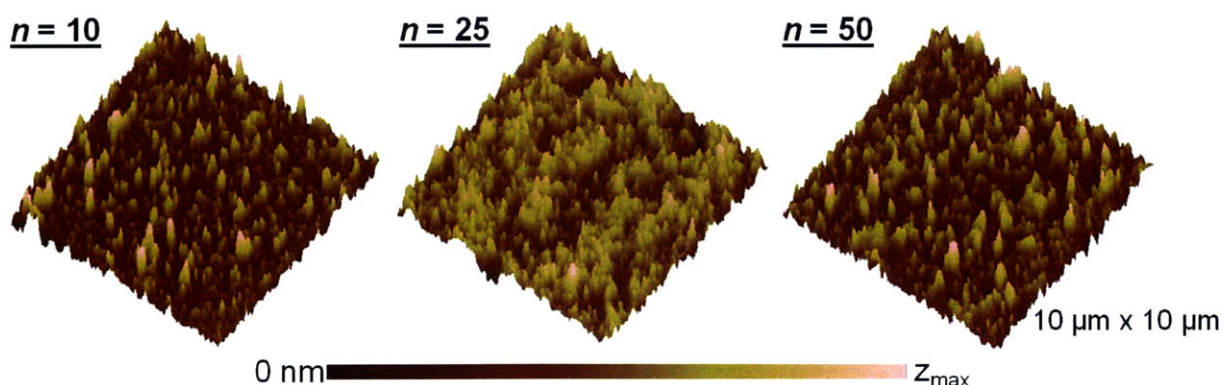

Figure 6-3: Sprayed (thrombin/tannic acid)$_n$ film morphology measured by atomic force microscopy for n = 10, 25, and 50. Each image is 10 μm x 10 μm, and z_{max} = 360 nm, 380 nm, and 440 nm for n = 10, 25, and 50, respectively.

Table 6-1: Sprayed (thrombin/tannic acid)$_n$ film characteristics.

Number of bilayers	$n = 10$	$n = 25$	$n = 50$
Average thickness (nm)	108.6 ± 12.4	185.6 ± 19.6	240.9 ± 28.4
RMS roughness (nm)	46.3 ± 3.7	51.9 ± 4.2	66.8 ± 11.5
Y_o (nm)	89.0	173.3	208.1
R^2	0.75	0.95	0.87
k (hours^{-1})	8.2×10^{-3}	7.5×10^{-3}	6.5×10^{-3}
Release $t_{1/2}$ (hours)	84.8	92.6	107.3

Following assembly of films at $n = $ 10, 25, and 50 bilayers, the dissolution of each of these films on flat substrates was examined. Figure 6-4 shows the absolute and normalized thickness over approximately 10 days in PBS. The following model for one-phase decay was fit to each of these data sets:

$$Y = Y_o e^{-kt}.$$

In this equation, Y is the film thickness, Y_o is the initial film thickness, t is the time, and k is the rate constant (hours^{-1}). By fitting this data, we estimated the dissolution rate constants for these films in PBS and the half-life for release ($t_{1/2}$). The Y_o, goodness of fit (R^2), k, and $t_{1/2}$, for $n = $ 10, 25, and 50, are given in Table 1.
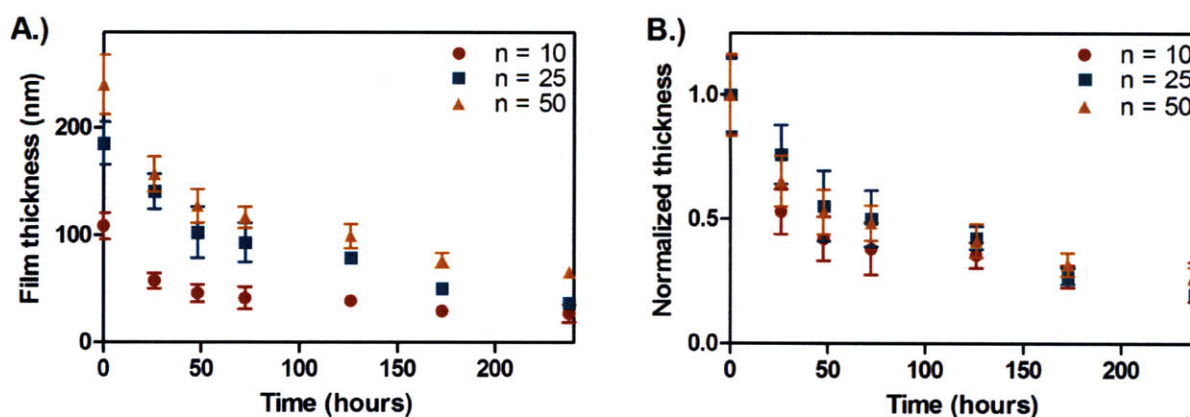

Figure 6-4: Sprayed (thrombin/tannic acid)$_n$ film degradation for $n = $ 10, 25, and 50. A.) Film thickness over time. B.) Normalized film thickness over time.

Overall, dissolution of these films is slow following the initial loss of approximately 25 to 47% of the film thickness in the first few hours of release. This can be expected as there is no

significant driving force for film dissolution at these release conditions (the same pH and ionic strength in which the films were initially assembled); release is simply diffusion based.

6.3.3 Film Activity

To enhance hemostatic capabilities of the absorbent gelatin sponge, Surgifoam®, the sponge is soaked in thrombin solution immediately prior to use, which can often waste crucial time [139]. In this work, we sought to prefunctionalize these sponges with our hemostat containing films, eliminating the need for sponge preparation prior to use. After characterizing the properties of these LbL films on flat substrates, the films were assembled on Surgifoam® using the vacuum spray assembly technique described in Chapter 5. Aerial scanning electron microscopy images of films assembled on these sponges at $n = 10$, 25, and 50 bilayers are shown in Figure 6-5 along with an uncoated sponge. Overall, the thin film is visible as a coating of the pores, but the underlying sponge architecture is completely maintained. A quick test of PBS absorption in each of these coated sponges compared to uncoated sponges, did not lead to any notable change in sponge absorption compared to uncoated sponges. This is in contrast to the increased absorption of Surgifoam® coated with antibiotic containing films described in Chapter 5, which were significantly thicker than the thrombin films developed here and shown to be significantly hydrophilic compared to the Surgifoam®.
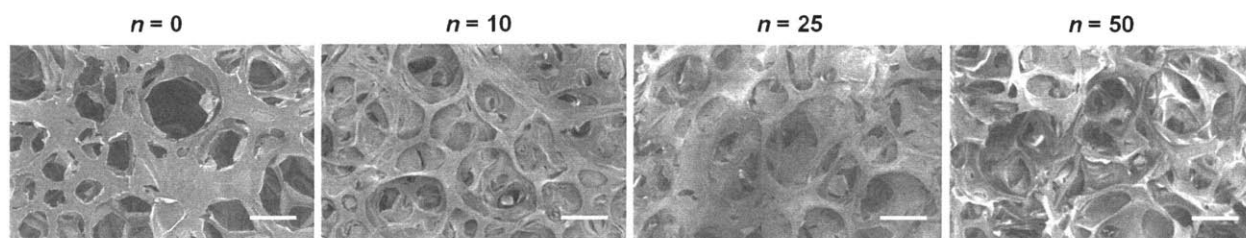
Figure 6-5: Sprayed (thrombin/tannic acid)$_n$ coated Surgifoam® morphology for $n = 0$, 10, 25, and 50 (scale bar = 200 μm).

Following spray coating of the LbL film architecture on the Surgifoam®, the activity of these sponges was tested both *in vitro* and *in vivo*. *In vitro*, films were soaked in buffer solution and activity was monitored by looking at fibrin clot formation upon exposing this solution to fibrinogen. Activity was monitored after soaking the coated sponge for various times ranging from 10 minutes up to 6 days. No change in film activity was seen over this time which may be attributed either to the very slow dissolution of these films or the possibility that all of the

thrombin releases rapidly. Figure 6-6 shows the activity of the solution in which coated sponges were soaked for 10 minutes expressed in both international units (IU) per milligram of sponge and IU per square centimeter of sponge. Additionally, Figure 6-6 shows a plot of activity simultaneously with increasing film thickness; the activity increases in a similar manner to the film thickness as expected. The activity seen at each of the three bilayer numbers are clinically relevant, where 1 IU of thrombin activity is known to clot 1 mL of plasma in 15 seconds [151, 152].
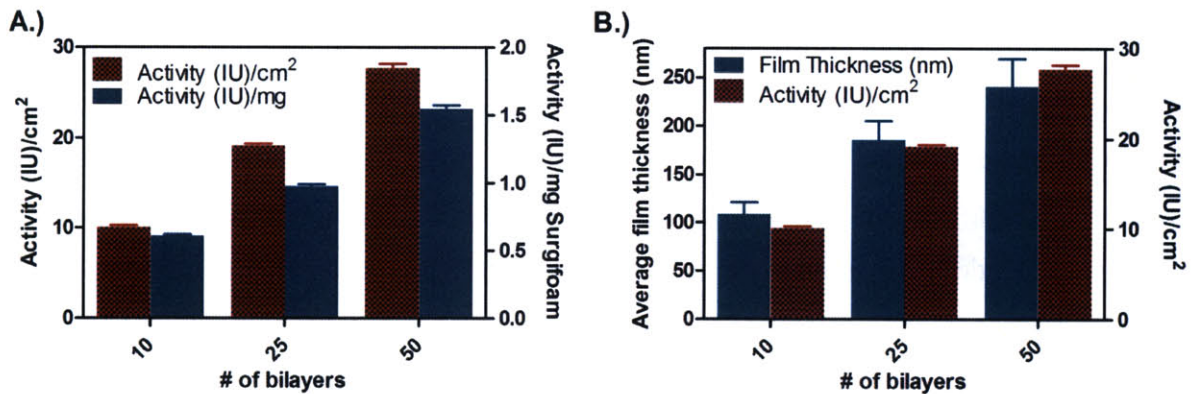
Figure 6-6: Activity of film coated Surgifoam® at *n* = 10, 25, and 50. A.) Activity expressed as international units (IU) per square centimeter of coated Surgifoam® and IU per milligram of Surgifoam®. B.) Flat surface film thickness and activity of coated Surgifoam® (IU/cm^2). Activity data was provided by Ferrosan (Soeborg, Denmark).

To examine the *in vivo* activity of these films, coated Surgifoam® sponges were tested in a porcine spleen bleeding model. As controls, a sponge coated with a monolayer of BPEI and uncoated gauze were also tested. A representative surgery image and the results of this study are shown in Figure 6-7. The results for application of the uncoated gauze control are not shown in Figure 6-7B; these samples did not promote any hemostasis over the 12 minute test period. From Figure 6-7B, we can see the results for time to hemostasis for each of the three bilayer formulations and the BPEI control. Once the test sample was placed on the bleeding wound, 60 seconds of digital compression was always applied. Following this initial compression, it can be seen that none of the three bilayer formulations required any additional time or compression to promote hemostasis. The wound had essentially stopped bleeding during the 60 second compression period. For the BPEI control, however, an additional 104 ± 27 seconds were needed to stop bleeding from the wound, including an additional 30 second compression period

following the first compression. The potential differences between each of the varying bilayer number coatings could not be differentiated in this *in vivo* assay, most likely due to the standard 60 second compression period and/or the positive feedback of thrombin. However, from *in vitro* assays, we know that there are varying concentrations of thrombin in these films as expected based on studies of film growth, morphology, and degradation. Overall, all of the film coated sponges act instantaneously following the initial compression, with greatly enhanced activity compared to a BPEI coated sponge control which requires additional compression and time to reach hemostasis. Therefore, the (thrombin/tannic acid)$_n$ film architecture appears to be highly promising in promoting hemostasis in a clinically relevant animal model at as few as 10 bilayers.
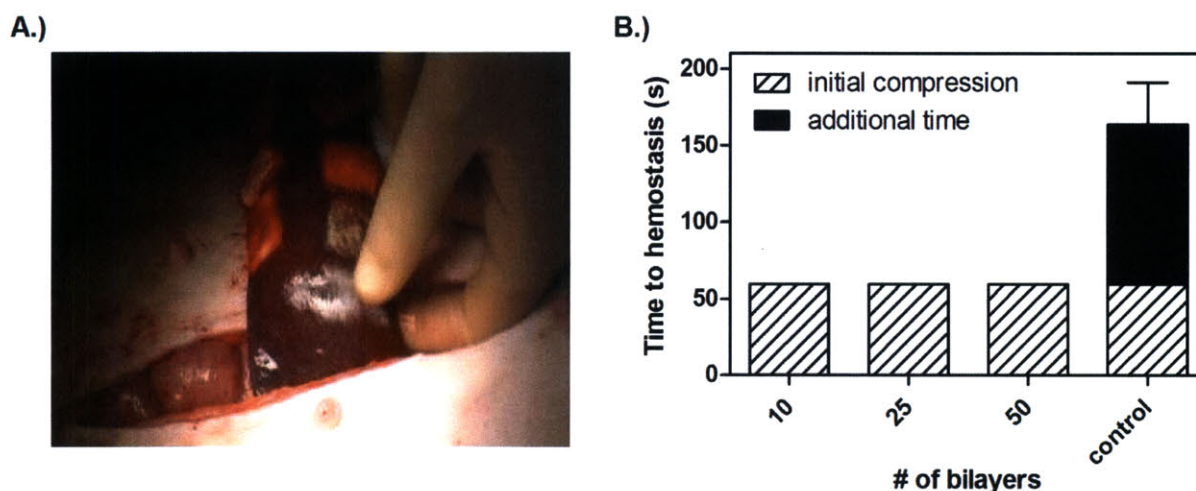
Figure 6-7: *In vivo* **activity of (thrombin/tannic acid)**$_n$ **coated Surgifoam® for** *n* **= 10, 25, and 50, and BPEI control in a porcine spleen bleeding model. A.) Representative image of the porcine spleen bleeding model. B.) Time to hemostasis following sample application. Figure data provided by Ferrosan (Soeborg, Denmark).**

6.4 Conclusions

In this work, we have formulated a novel multilayer film aimed at promoting hemostasis, by using the spray LbL assembly technique. In contrast to traditional multilayer films, our architecture does not contain any polymeric component. The films were formulated based on novel interactions found to exist between a clotting factor, thrombin, and a small polyphenol, tannic acid at physiologic pH. Each of these materials is FDA approved, making these films amenable to rapid clinical translation. We demonstrated the practical applicability of these films to a clinically relevant absorbent gelatin sponge, Surgifoam®. The efficacy of these sponges

was shown in a porcine spleen bleeding model, where film coated sponges instantaneously promoted hemostasis following a short digital compression period. Due to the versatility of the spray LbL assembly technique, these films have the potential to be used on a variety of substrates like Surgifoam® to address the unmet challenge of promoting rapid hemostasis at complex wound sites which are not amenable to traditional mechanical methods of bleeding control.

Chapter 7

Effects of Side Group Functionality and Molecular Weight on the Activity of Synthetic Antimicrobial Polypeptides

7.1 Introduction

Infectious diseases cause serious complications in a wide range of medical procedures. The severity of these infections is augmented by two primary factors: (1) biofilm formation and (2) drug-resistant bacteria [153]. Several methods for controlling the formation and growth of biofilms have been proposed; however, the use of appropriately functionalized surfaces that prevent the critical step of microbial attachment on an implant may be the most effective method for preventing biofilm formation entirely. Along with chronic infection due to biofilms, drug resistance in planktonic bacteria is a prominent factor that is making treatment of infections increasingly more difficult [65]. The systemic overuse of broad-spectrum antibiotics has led to a severe rise in multi-drug resistant bacteria over the last several decades. Compounded by a lack of discovery and approval of new classes of antibiotics, there is a pressing need for the development of novel antimicrobial agents [65, 153].

The use of naturally occurring antimicrobial peptides (AmPs) for infection treatment is being explored as a new class of therapeutics [13, 98]. These cationic peptides are part of the eukaryote immune system and are highly broad-spectrum, active against Gram-positive, Gram-negative, and drug-resistant bacteria, as well as fungi and viruses. Several modes of AmP activity have been proposed, all suggesting a low propensity for the development of resistance [69, 70]. Additionally, AmPs have been shown to act rapidly [154] prevent biofilm formation,[8] and be successfully incorporated and released from polymer multilayers [13, 72, 155]. Despite their therapeutic potential for infection control, the practical applicability of AmPs is thus far limited. AmP production methods are traditionally expensive and are implicated as the principal obstacle in preventing widespread AmP use [154]. Additionally, significantly larger doses of

AmPs are required for activity comparable to conventional antibiotics; however, at these large concentrations, AmPs have been shown to induce toxicity in mammalian cells [13, 81, 95, 154]. The cost-effective and efficient development of novel AmPs which yield comparable activity to natural AmPs and have a high degree of biocompatibility, will ultimately allow for clinical translation of these promising therapeutics.

Cationic polymers can be selectively designed to exhibit high levels of antimicrobial activity, are relatively inexpensive to synthesize, and can be produced on a large scale [153]. To design these antimicrobial polymers, typically a combination of cationic and hydrophobic groups are dispersed along a polymer backbone [156-160], or hydrophobic long chain N-alkylated quarternary ammonium groups are utilized [17, 18, 161-163]. It is hypothesized that the quaternary amine polymers function by interacting with the bacterial membrane, which leads to loss in membrane integrity and cell death. Several polymers synthesized utilizing these strategies, including polyethyleneimines [17, 18, 161, 164], polymethacrylates [156, 163], polydiallyammonium salts [16, 162, 165], polyarylamides [157, 158], protonated polystyrenes [166], and polynorbornenes [167], have shown a high degree of antimicrobial activity; however these polymers are non-biodegradable and in some cases, cytotoxic, rendering them unsuitable for many biomedical applications. Alternatively, it was recently demonstrated that synthetic antimicrobial polypeptides can be synthesized by the ring opening polymerization (ROP) of the N-carboxyanhydrides (NCA) of cationic (lysine) and hydrophobic (alanine, phenylalanine, or leucine) amino acid residues, creating a biodegradable synthetic AmP mimic. These polymers showed antimicrobial activity comparable to naturally occurring AmPs but have a high degree of hemolytic activity [159], making them unsuitable for systemic administration.

We recently introduced a new strategy to synthesize polypeptides that can be quantitatively modified with a broad range of side functional groups through the direct ring opening polymerization (ROP) of γ-propargyl-L-glutamate to generate poly(propargyl-L-glutamate) (PPLG) and the subsequent alkyne-azide cycloaddition click reaction of substituted alkynes [168, 169]. This strategy of a clickable polypeptide backbone was first used to synthesize densely grafted polypeptide brushes and, more recently, glycopeptides with near quantitative side group functionalization [168, 170]. This paper reports the first use of clickable polypeptides for synthesizing antimicrobial agents. As a promising alternative to currently existing antimicrobial polymers, we have synthesized and characterized a library of synthetic

cationic homopolypeptides that mimic naturally occurring AmPs, shown in Figure 7-1. The new antimicrobial polypeptides range in length from 30 to 140 repeat units and they have varied side group functionality, including primary, secondary, tertiary, and quaternary amines with hydrocarbon side chains ranging from 1 to 12 carbons long. Table 7-1 summarizes the polymers investigated and indicates whether they were tested for coating applications and/or solution antimicrobial activity. We have denoted the quaternary amine polypeptides as QCn, where Q indicates that the amine is quaternary and Cn indicates a carbon side chain of length n. The effect of the side chain functionality and the polypeptide length was evaluated using a modified microdilution assay to determine the minimum inhibitory concentration (MIC), or the lowest point at which visible bacteria growth is inhibited [104], against a model Gram-negative (*Escherichia coli K-1*) and a model Gram-positive bacteria (*Staphylococcus aureus* 25923). A bacteria attachment assay was also carried out on polypeptide coatings to evaluate their potential efficacy for use as antimicrobial surface coatings. As an initial measure of biocompatibility, red blood cell (RBC) lysis was monitored in the presence of these polypeptides.
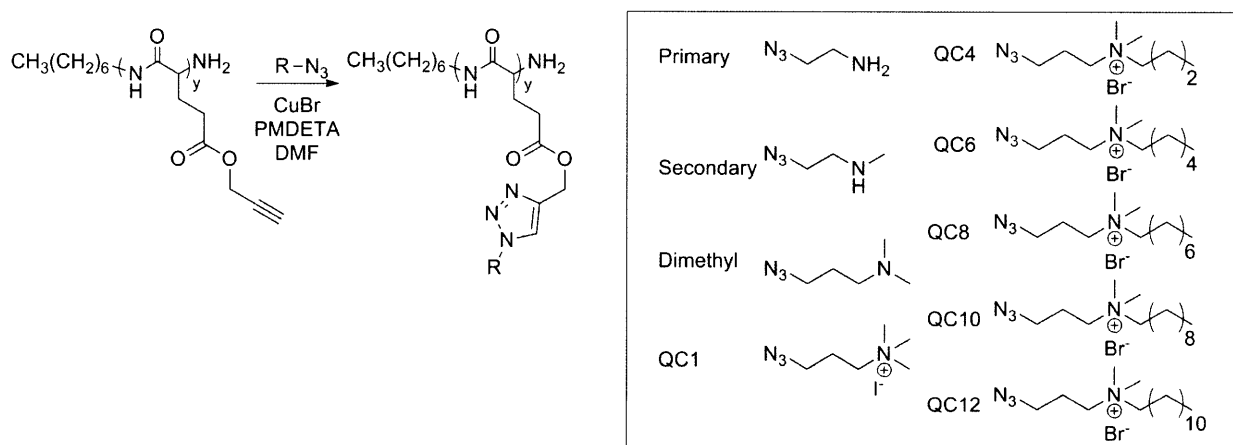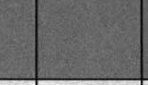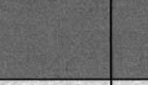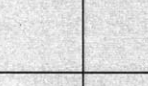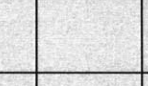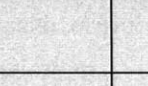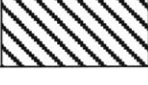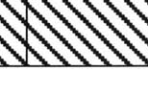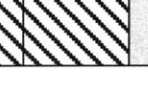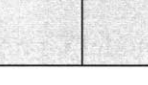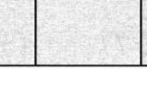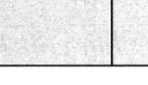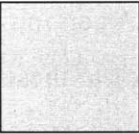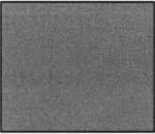

Figure 7-1: Alkyne-azide cycloaddition click functionalization of PPLG and various amine side groups. The abbreviation Q indicates that the amine is quaternary and Cn indicates a carbon chain length with n repeat units.

Table 7-1: Summary of polypeptides tested.[a]

DP	Primary	Secondary	Tertiary	Quaternary					
				QC1	QC4	QC6	QC8	QC10	QC12
30									
56									
75									
140									

Tested for MIC

Tested for MIC and coatings

Not tested

[a]Here DP is the degree of polymerization of the polypeptide. Primary, secondary, tertiary, and quaternary represent the degree of the amine functionalized side chains. For polypeptides defined as QCn, Q = quaternary and Cn = carbon side chain length of n.

7.2 Materials and Methods

7.2.1 Polypeptide Synthesis and Physical Characterization

7.2.1.1 Materials

L-(+)-glutamic acid, 99% minimum was purchased from EMD Chemicals (Gibbstown, NJ). 3-dimethylaminopropylchloride hydrochloride, 99% was purchased from Acros Organics (Geel, Belgium). All other chemicals were purchased from Sigma-Aldrich (St. Louis, MO). All materials were used as received.

7.2.1.2 General Experimental Methods

^{1}H-NMR and ^{13}C NMR were recorded on Bruker 400 MHz FT-NMR spectrometers. Fourier transform infrared (FTIR) spectra were recorded on a Thermo Nicolet NEXUS 870 series spectrophotometer. Atomic force microscopy images were taken with a Dimension 3100

scanning probe microscope (Veeco). Polymer film thicknesses were obtained using a Dektak 150 surface profiler (Veeco). Gel permeation chromatography measurements were carried out using a Waters' Breeze 1525 HPLC system equipped with two Polypore columns operated at 75°C, series 2414 refractive index detector, series 1525 binary HPLC pump, and 717 plus autosampler. Waters' Breeze Chromatography Software Version 3.30 was used for data collection as well as data processing. DMF with 0.01M LiBr was the eluent for analysis, and samples were dissolved at 4-6 mg/mL in DMF. The average molecular weight of the sample was calibrated against narrow molecular weight poly(methyl methacrylate) standards. Circular dichroism (CD) spectroscopy of polymer solution was carried out by using an Aviv model 202 CD spectrometer. Measurements were performed at $25 \pm 0.1°C$, sampling every 1 nm with a 3 s averaging time over the range of 195–260 nm (bandwidth = 1.0 nm). Measurements were taken using a cell with a 1 mm path length.

7.2.1.3 Synthesis of Poly(γ-propargyl L-glutamate)

PPLG was synthesized as previously described [168, 169]. Briefly, L-(+)-glutamate was reacted with propargyl alcohol to form γ-propargyl L-glutamate, using chlorotrimethylsilane [171]. The NCA ring was formed by reacting γ-propargyl L-glutamate with triphosgene [172]. PPLG was prepared by ROP of γ-propargyl L-glutamate NCA, initiated with heptylamine. The reaction was performed in DMF at room temperature and the polymer was recovered by precipitation into diethylether.

7.2.1.4 Synthesis of Amino Azides

Primary, secondary, and tertiary amino azides were synthesized as previously described [169, 173]. The quaternary amines were prepared following the protocol presented by Vial et al [174]. Briefly, in a typical experiment, 3-azido-N,N-dimethylpropan-1-amine (0.5 g, 3.9 mmol) was dissolved in methanol (5 mL) and added to the haloalkane (bromododecane 0.88 g, 3.54 g) dissolved in methanol (5 mL). The reaction mixture was refluxed for 20 hours and then cooled to room temperature. The methanol and any unreacted 3-azido-N,N-dimethylpropan-1-amine was removed under high vacuum. QC12 ^{1}H-NMR (400MHz, CDCl$_3$) δ=3.71 (m, 2H, CH$_2$N), 3.56 (t, 2H, N$_3$CH$_2$), 3.46 (m, 2H, NCH$_2$), 3.40 (s, 6H, CH$_3$), 2.04 (m, 2H, CH$_2$), 1.70 (m, 2H, CH$_2$), 1.33 (m, 2H, CH$_2$), 1.23 (m, 18H, (CH$_2$)$_9$), 0.85 (t, 3H, CH$_3$). QC8 ^{1}H-NMR (400MHz, CDCl$_3$) δ=3.66 (m, 2H, CH$_2$N), 3.54 (t, 2H, N$_3$CH$_2$), 3.43 (m, 2H, NCH$_2$), 3.36 (s, 6H, CH$_3$),

2.01 (m, 2H, CH$_2$), 1.68 (m, 2H, CH$_2$), 1.31 (m, 4H, CH$_2$CH$_2$), 1.23 (m, 6H, (CH$_2$)$_3$), 0.82 (m, 3H, CH$_3$). QC4 ^{1}H-NMR δ=3.66 (m, 2H, CH$_2$N), 3.55 (t, 2H, N$_3$CH$_2$), 3.49 (m, 2H, NCH$_2$), 3.33 (s, 6H, CH$_3$), 2.01 (m, 2H, CH$_2$), 1.66 (m, 2H, CH$_2$), 1.37 (m, 2H, CH$_2$), 0.94 (m, 3H, CH$_3$) (400MHz, CDCl$_3$). QC1 ^{1}H-NMR (400MHz, D$_2$O) δ=3.50 (t, 2H, N$_3$CH$_2$), 3.45 (m, 2H, NCH$_2$), 3.15 (s, 9H, CH$_3$), 2.10 (m, 2H, CH$_2$).

7.2.1.5 Synthesis of Amino Functionalized PPLG

A typical procedure started with a feed ratio of alkyne/azide/CuBr/N,N,N',N',N''-pentamethyldiethylenetriamine (PMDETA) equal to 1/1.2/0.1/0.1 for primary, secondary, tertiary, and QC1 amines and a feed ratio of 1/1.1/0.1/0.1 for QC4-QC12. PPLG (0.050 g, 0.299 mmol alkyne repeat units), amino azide (0.124 g, 0.329 mmol QC12 azide), and PMDETA (6.25 µL, 0.0299 mmol) were all dissolved in DMF (3 mL). After the solution was degassed, the CuBr catalyst (0.0043 g, 0.0299 mmol) was added and the reaction solution was stirred at room temperature. Once the reaction was complete, the reaction solution was purified by dialysis against water acidified by HCl (pH < 4) for 2-3 days to remove excess amino azide and copper catalyst. The polymer structure was verified by ^{1}H-NMR.

7.2.1.6 Water Solubility and Substrate Coating Experiments

All polypeptides were tested for their water solubility characteristics. Each polypeptide (50 mg) was placed in a glass vial and water (1 mL) was added. The polymers were agitated at 37°C. Upon visual inspection for clouding or precipitation, polypeptide solubility was determined. For coating experiments, the QCn (n ≥ 4) polypeptides were dissolved at 5 mg/mL in methanol. These polymers were solvent cast by applying 75 µL of polymer solution to each side of a round glass cover slip (VWR, West Chester, PA) and allowing the substrates to dry. Following this, the thickness of each solvent cast polymer film was obtained. Surface morphology was characterized using atomic force microscopy. Coated substrates and uncoated control samples were subsequently placed in 3 mL of bacteria culture media for 2 hours at 37°C. Following incubation, substrates were removed, rinsed with DI-water, and dried. Film thickness and surface morphology was examined again.

7.2.2 Polypeptide Antimicrobial Characterization

7.2.2.1 Materials

Staphylococcus aureus 25923 (*S. aureus*) and *Escherichia coli K-12* (*E. coli*) were obtained from ATCC (Manassas, VA) and the *E. coli* Genetic Stock Center (New Haven, CT), respectively. Cation-adjusted Mueller Hinton Broth (CaMHB), LB-Miller Broth (LB), Bacto agar, and trypticase soy agar plates (w/ 5% sheep blood) were obtained from BD Biosciences (San Jose, CA). Bovine RBCs were obtained from Innovative Research (Novi, MI). Trizma hydrochloride buffer and ultrapure distilled water were obtained from Sigma-Aldrich (St. Louis, MO) and Invitrogen (Carlsbad, CA), respectively. Triton-X 100 was purchased from Electron Microscopy Sciences (Hatfield, PA).

7.2.2.2 General Experimental Methods

A BioTek PowerWave XS plate reader was used for all 96 well plate absorbance measurements. Samples in all experiments were tested in triplicate; experiments were repeated a minimum of three times. All error bars reported are standard deviations of these experimental repeats.

7.2.2.3 Bacterial Growth Inhibition

Bacterial growth inhibition was examined to determine MIC values for the polypeptides. Bacterial growth inhibition for primary, secondary, tertiary, and QC1 polypeptides was monitored using a modified microdilution assay, as described in Chapter 2 and 3 [13, 14]. To summarize, polypeptide samples were serially diluted in a 96 well clear bottom plate in DI-water upon sterile filtration (0.2 μm pore size); the range of concentrations tested spanned from 70 – 4500 μg/mL. QCn (n$\geq$ 4) polypeptides were dissolved and diluted in methanol. The methanol was allowed to evaporate, leaving a polymer coating on the surface; the range of concentrations tested spanned from 20 – 2500 μg/mL (corresponding to a surface density of average mass of polymer per unit area of 6.1 – 780 μg/cm^2 calculated by dividing the total polymer mass in the well by the surface area of the well). This method of sample preparation was selected to mirror the attachment assay sample preparation outlined below. Bacteria (*S. aureus* or *E. coli*) were added to these wells in their exponential growth phase at a final concentration of 10^5 CFU/mL. Positive controls with no polypeptide and only bacteria treatment and negative controls with no

bacteria (containing only CaMHB or LB) were included on each plate. Plates were incubated at 37 °C for 16-18 hours with constant shaking. Following incubation, the absorbance of each well was read at 600 nm for *S. aureus* and 540 nm for *E. coli*. Normalized bacteria density was calculated as follows:

$$Normalized\ Bacteria\ Density = \frac{(Sample\ Abs - Negative\ Control\ Abs)}{(Positive\ Control\ Abs - Negative\ Control\ Abs)}.$$

7.2.2.4 Bacterial Attachment Inhibition

Inhibition of bacterial attachment to QCn ($n \geq 4$) polypeptide coatings was assessed as previously described in Chapter 2 [13]. Briefly, solvent cast polypeptide substrates were prepared by dissolving these polymers at a concentration of 5 mg/mL in methanol and evenly coating round glass cover slips with a 12 mm diameter (VWR, West Chester, PA) yielding a final polypeptide coverage of 330 μg/cm^2 upon drying. These samples were incubated at 37°C in either *S. aureus* or *E. coli* suspensions at a concentration of 10^6 CFU/mL for 2 hours. Controls of uncoated substrates were also incubated in these bacteria suspensions. Following incubation, substrates and controls were removed and rinsed briefly in three separate sterile water baths and placed immediately on trypticase soy agar plates (w/ 5% sheep blood). These agar plates were incubated at 37 °C for 16-18 hours. The presence of colonies upon incubation was monitored via digital imaging.

7.2.2.5 Polymer Hemolytic Activity

Bovine RBC hemolysis was monitored as a measure of polypeptide biocompatibility adapted from previously reported protocols [159, 175]. Polypeptide samples were prepared for testing by dissolving in tris buffer (10 mM tris hydrochloride, 150 mM sodium chloride) for primary, secondary, tertiary, and QC1 polymers and methanol for QCn ($n \geq 4$) polymers. Samples were added in triplicate to a 96 well clear bottom plate and serial diluted (100 μL final volume in each well), with a concentration range of 39 to 5000 μg/mL. For QCn ($n \geq 4$) polymers, solutions were allowed to evaporate, leaving a thin polymer coating on each well with surface coverage ranging from 12.2 - 1560 μg/cm^2. Negative controls of untreated wells and positive controls of 1% triton-X solution were added to control wells in each plate. Upon evaporation of methanol for QCn ($n \geq 4$) polypeptides, tris buffer (100 μL) was added to each well. Bovine RBCs (5% in tris buffer) were added to each sample and control wells (100 μL).

These plates were subsequently incubated with agitation at 37°C. Following incubation, plates were centrifuged at 1000 RPM for 5 minutes. Samples (75 μL) were transferred to a fresh 96 well clear bottom plate and the absorbance of each well at 540 nm was determined. Final normalized hemolysis was calculated as follows:

$$Normalized\ Hemolysis = \frac{(Sample\ Abs_{540} - Negative\ Control\ Abs_{540})}{(Positive\ Control\ Abs_{540} - Negative\ Control\ Abs_{540})}.$$

7.3 Results and Discussion

7.3.1 Antimicrobial Polypeptide Synthesis

To design and synthesize a family of antimicrobial synthetic polypeptides that mimic naturally occurring AmPs, we systematically varied the amino side chain functionality and polymer chain length of PPLG to determine the optimal polymer composition for the growth inhibition of both Gram-negative and Gram-positive bacteria as well as the prevention of biofilm formation by these bacteria. PPLG at four different degrees of polymerization (DP) from 30 to 140 repeat units was synthesized as previously described [168]. Figure 7-2A shows a representative ^{1}H-NMR spectrum of PPLG (DP = 140) which confirms the polymer structure. GPC traces of the PPLG backbone indicate that these polymers have a narrow molecular weight distribution with polydispersities (PDI) between 1.09 and 1.25, as shown in Figure 7-3. Various amine functional groups were coupled to the PPLG using the copper catalyzed alkyne-azide cycloaddition click reaction, shown in Figure 7-1. ^{1}H-NMR was used to confirm the coupling efficiency of the click reaction. Representative ^{1}H-NMR of QC1 and QC6 substituted PPLG (DP = 140) compared to the ^{1}H-NMR of PPLG (DP = 140) are shown in Figure 7-2. In all cases, the coupling efficiency of the click reaction was near quantitative, as indicated by the disappearance of the PPLG alkyne peak (a, 3.4 ppm) and ester peak (b, 4.7 ppm) in Figure 7-2A and the appearance of a new ester peak (k, 5.2 ppm) in Figures 7-2B and 7-2C. Furthermore, the peak integration for all samples tested was as expected for near quantitative substitution. For polymers analyzed in D_2O, the original backbone peak (d, 2.0 ppm) did not overlap with the newly added side chains. This peak was used to determine the percent conversion of alkyne to triazole ring. For example, in Figure 7-2B, the integration of the backbone peak (d, 2.0 ppm) was compared to the integration of the triazole peak (m, 8.1 ppm) giving a substitution of 99.3%. When comparing the integration to other peaks, the substitution rate ranged from 94.4-99.7%.
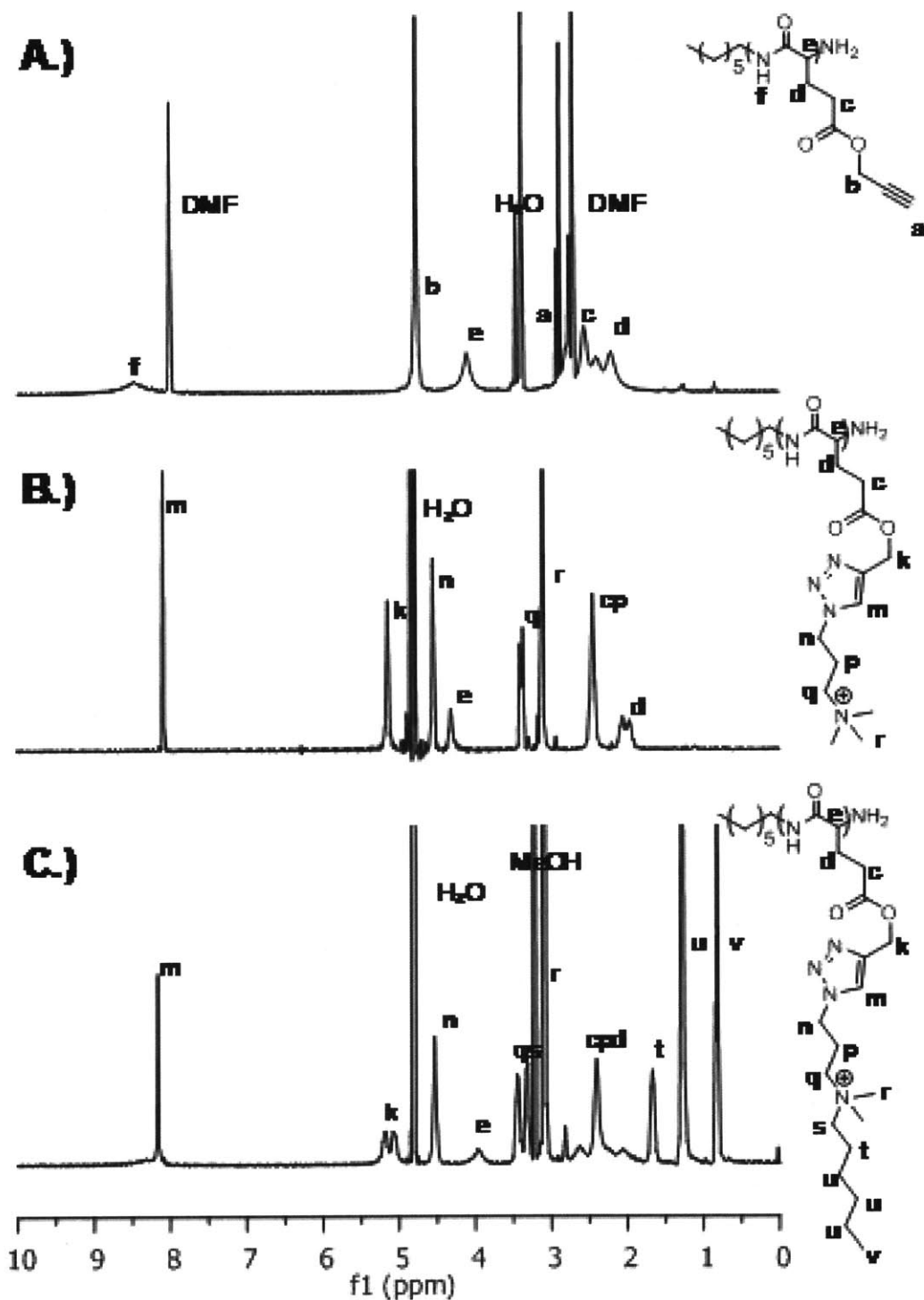
Figure 7-2: A.) ¹H-NMR spectrum of PPLG (DP = 140) in d₇ DMF. B.) ¹H-NMR spectrum of PPLG (DP = 140) functionalized with QC1 in D₂O. C.) ¹H-NMR spectrum of PPLG (DP = 140) functionalized with QC6 in CD₃OD.
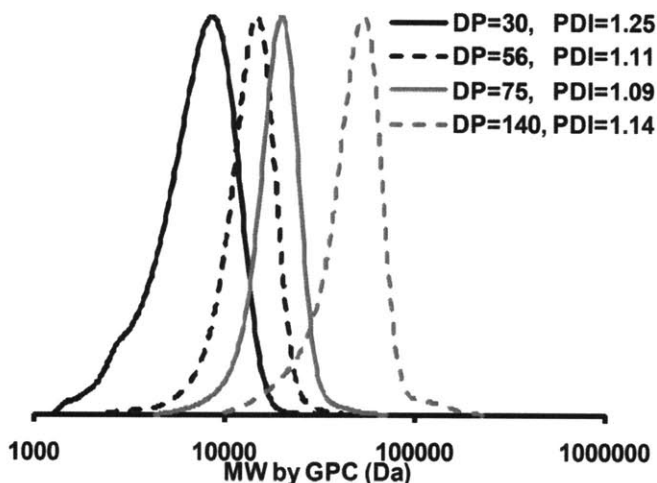
Figure 7-3: Molecular weight distribution of PPLG obtained using a DMF GPC and calculated using PMMA standards. The degree of polymerization was determined by ^{1}H-NMR.

Table 7-1 summarizes the polymers synthesized and how they were tested. To determine how to best test these polymers, water solubility and substrate coating experiments were performed. The water solubility of all polypeptides (except QC12 which is completely water insoluble) was determined to be greater than 50 mg/mL which was assumed to exceed what is necessary for MIC testing. Substrate coating experiments were performed to determine if these polymers are candidates for anti-biofilm coatings. Although, they have high water solubility, the QCn (n≥ 4) polymers also have surfactant like properties, c ausing them to readily adhere to surfaces. Glass substrates were coated by solvent casting these polymers from a methanol solution at a set concentration and dry film thicknesses were measured. Following exposure to bacteria culture media, film thicknesses were measured again. A significant amount of smooth polymer film remained on the substrate, which was estimated to be equivalent to at least 30 monolayers of packed polypeptide. A detailed discussion of this calculation as well as the thickness measurements can be found in Appendix C. Based on the solubility and surface adsorption characteristics, the primary, secondary, tertiary, and QC1 polymers were tested for bacteria growth inhibition using the microdilution assay, and QCn (≥ 4) polymers were t ested for both bacteria growth inhibition and activity against bacteria attachment. Several of these polymers have potential for use in systemic or localized antimicrobial delivery applications; the QCn (n≥ 4) polymers may be suitable for semi -permanent antimicrobial coatings on medical devices.

7.3.2 *Bacterial Growth Inhibition*

We quantified the activity of all polypeptides synthesized in this work against two classes of bacteria that are commonly associated with infection. *S. aureus* and *E. coli* were chosen as model Gram-positive and Gram-negative bacteria, respectively. The effect of the polypeptides on the inhibition of bacterial growth was examined using a modified liquid microdilution assay for the primary, secondary, tertiary, and QC1 polypeptides as highlighted in Table 7-1. For the purposes of this work, we have expressed MIC as a polypeptide concentration range over which bacteria density normalized to a positive control of untreated bacteria and a negative control of growth media is found to decrease from greater than or equal to 0.1 to less than or equal to 0.02 (where 1.0 indicates the positive control). Samples that did not exhibit a significant decrease over the polypeptide concentration range of 70 – 4500 µg/mL and maintained a normalized bacteria density ≥ 1.0 at the highest tested concentration were defined as inactive. Figures 7-4A and 4B show the results of this assay for the primary amine functionalized polypeptides of varying molecular weight for *S. aureus* and *E. coli*, respectively. As seen in Figure 7-4A, there is a clear molecular weight dependence on *S. aureus* growth inhibition, for which the lowest molecular weight primary amine polypeptide (DP = 30) shows no *S. aureus* inhibition and the highest molecular weight (DP = 140) is the most active, with a MIC between 70.3 – 140.6 µg/mL. This MIC for *S. aureus* is comparable and in some cases lower than many highly effective naturally occurring antimicrobial peptides, including cecropin A and B, magainin 1 and 2, and defensin [158, 159]. Table 7-2 summarizes the MIC for the primary, secondary, tertiary, and QC1 polypeptides tested against *S. aureus* as well as the normalized bacteria inhibition at the highest polypeptide concentration tested, 4500 µg/mL. Along with the highest molecular weight primary amine, the highest molecular weight secondary amine polypeptide also exhibits an MIC for *S. aureus* that is comparable to natural AmPs, between 140.6 – 281.3 µg/mL. The tertiary and quaternary (QC1) amine samples do not show any significant *S. aureus* growth inhibition.
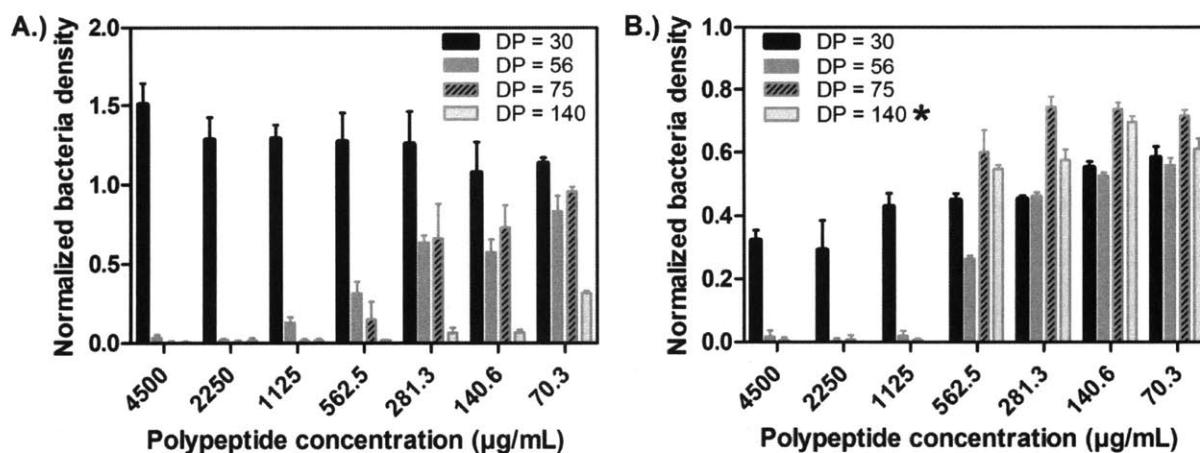
Figure 7-4: Bacteria growth inhibition for primary amine functionalized polymers based on normalized turbidity measurements. A.) *S. aureus* normalized bacteria density at varying polymer concentrations. B.) *E. coli* normalized bacteria density at varying polymer concentrations (*high turbidity was observed for DP = 140 polypeptides at concentrations of 4500 – 1125 µg/mL due to polypeptide precipitate forming; in these cases, however, complete bacteria growth inhibition was observed based on clear solution surrounding the polypeptide precipitate).

Table 7-2: *Staphylococcus aureus* growth inhibition properties.

DP	Primary		Secondary		Tertiary		Quaternary (QC1)	
	MIC[a]	Normalized density[b]	MIC[a]	Normalized density[b]	MIC[a]	Normalized density[b]	MIC[a]	Normalized density[b]
30	NA	1.4 ± 0.1	NA	1.6 ± 0.2	NA	1.5 ± 0.4	NA	1.1 ± 0.2
56	1125-2250	< 0.05	NA	1.2 ± 0.1	NA	0.9 ± 0.1	NA	1.3 ± 0.05
75	562.5-1125	< 0.05	>4500	0.8 ± 0.2	NA	1.2 ± 0.3	NA	1.1 ± 0.2
140	70.3-140.6	< 0.05	140.6-281.3	< 0.05	NA	1.0 ± 0.2	>4500	0.6 ± 0.1

[a]MIC is in µg/mL. No activity (NA) was defined as normalized density 1.0 at polypeptide concentration of 4500 µg/mL.
[b]Normalized density is shown for bacteria exposed to 4500 µg/mL polypeptide.

Examining the polypeptides against *E. coli* growth, the primary amine samples were again found to be highly active against growth of this Gram-negative bacteria. Figure 7-4B

shows the results of *E. coli* growth inhibition for the four primary amine functionalized polypeptides. The molecular weight dependence is not as strongly visible with *E. coli* as with *S. aureus*; here the MIC against *E. coli* is found to lie between 562.5 – 1125 μg/mL for the three highest molecular weight primary amine polypeptides (DP = 56, 75, and 140). What appears as a bacteria density ≥ 1.0 in Figure 7-4B (for DP = 140) was optically visible polypeptide precipitate due to the test media conditions in a clear bacteria solution (signifying no bacteria present). Even the lowest molecular weight primary amine (DP = 30) exhibited approximately 70% inhibition of *E. coli* bacteria growth upon exposure to the 4500 μg/mL polypeptide concentration, although the same polymer was inactive at all concentrations for *S. aureus*. This was an unexpected finding, as traditionally, treatment of Gram-negative bacteria has been more difficult than Gram-positive strains due to the more complex membrane structure of these bacteria [65].

Table 7-3: *Escherichia coli* growth inhibition properties.

	Primary		Secondary		Tertiary		Quaternary (QC1)	
DP	MIC[a]	Normalized density[b]	MIC[a]	Normalized density[b]	MIC[a]	Normalized density[b]	MIC[a]	Normalized density[b]
30	>4500	0.3 ± 0.03	NA	1.0 ± 0.2	NA	1.0 ± 0.02	NA	0.8 ± 0.2
56	562.5-1125	<0.05	>4500	0.5 ± 0.04	NA	0.06	>4500	0.6 ± 0.06
75	562.5-1125	<0.05	>4500	0.2 ± 0.006	NA	0.9 ± 0.2	>4500	0.2 ± 0.006
140	562.5-1125	1.6 ± 0.2[c]	>4500	0.3 ± 0.02	>4500	0.4 ± 0.04	>4500	0.3 ± 0.01

[a]MIC is in μg/mL. No activity (NA) was defined as normalized density 1.0 at polypeptide concentration of 4500 μg/mL.
[b]Normalized bacteria density is shown for bacteria exposed to 4500 μg/mL polypeptide.
[c]Polypeptide precipitate was optically visible in the clear bacteria solution, indicating growth inhibition, but leading to a large optical density reading resulting in large normalized bacteria density.

Table 7-3 summarizes the MIC of the tested polypeptides against *E. coli* along with the normalized bacteria density at the highest tested concentration of 4500 μg/mL. The highest molecular weight secondary amine shows activity against *E. coli*, although the MIC is above

138

4500 µg/mL. Interestingly, unlike *S. aureus* the mid-range molecular weight secondary amines show *E. coli* inhibition at the highest tested concentration (approximately 50% and 20% for DP = 56 and 75, respectively). Additionally, the DP = 140 tertiary amine and DP 56 QC1 polypeptides exhibited *E. coli* growth inhibition as shown in Table 7-3 at the highest tested concentration, which was not observed for *S. aureus*. Many of the polymers developed in this work appear to be excellent candidates for infection prevention by delivery from drug-eluting coatings, as has been previously examined for naturally occurring AmPs [13, 36].

The quaternary amine functionalized polypeptides containing hydrophobic side chains (QCn, n ≥ 4), as highlighted in Table 7-1, were examined for bacterial growth inhibition from surface coatings. Polypeptides dissolved in methanol were allowed to coat a well plate via solvent evaporation to yield a polymer film, and these surfaces were subsequently exposed to bacteria solution. Table 7-4 summarizes the MIC for each of the tested polypeptides for both *S. aureus* and *E. coli*. Here, MIC again represents the polypeptide concentration range over which the normalized bacteria density transitions from greater than or equal to 0.1 to less than or equal to 0.02. Any polypeptides which exhibited a normalized bacteria density 1.0 at the highest tested surface concentration were defined as inactive. For *S. aureus*, bacteria growth inhibition was not seen for the QC4 and QC6 polypeptides. At an increased polymer hydrophobicity, QC8 was found to have a MIC between 156.3-312.5 µg/mL and 78.1-156.3 µg/mL for the DP = 75 and 140 polymers, respectively. The QC12 had the lowest MIC observed for *S. aureus* between 39.1-78.1 µg/mL (corresponding to a surface coverage of 12.2-24.4 µg/cm^2 for this water insoluble polypeptide). QC10 also exhibited a low MIC between 312.5-625 µg/mL against *S. aureus*. These results are consistent with what has been observed for antimicrobial activity against *S. aureus* of similar alkylated quaternary polyethylenimines [161]. We found that the quaternary amine polypeptides were more active against *E. coli* than *S. aureus* for QC6, had comparable activity for QC8, and were less active for QC10 and QC12 against *E. coli* than *S. aureus*. Figure 7-5 shows the results of this polypeptide coating dose response assay for the QC8 samples (DP = 75) for both *S. aureus* and *E. coli*. For *E. coli*, bacteria growth inhibition increased with increasing hydrophobicity up to an alkyl chain length of 8 and decreased with alkyl chain lengths of 10 and 12. The lowest MIC was observed for the QC8 samples with a range of 156.3-312.5 µg/mL. This trend is similar to what has been observed with pendant quaternary amine containing methacrylate polymers, where the carbon side chain lengths tested

were 12, 14, and 16. As the length of the carbon side chain increased, the methacrylate polymer antimicrobial activity increased for *S. aureus* but decreased for *E. coli* [163]. We hypothesize that the difference in MIC trends observed for *S. aureus* and *E. coli* is a result of the different membrane structure of these bacteria.

Table 7-4: Bacteria response to QCn (n ≥ 4) polypeptides.[a]

Bacteria	DP	Quaternary (QC4) MIC	Quaternary (QC6) MIC	Quaternary (QC8) MIC	Quaternary (QC10) MIC	Quaternary (QC12) MIC[b]
S. aureus	75	NA	NA	156.3-312.5	312.5-625	39.1-78.1
	140	NA	NA	78.1-156.3	312.5-625	39.1-78.1
E. coli	75	NA	312.5-625	156.3-312.5	1250-2500	1250-2500
	140	NA	312.5-625	156.3-312.5	1250-2500	1250-2500

[a]MIC is in μg/mL. No activity (NA) was defined as normalized density ≥ 1.0 at polypeptide concentration of 2500 μg/mL.
[b]QC12 is completely water insoluble; the MIC values for DP = 75 and 140 correspond to a surface coverage of 12.2-24.4 μg/cm^2 and 390-780 μg/cm^2, for *S. aureus* and *E. coli*, respectively.
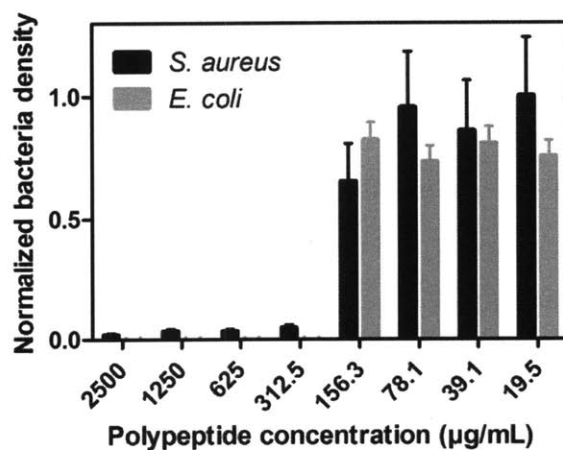
Figure 7-5: Bacteria growth inhibition by QC8 (DP = 75) coating for both *S. aureus* and *E. coli*.

The exact mechanism of action of the QCn (≥4) polypeptides is currently under investigation. CD studies performed when the molecules were dissolved in methanol indicate that the QCn (≥ 4) polymers adopt an α -helical conformation in solution before they are

solvent cast, as indicated by the strong minimums at 208 nm and 222 nm as shown in Figure 7-6 [176].
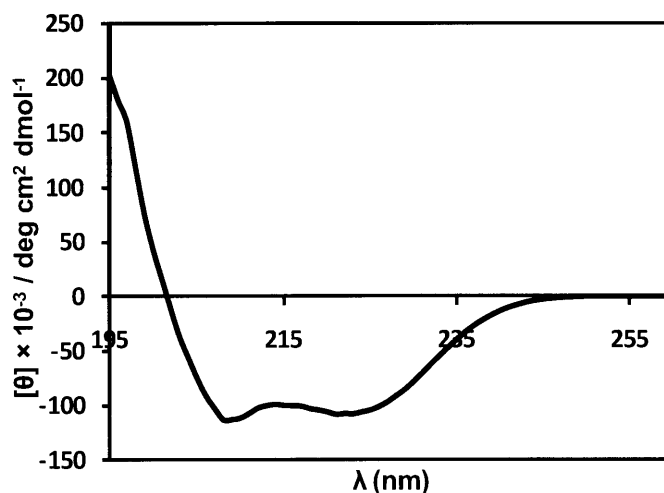
Figure 7-6: Circular Dichroism of QC8 functionalized PPLG in methanol (DP = 75, concentration = 1.67 mg/mL)

After solvent casting, FTIR was used to determine if the polymer backbone maintained a helical structure. The strong amide I peak at 1653 nm is characteristic of an α-helical structure [177]. A representative spectrum for the QC8 functionalized polypeptide is shown in Figure 7-7. As with other antimicrobial polycations, it is believed that these polymers function by electrostatic association with the negatively charged bacteria cell surface and subsequent disruption of the plasma membrane [178]. Due to the rigidity of the polypeptide backbone, we hypothesize that these polymers act by complexing with the exterior surface of the bacterial cell membrane, rather than inserting fully across the membrane, as with more flexible polymers [179]. One of the advantages of applying a systematic approach to design synthetic antimicrobial polypeptides is that different properties can be decoupled and explored. For the current system, we are using a rigid α-helical backbone, but in the future, utilizing a mixture of D-L monomers, it is also possible to explore the effect of polymer backbone rigidity on the antimicrobial activity and mechanism of membrane disruption.
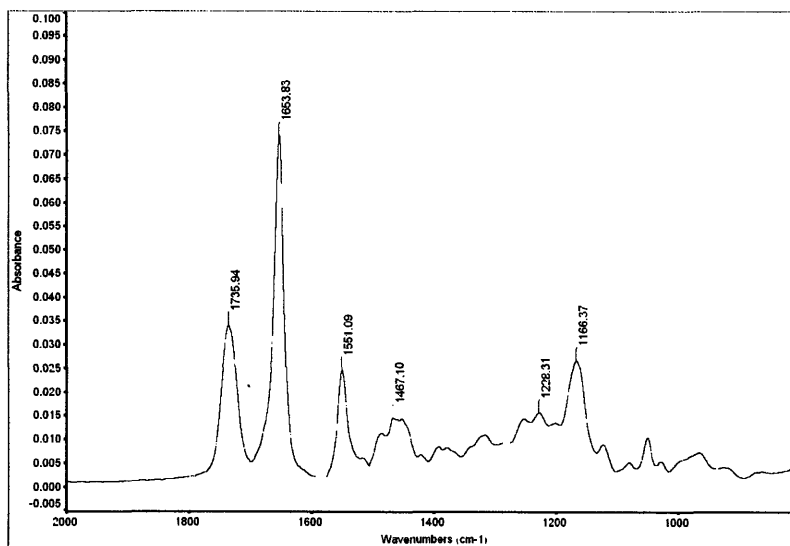
Figure 7-7: Representative FTIR of QC8 functionalized PPLG.

7.3.3 Bacteria Attachment Inhibition

An increasingly common cause of medical device failure and the spread of infection is the formation of biofilms on implants and dead tissue [7]. The first critical step necessary for biofilm formation is the attachment of bacteria on a surface. Preventing this attachment step will ultimately prevent biofilm formation and is a desirable characteristic of functionalized surfaces. To examine whether the QCn (n ≥ 4) polypeptides have the potential to make anti-biofilm device coatings for orthopedic implants or intraocular lenses for example, the ability of substrates coated with these polypeptides to inhibit bacteria attachment was examined. Round glass substrates were coated with quaternary amine functionalized polypeptide samples with varying degrees of hydrophobicity at two different molecular weights (DP = 75 and 140) and allowed to evaporate to evenly coat these substrates, yielding a final coating of 330 $\mu g/cm^2$. These substrates were then tested for prevention of bacterial attachment for both *S. aureus* and *E. coli*. Figures 7-8 and 7-9 show the results for attachment inhibition of *S. aureus* and *E. coli*, respectively, by these coated substrates. It was found that increasing hydrophobicity of polypeptide functional groups leads to increased inhibition of bacterial attachment for *S. aureus* and *E. coli* up to an alkyl chain length of 10. Beyond this point, increasing hydrophobicity (alkyl chain length of 12) seems to decrease inhibition capability. Although the QC12 sample did have a comparable MIC to the QC10 in the polypeptide dose response liquid assay testing for bacteria growth inhibition, its attachment inhibition activity is not comparable to QC10. Increased

142

hydrophobicity may assist penetration of the bacteria cell based on hydrophobic interactions with the lipid bilayer membranes; however, it is also possible that this behavior is no longer sustained at greater alkyl chain lengths (i.e. QC12) in the case of *E. coli* due to changes in the compatibility between the cationic hydrophobic side chain and the amphiphilic lipid membrane of the cell. These changes may more significantly affect *E. coli* than *S. aureus* due to the more complex membrane structure of Gram-negative bacteria, which may explain why there is no significant decrease in *S. aureus* attachment inhibition by the QC12 polypeptide compared to the QC8 and QC10 polymers. These results agree with the results of bacteria growth inhibition, where the QC12 has the lowest MIC for *S. aureus* and the QC8 and QC10 are also quite active against *S. aureus* growth. Additionally, both molecular weights tested displayed the same trends in activity.
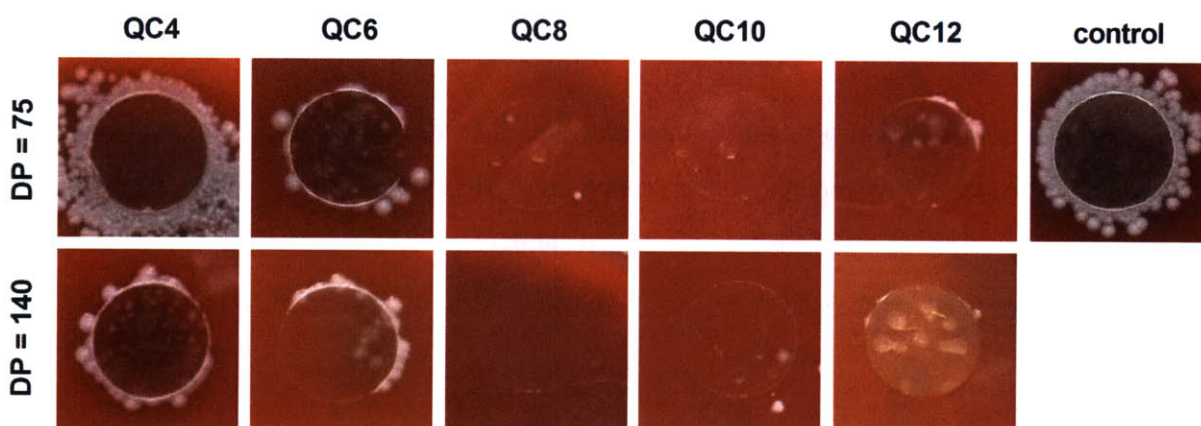
Figure 7-8: *S. aureus* **attachment inhibition by quarternary amine functionalized polypeptides with varying hydrophobicity (QC4 – QC12; control = uncoated substrate).**
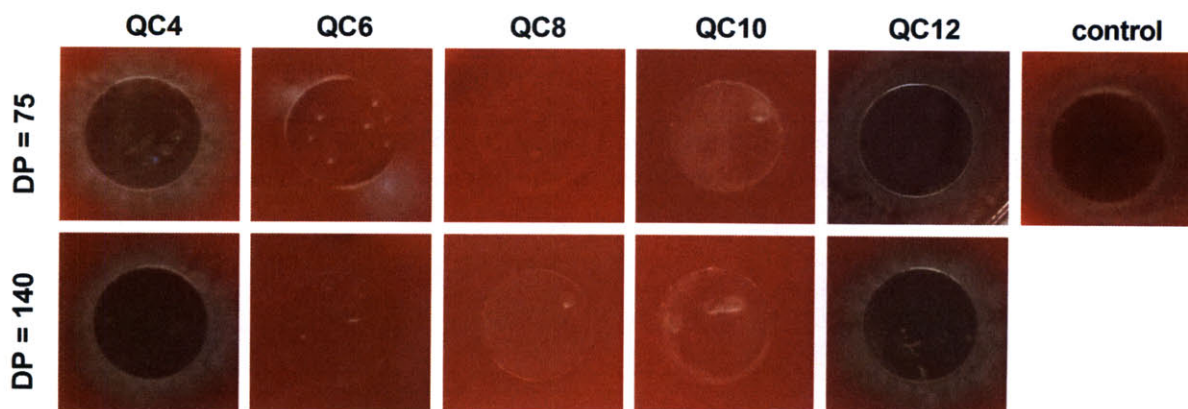
Figure 7-9: *E. coli* **attachment inhibition by quarternary amine functionalized polypeptides with varying hydrophobicity (QC4 – QC12; control = uncoated substrate).**

7.3.4 Polypeptide Biocompatibility

As an initial test of biocompatibility RBC lysis (hemolysis) in response to these polypeptides was examined by monitoring free hemoglobin absorbance. Table 7-5 shows results for all polypeptides that displayed a normalized hemolysis greater than 0.005 at the highest tested polypeptide concentration of 5000 μg/mL. All polypeptides were found to be non-cytotoxic, displaying low hemolytic activity in comparison to many naturally occurring AmPs as well as several antimicrobial polymers that have recently been developed [158, 159]. In all cases in which hemolysis above 0.5% was observed, the concentration at which this occurred far exceeded the polypeptide MIC against *S. aureus* and *E. coli*. This is a necessary requirement for antimicrobial polymers to attain utility in clinical applications. The largest level of hemolysis was observed for the QC8 polypeptide, with a maximum of approximately 23% for the DP = 75 polypeptide at a 5000 μg/mL concentration. Figure 7-10 shows hemolysis in response to varying QC8 polypeptide concentrations. This polymer was also found to exhibit high activity against both Gram-positive and Gram-negative bacteria, and therefore, it was expected to have some degree of hemolysis. However, the concentrations at which the QC8 polymer exhibits complete bacteria growth inhibition were 78.1-156.3 μg/mL and 156.3-312.5 μg/mL for *S. aureus E. coli* respectively, which are far lower than the concentration at which significant hemolysis is observed (approximately less than 8%).

Table 7-5: Normalized red blood cell lysis.[a]

DP	Primary	Quaternary (QC8)	Quaternary (QC10)	Quaternary (QC12)
75	<0.005	0.23 ± 0.013	0.20 ± 0.024	0.085 ± 0.029
140	0.032 ± 0.003	0.11 ± 0.007	0.15 ± 0.008	0.052 ± 0.008

[a]Secondary, tertiary, and quaternary (QC1, QC4, QC6) amine samples showed less than 0.005 normalized red blood cell hemolysis at the highest tested concentration.
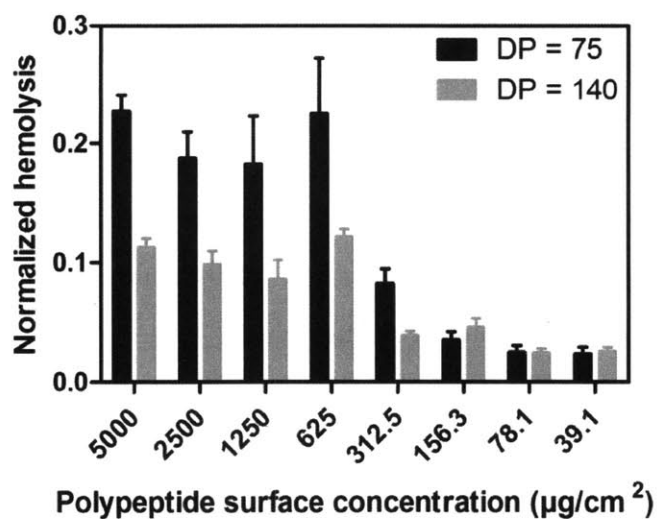
Figure 7-10: Normalized hemolysis for QC8 polypeptide.

7.4 Conclusions

In this work, we created a library of synthetic antimicrobial polypeptides that mimic naturally occurring AmPs. These polypeptides were designed by systematically varying the side chain functionality (primary to quaternary amine) and alkyl side chain length of a PPLG backbone of varying molecular weights. To assess the antimicrobial potential of these polypeptides, they were tested based on the criteria of bacteria growth and attachment inhibition for both Gram-negative and Gram-positive bacteria, as well as for hemolytic activity (a preliminary indication of biocompatibility). With respect to bacteria growth inhibition, several polymers were found to exhibit MIC values that rival naturally existing AmPs. For the quaternary amine series, increasing side chain hydrophobicity led to increased bacteria growth inhibition within a certain limit. In particular, QC12 was the most potent polypeptide against *S. aureus*, while both QC6 and QC8 were most effective in inhibiting *E. coli* growth. The QC8 and QC10 polypeptides were optimal in completely preventing bacteria attachment for both *S. aureus* and *E. coli*. Finally, with regards to biocompatibility, all of the antimicrobial polypeptides were found to be non-cytotoxic with extremely low hemolytic activity in comparison to many naturally occurring AmPs. Overall, these polymers possess many of the beneficial characteristics of naturally occurring AmPs, including effective MIC values, broad-spectrum activity, and potential for preventing biofilm formation by mitigating microbial attachment; at the same time, these synthetic polypeptides are efficiently produced, cost-effective, and

biocompatible. The antimicrobial polypeptides developed in this work are an important step forward in the production of a new class of antimicrobial therapeutics which have the potential for clinical translation in both systemic and local delivery applications as well as for use in semi-permanent medical device coatings. The flexibility of this system allows for the systematic variation of polymer properties, ranging from side chain functionality to backbone rigidity, which will provide insight into the mechanism of action of antimicrobial agents and aid in the rational design of future antimicrobial therapeutics.

Chapter 8

Conclusions and Future Directions

8.1 Thesis Summary

This thesis has focused on developing layer-by-layer (LbL) assembled films for the effective treatment of infection, inflammation, and bleeding. The primary findings of each thesis chapter are highlighted as follows.

- In Chapter 2, the delivery of antimicrobial peptide (AmP), ponericin G1, from hydrolytically degradable films was described. The use of various polyanions allowed tunable AmP dosage and release timescales for these films. The released ponericin G1 maintained activity against *Staphylococcus aureus* both in solution and by preventing attachment of bacteria to film coated surfaces. Additionally, although ponericin G1 was found to significantly decrease fibroblast viability in AmP treated media, film release components, including the AmP, did not affect mammalian cell viability [13].

- The development of a hydrolytically degradable film for the delivery of vancomycin was examined in Chapter 3. Drug loading and release characteristics were directly related to film growth properties which depended on the film architecture (including polyanion choice) and the method of LbL assembly utilized (spray versus dip LbL). Dip assembled films had a significant degree of interdiffusion compared to sprayed films, which allowed for the formation of favorable non-electrostatic secondary interactions leading to linear drug release over a period of approximately 2.5 days compared to a large bolus release of drug from sprayed films. It was also found that by continuing to spray more layers, interdiffusion in these films could eventually be induced, increasing drug release profile linearity and length of release. Additionally, spray assembled films were shown to have significantly high drug loadings compared to dipped films due to lack of out-diffusion of drug during the assembly process. Drug loading up to 20 weight percent was attained, compared to maximum loadings of approximately 7 and 3 weight percent previously reported for polyurethane scaffolds and

poly(methyl methacrylate) beads, respectively [10]. It was shown that these films could be coated upon drugstore bandages and retain complete vancomycin activity against *S. aureus* [14]. Finally, the long term storage stability of these films was examined. The films remained stable upon storage at both room (25 °C) and elevated temperatures (37 °C) for at least 6 months and 1 month, respectively, maintaining release profiles and minimum inhibitory concentrations comparable to films used directly upon assembly. These films may therefore be suitable alternatives for use in situations where rapid care is desirable but refrigeration of vancomycin solutions is not possible

- After thoroughly examining the properties of vancomycin releasing films in Chapter 3, they were modularly combined with previously developed non-steroidal anti-inflammatory (NSAID) delivering LbL films [58] in Chapter 4. The goal was to create a single film that could target both infection and inflammation. The NSAID used in these studies was diclofenac. Studies of film component interactions prior to composite film assembly uncovered two novel interactions, namely the interaction of vancomycin with poly(carboxymethyl-β-cyclodextrin) and the interaction of diclofenac with vancomycin. Additionally, studies of single-therapeutic films allowed the determination of diffusion and exchange behavior within these films upon exposure to film deposition or wash solutions of the complementary film. With the knowledge of these interactions and film behavior, several optimal composite film architectures were developed for both prolonged and short-term release of the NSAID and the antibiotic. Both dip and spray assembly were utilized to best manipulate the interactions that were uncovered between film components and obtain the desired release profiles. The successful application of these films to clinically-relevant substrates, including bandages, intraocular lenses, and sutures, was demonstrated. Additionally, both vancomycin and diclofenac were found to retain complete *in vitro* activity upon delivery from these films.

- In Chapter 5, the application of the vancomycin delivery films developed in Chapter 3 to a clinically relevant substrate was explored. These films were used to coat a porous and absorbent gelatin bandage, Surgifoam®, using the spray LBL assembly technique with vacuum application to draw film components through the porous sponge. The hydrophilic

LbL coating enhanced the absorbent nature of the sponge by a factor of approximately 2-fold. Additionally, the porosity of the sponge increased drug loading approximately 880% compared to a flat substrate, and increased the release time up to 6.2 days compared to 1.9 days for a vancomycin film on a flat substrate.

- To address current issues with hemorrhage control, Chapter 6 examined the development of a thin hemostatic coating for application to existing medical devices. The coating was assembled based on novel hydrogen bonding interactions found to occur between the clotting factor, thrombin, and a small polyphenol, tannic acid. Unlike traditional multilayer films, these films incorporated no polymeric component, and unlike the other film systems developed in this work, these films were not designed to be hydrolytically degradable. Therefore, the films degrade slowly overtime using a diffusion based mechanism. The films were applied to Surgifoam® and tested in a porcine spleen injury model and found to instantaneously promote hemostasis following a single short digital compression period compared to several minutes and application of multiple compressions for control samples.

- Lastly, in Chapter 7, the potential to economically develop antimicrobial polypeptides that mimic the favorable properties of natural AmPs was explored. A library of synthetic antimicrobial polypeptides was designed by systemically varying the side-chain functionality (primary to quaternary amine) with different alkyl side chain lengths clicked on a poly-(propargyl-L-glutamate) backbone of varying molecular weight. Several of these polypeptides exhibited broad-spectrum growth inhibition of a model Gram-negative and Gram-positive bacteria, *Escherichia coli* and *S. aureus*, respectively. Additionally, several of the polypeptides also prevented attachment of these bacteria on polypeptide coated substrates. Additionally, these polypeptides had low red blood cell hemolytic activity compared to many naturally occurring antimicrobial peptides.

8.2 Future Directions

There are many potential future directions that could be taken to build upon the findings of this thesis. First, some of the most obvious future steps would be to prove *in vivo* efficacy of both the infection and inflammation related films developed here and examine the long term

storage stability of these films coated on relevant clinical substrates. The eventual goal of this work is to create a single device that is able to simultaneously address infection, inflammation, and bleeding. In this thesis, single films that control both infection and inflammation were developed. The next logical step is to work on a method for combining these films with the hemostatic films developed in this thesis. This is complicated by issues related to film component interdiffusion and the fact that the hemostatic film is built primarily based on hydrogen bonding interactions whereas the other therapeutics have been assembled into films via electrostatic means. It has previously been shown that a single film containing stacks of hydrogen bonded components and stacks of electrostatically interacting layers can be assembled [180]. Similar methods could be employed to accomplish the goal of combining all films developed in this thesis to create a single multi-functional therapeutic device. Additionally, methods must be explored to control interdiffusion between the various therapeutic segments of this multi-functional film. When concurrent release of therapeutics is desired, such as the films developed in Chapter 4 to simultaneously address infection and inflammation, interdiffusion between film components can be very useful in promoting favorable interactions between film components. However, in cases where sequential drug delivery is needed, interdiffusion of film components is not desirable. Aside from techniques that have been employed and are currently under investigation for producing barrier layers to prevent film components from interacting, there is potential for applying findings from this thesis regarding the ability of spray assembled films to greatly reduce the level of interdiffusion that occurs during film assembly [14] to further assist in separating the interactions of film components.

Additionally, in this thesis it was shown that thrombin is a hydrogen bond acceptor, interacting strongly with tannic acid, a hydrogen bond donor. It is conceivable that films could be constructed that are entirely composed of the therapeutic components that are of interest to this work, including thrombin and vancomycin. There are numerous potential hydrogen bond donors on the vancomycin molecule, which like tannic acid, may interact directly with thrombin. It may, therefore, be possible to assemble ultra-thin therapeutic coatings that contain only large densities of thrombin and vancomycin. A film like this would allow for immediate action against both bleeding and infection.

It may also be desirable to examine other methods of stimuli-responsiveness aside from degradation based on molecular diffusion and polymer hydrolysis, which were the primary

means of drug release explored in this thesis. Numerous other methods of stimuli-responsive drug release have previously been employed. Particularly interesting to the applications of this thesis would be triggered drug release based on either temperature or pH. Both of these have been explored in the context of hydrogen bonded films [180, 181]. By incorporating polymeric components like poly(N-isopropyl acrylamide), which are responsive near physiologic temperatures, the film may undergo rearrangement or disruption upon exposure to these temperatures, triggering drug release. Additionally, by using materials that undergo large changes in degree of ionization between film deposition and release, a similar stimuli-responsive behavior may be attained. For example, deposition of poly(acrylic acid) containing films at low pH where poly(acrylic acid) is fully protonated and acts as a good hydrogen bond donor, and subsequent release at higher pH conditions in which the acid groups are fully ionized disrupting hydrogen bonding interactions, may allow for triggered drug release. For conditions in which rapid treatment is needed, such as bleeding, having a film that contains a large density of drug and then rapidly deconstructs at physiologic pH or temperature would be highly desirable.

Finally, there is great potential for clinical translation of the therapeutic films developed in this thesis. The hemostatic films developed in Chapter 6 are composed entirely of materials that are approved by the United States Food and Drug Administration (FDA) and these films have already shown *in vivo* efficacy in a large animal model. These coatings are therefore readily translatable. Therapeutic films developed in this thesis for infection and inflammation control described in Chapters 3 through 5 also contain materials that are approved by the FDA (such as the therapeutics and polyanions used) or are in the in the process of approval, such as the poly(β-amino esters), which have recently found utility in commercial hair products. By developing coatings that are composed of materials that are commonly used and approved by the FDA, clinical translation is greatly facilitated, compared to developing or using materials whose properties are not well characterized. The next step towards translation for films developed in Chapters 3 through 5 would be characterization of efficacy in infection and inflammation animal models.

8.3   Concluding Remarks

This thesis has enhanced the understanding of designing tunable drug releasing multilayer films. Overall, it was shown that drug loading and release behavior of therapeutic

containing films are strong functions not only of the film architecture but also of the film assembly technique utilized (spray versus dip LbL). Both film architecture and assembly technique greatly influence the formation of favorable secondary interactions which may be crucial to stability of a particular film. Prior to the findings of this thesis, the understanding of small molecule behavior in spray LbL assembled films was limited. Additionally, this thesis showed that film architecture can be better informed by performing studies to explore interactions between film components prior to film assembly, a previously unexplored design approach.

The novel drug delivery coatings developed in this thesis using LbL assembly have greatly improved the treatment potential for traumatic injury resulting in bleeding, infection, and inflammation. These versatile coatings were designed to specifically overcome the drawbacks of current drug delivery methods for each of these conditions which lead to inferior treatment options for patients. This includes treatment over inappropriate timescales or inappropriate drug concentrations or lack of methods that are easily applicable and do not require long-term patient hospitalization. Although the films in this work were developed specifically to target infection, inflammation, and bleeding, the findings of this thesis can be applied to the development of various other drug delivery or self-assembling systems.

Bibliography

[1] H.B. Alam, D. Burris, J.A. DaCorta, P. Rhee, Hemorrhage Control in the Battlefield - Role of New Hemostatic Agents, Military Medicine, 170 (2005) 63-69.

[2] J.L. Sondeen, A.E. Pusateri, V.G. Coppes, C.C.E. Gaddy, J.B. Holcomb, Comparison of 10 Different Hemostatic Dressings in an Aortic Injury, The Journal of Trauma, 54 (2003) 280-285.

[3] C.K. Murray, S.A. Roop, D.R. Hospenthal, D.P. Dooley, K. Wenner, J. Hammock, N. Taufen, E. Gourdine, Bacteriology of War Wounds at the Time of Injury, Military Medicine, 171 (2006) 826-829.

[4] I. Wedmore, J.G. McManus, A.E. Pusateri, J.B. Holcomb, A Special Report on the Chitosan-based Hemostatic Dressing: Experience in Current Combat Operations, The Journal of Trauma, 60 (2006) 655-658 610.1097/1001.ta.0000199392.0000191772.0000199344.

[5] K. King, M.C. Neuffer, J. McDivitt, D. Rose, C.C. Cloonan, J.S. Vayer, Hemostatic Dressings for the First Responder - A Review, Military Medicine, 169 (2004) 716-720.

[6] H.S. Gold, R.C. Moellering, Antimicrobial-Drug Resistance, N Engl J Med, 335 (1996) 1445-1453.

[7] J.W. Costerton, P.S. Stewart, E.P. Greenberg, Bacterial Biofilms: A Common Cause of Persistent Infections, Science, 284 (1999) 1318-1322.

[8] M. Zilberman, J.J. Elsner, Antibiotic-Eluting Medical Devices for Various Applications, Journal of Controlled Release, 130 (2008) 202-215.

[9] S.-S. Lin, S.W.N. Ueng, S.-S. Lee, E.-C. Chan, K.-T. Chen, C.-Y. Yang, C.-Y. Chen, Y.-S. Chan, In Vitro Elution of Antibiotic from Antibiotic-Impregnated Biodegradable Calcium Alginate Wound Dressing, The Journal of Trauma, 47 (1999) 136-141.

[10] B. Li, K.V. Brown, J.C. Wenke, S.A. Guelcher, Sustained Release of Vancomycin from Polyurethane Scaffolds Inhibits Infection of Bone Wounds in a Rat Femoral Segmental Defect Model, Journal of Controlled Release, 145 (2010) 221-230.

[11] L.F. Zhang, D.J. Yang, H.C. Chen, R. Sun, L. Xu, Z.C. Xiong, T. Govender, C.D. Xiong, An Ionically Crosslinked Hydrogel Containing Vancomycin Coating on a Porous Scaffold for Drug Delivery and Cell Culture, International Journal of Pharmaceutics, 353 (2008) 74-87.

[12] H.F. Chuang, R.C. Smith, P.T. Hammond, Polyelectrolyte Multilayers for Tunable Release of Antibiotics, Biomacromolecules, 9 (2008) 1660-1668.

[13] A. Shukla, K.E. Fleming, H.F. Chuang, T.M. Chau, C.R. Loose, G.N. Stephanopoulos, P.T. Hammond, Controlling the Release of Peptide Antimicrobial Agents from Surfaces, Biomaterials, 31 (2010) 2348-2357.

[14] A. Shukla, S.N. Avadhany, J.C. Fang, P.T. Hammond, Tunable Vancomycin Releasing Surfaces for Biomedical Applications, Small, 6 (2010) 2392-2404.

[15] J.A. Lichter, M.F. Rubner, Polyelectrolyte Multilayers with Intrinsic Antimicrobial Functionality: The Importance of Mobile Polycations, Langmuir, 25 (2009) 7686-7694.

[16] J.C. Tiller, C.-J. Liao, K. Lewis, A.M. Klibanov, Designing Surfaces That Kill Bacteria on Contact, Proceedings of the National Academy of Sciences of the United States of America, 98 (2001) 5981-5985.

[17] D. Park, J. Wang, A.M. Klibanov, One-Step Painting-Like Coating Procedures to Make Surfaces Highly and Permanently Bactericidal, Biotechnology Progress, 22 (2006) 584-589.

[18] K. Mukherjee, J.J. Rivera, A.M. Klibanov, Practical Aspects of Hydrophobic Polycationic Bactericidal "Paints", Applied Biochemistry and Biotechnology, 151 (2008) 61-70.

[19] A.C. Engler, A. Shukla, S. Puranam, H.G. Buss, N. Jreige, P.T. Hammond, Effects of Side Group Functionality and Molecular Weight on the Activity of Synthetic Antimicrobial Polypeptides, Biomacromolecules, (2011) in press.

[20] P. Wu, D.W. Grainger, Drug/Device Combinations for Local Drug Therapies and Infection Prophylaxis, Biomaterials, 27 (2006) 2450-2467.

[21] K.E. Uhrich, S.M. Cannizzaro, R.S. Langer, K.M. Shakesheff, Polymeric Systems for Controlled Drug Release, Chemical Reviews, 99 (1999) 3181-3198.

[22] G. Decher, Fuzzy Nanoassemblies: Toward Layered Polymeric Multicomposites, Science, 277 (1997) 1232-1237.

[23] E. Kharlampieva, S.A. Sukhishvili, Hydrogen-Bonded Layer-by-Layer Polymer Films, Polymer Reviews, 46 (2006) 377 - 395.

[24] A.P.R. Johnston, E.S. Read, F. Caruso, DNA Multilayer Films on Planar and Colloidal Supports: Sequential Assembly of Like-Charged Polyelectrolytes, Nano Letters, 5 (2005) 953-956.

[25] J.B. Schlenoff, S.T. Dubas, T. Farhat, Sprayed Polyelectrolyte Multilayers, Langmuir, 16 (2000) 9968-9969.

[26] K.C. Krogman, N.S. Zacharia, S. Schroeder, P.T. Hammond, Automated Process for Improved Uniformity and Versatility of Layer-by-Layer Deposition, Langmuir, 23 (2007) 3137-3141.

[27] K.C. Krogman, J.L. Lowery, N.S. Zacharia, G.C. Rutledge, P.T. Hammond, Spraying Asymmetry Into Functional Membranes Layer-by-Layer, Nature Materials, 8 (2009) 512-518.

[28] N. Fukao, K.-H. Kyung, K. Fujimoto, S. Shiratori, Automatic Spray-LBL Machine Based on in-Situ QCM Monitoring, Macromolecules, (2011) in press.

[29] J. Cho, K. Char, J.-D. Hong, K.-B. Lee, Fabrication of Highly Ordered Multilayer Films Using a Spin Self-Assembly Method, Advanced Materials, 13 (2001) 1076-1078.

[30] M. Macdonald, N.M. Rodriguez, R. Smith, P.T. Hammond, Release of a Model Protein from Biodegradable Self Assembled Films for Surface Delivery Applications, Journal of Controlled Release, 131 (2008) 228-234.

[31] S. Facca, C. Cortez, C. Mendoza-Palomares, N. Messadeq, A. Dierich, A.P.R. Johnston, D. Mainard, J.-C. Voegel, F. Caruso, N. Benkirane-Jessel, Active Multilayered Capsules for In Vivo Bone Formation, Proceedings of the National Academy of Sciences, 107 (2010) 3406-3411.

[32] V.A. Izumrudov, E. Kharlampieva, S.A. Sukhishvili, Multilayers of a Globular Protein and a Weak Polyacid: Role of Polyacid Ionization in Growth and Decomposition in Salt Solutions, Biomacromolecules, 6 (2005) 1782-1788.

[33] M.L. Macdonald, N.M. Rodriguez, N.J. Shah, P.T. Hammond, Characterization of Tunable FGF-2 Releasing Polyelectrolyte Multilayers, Biomacromolecules, 11 (2010) 2053-2059.

[34] M.L. Macdonald, R.E. Samuel, N.J. Shah, R.F. Padera, Y.M. Beben, P.T. Hammond, Tissue Integration of Growth Factor-Eluting Layer-by-Layer Polyelectrolyte Multilayer Coated Implants, Biomaterials, 32 (2011) 1446-1453.

[35] O. Etienne, C. Picart, C. Taddei, Y. Haikel, J.L. Dimarcq, P. Schaaf, J.C. Voegel, J.A. Ogier, C. Egles, Multilayer Polyelectrolyte Films Functionalized by Insertion of Defensin: A New Approach to Protection of Implants from Bacterial Colonization, Antimicrobrial Agents and Chemotherapy, 48 (2004) 3662-3669.

[36] A. Guyomard, E. Dé, T. Jouenne, J.-J. Malandain, G. Muller, K. Glinel, Incorporation of a Hydrophobic Antibacterial Peptide into Amphiphilic Polyelectrolyte Multilayers: A Bioinspired Approach to Prepare Biocidal Thin Coatings, Advanced Functional Materials, 18 (2008) 758-765.

[37] C.M. Jewell, J. Zhang, N.J. Fredin, M.R. Wolff, T.A. Hacker, D.M. Lynn, Release of Plasmid DNA from Intravascular Stents Coated with Ultrathin Multilayered Polyelectrolyte Films, Biomacromolecules, 7 (2006) 2483-2491.

[38] E.M. Saurer, C.M. Jewell, J.M. Kuchenreuther, D.M. Lynn, Assembly of Erodible, DNA-Containing Thin Films on the Surfaces of Polymer Microparticles: Toward a Layer-by-Layer Approach to the Delivery of DNA to Antigen-Presenting Cells, Acta Biomaterialia, 5 (2009) 913-924.

[39] J. Zhang, L.S. Chua, D.M. Lynn, Multilayered Thin Films that Sustain the Release of Functional DNA under Physiological Conditions, Langmuir, 20 (2004) 8015-8021.

[40] J. Zhang, D.M. Lynn, Ultrathin Multilayered Films Assembled from "Charge-Shifting" Cationic Polymers: Extended, Long-Term Release of Plasmid DNA from Surfaces, Advanced Materials, 19 (2007) 4218-4223.

[41] P.T. Hammond, Form and Function in Multilayer Assembly: New Applications at the Nanoscale, Advanced Materials, 16 (2004) 1271-1293.

[42] D.M. Lynn, Layers of Opportunity: Nanostructured Polymer Assemblies for the Delivery of Macromolecular Therapeutics, Soft Matter, 2 (2006) 269-273.

[43] D.M. Lynn, Peeling Back the Layers: Controlled Erosion and Triggered Disassembly of Multilayered Polyelectrolyte Thin Films, Advanced Materials, 19 (2007) 4118-4130.

[44] A.N. Zelikin, Drug Releasing Polymer Thin Films: New Era of Surface-Mediated Drug Delivery, ACS Nano, 4 (2010) 2494-2509.

[45] A.L. Becker, A.P.R. Johnston, F. Caruso, Drug Delivery: Layer-by-Layer-Assembled Capsules and Films for Therapeutic Delivery, Small, 6 (2010) in press.

[46] C. Picart, Polyelectrolyte Multilayer Films: From Physico-Chemical Properties to the Control of Cellular Processes, Current Medicinal Chemistry, 15 (2008) 685-697.

[47] T. Boudou, T. Crouzier, K. Ren, G. Blin, C. Picart, Multiple Functionalities of Polyelectrolyte Multilayer Films: New Biomedical Applications, Advanced Materials, 22 (2010) 441-467.

[48] S. Mansouri, Y. Merhi, F.o.M. Winnik, M. Tabrizian, Investigation of Layer-by-Layer Assembly of Polyelectrolytes on Fully Functional Human Red Blood Cells in Suspension for Attenuated Immune Response, Biomacromolecules, 12 (2011) 585-592.

[49] N.G. Veerabadran, P.L. Goli, S.S. Stewart-Clark, Y.M. Lvov, D.K. Mills, Nanoencapsulation of Stem Cells within Polyelectrolyte Multilayer Shells, Macromolecular Bioscience, 7 (2007) 877-882.

[50] A. Agarwal, K.M. Guthrie, C.J. Czuprynski, M.J. Schurr, J.F. McAnulty, C.J. Murphy, N.L. Abbott, Polymeric Multilayers that Contain Silver Nanoparticles can be Stamped onto Biological Tissues to Provide Antibacterial Activity, Advanced Functional Materials, (2011) in press.

[51] S.T. Dubas, J.B. Schlenoff, Factors Controlling the Growth of Polyelectrolyte Multilayers, Macromolecules, 32 (1999) 8153-8160.

[52] N.S. Zacharia, M. Modestino, P.T. Hammond, Factors Influencing the Interdiffusion of Weak Polycations in Multilayers, Macromolecules, 40 (2007) 9523-9528.

[53] C. Porcel, P. Lavalle, G. Decher, B. Senger, J.C. Voegel, P. Schaaf, Influence of the Polyelectrolyte Molecular Weight on Exponentially Growing Multilayer Films in the Linear Regime, Langmuir, 23 (2007) 1898-1904.

[54] J.S. Moskowitz, M.R. Blaisse, R.E. Samuel, H.-P. Hsu, M.B. Harris, S.D. Martin, J.C. Lee, M. Spector, P.T. Hammond, The Effectiveness of the Controlled Release of Gentamicin from Polyelectrolyte Multilayers in the Treatment of Staphylococcus aureus Infection in a Rabbit Bone Model, Biomaterials, 31 (2010) 6019-6030.

[55] S. Pavlukhina, Y. Lu, A. Patimetha, M. Libera, S. Sukhishvili, Polymer Multilayers with pH-Triggered Release of Antibacterial Agents, Biomacromolecules, 11 (2010) 3448-3456.

[56] P.M. Nguyen, N.S. Zacharia, E. Verploegen, P.T. Hammond, Extended Release Antibacterial Layer-by-Layer Films Incorporating Linear-Dendritic Block Copolymer Micelles, Chemistry of Materials, 19 (2007) 5524-5530.

[57] B.-S. Kim, H.-i. Lee, Y. Min, Z. Poon, P.T. Hammond, Hydrogen-Bonded Multilayer of pH-Responsive Polymeric Micelles with Tannic Acid for Surface Drug Delivery, Chemical Communications, (2009) 4194-4196.

[58] R.C. Smith, M. Riollano, A. Leung, P.T. Hammond, Layer-by-Layer Platform Technology for Small-Molecule Delivery, Angewandte Chemie International Edition, 48 (2009) 8974-8977.

[59] C. Vodouhê, E.L. Guen, J.M. Garza, G. Francius, C. Déjugnat, J. Ogier, P. Schaaf, J.-C. Voegel, P. Lavalle, Control of Drug Accessibility on Functional Polyelectrolyte Multilayer Films, Biomaterials, 27 (2006) 4149-4156.

[60] N. Jessel, M. Oulad-Abdelghani, F. Meyer, P. Lavalle, Y. Haîkel, P. Schaaf, J.-C. Voegel, Multiple and Time-Scheduled In Situ DNA Delivery Mediated by β-Cyclodextrin Embedded in a Polyelectrolyte Multilayer, Proceedings of the National Academy of Sciences, 103 (2006) 8618-8621.

[61] D.M. Lynn, R. Langer, Degradable Poly(β-Amino Esters): Synthesis, Characterization, and Self-Assembly with Plasmid DNA, Journal of the American Chemical Society, 122 (2000) 10761-10768.

[62] K.C. Wood, J.Q. Boedicker, D.M. Lynn, P.T. Hammond, Tunable Drug Release from Hydrolytically Degradable Layer-by-Layer Thin Films, Langmuir, 21 (2005) 1603-1609.

[63] Renée C. Smith, A. Leung, B.-S. Kim, P.T. Hammond, Hydrophobic Effects in the Critical Destabilization and Release Dynamics of Degradable Multilayer Films, Chemistry of Materials, 21 (2009) 1108-1115.

[64] K.C. Wood, H.F. Chuang, R.D. Batten, D.M. Lynn, P.T. Hammond, Controlling Interlayer Diffusion to Achieve Sustained, Multiagent Delivery from Layer-by-Layer Thin Films, Proceedings of the National Academy of Sciences, 103 (2006) 10207-10212.

[65] G. Taubes, The Bacteria Fight Back, Science, 321 (2008) 356-361.

[66] A.S. Lynch, G.T. Robertson, Bacterial and Fungal Biofilm Infections, Annual Review of Medicine, 59 (2008) 415-428.

[67] P.S. Stewart, J.W. Costerton, Antibiotic Resistance of Bacteria in Biofilms, The Lancet, 358 (2001) 135-138.

[68] H.P. Stallmann, C. Faber, E.T. Slotema, D.M. Lyaruu, A.L.J.J. Bronckers, A.V.N. Amerongen, P.I.J.M. Wuisman, Continuous-Release or Burst-Release of the Antimicrobial Peptide Human Lactoferrin 1-11 (hLF1-11) from Calcium Phosphate Bone Substitutes, Journal of Antimicrobial Chemotherapy, 52 (2003) 853-855.

[69] R.E.W. Hancock, G. Diamond, The Role of Cationic Antimicrobial Peptides in Innate Host Defences, Trends in Microbiology, 8 (2000) 402-410.

[70] T. Ganz, The Role of Antimicrobial Peptides in Innate Immunity, Integrative and Comparative Biology, 43 (2003) 300-304.

[71] C. Loose, K. Jensen, I. Rigoutsos, G. Stephanopoulos, A Linguistic Model for the Rational Design of Antimicrobial Peptides, Nature, 443 (2006) 867-869.

[72] P.K. Singh, M.R. Parsek, E.P. Greenberg, M.J. Welsh, A Component of Innate Immunity Prevents Bacterial Biofilm Development, Nature, 417 (2002) 552-555.

[73] K.A. Brogden, Antimicrobial Peptides: Pore Formers or Metabolic Inhibitors in Bacteria?, Nature Reviews Microbiology, 3 (2005) 238-250.

[74] B.-S. Kim, S.W. Park, P.T. Hammond, Hydrogen-Bonding Layer-by-Layer-Assembled Biodegradable Polymeric Micelles as Drug Delivery Vehicles from Surfaces, ACS Nano, 2 (2008) 386-392.

[75] K.C. Wood, N.S. Zacharia, D.J. Schmidt, S.N. Wrightman, B.J. Andaya, P.T. Hammond, Electroactive Controlled Release Thin Films, Proceedings of the National Academy of Sciences, 105 (2008) 2280-2285.

[76] F. Caruso, K. Niikura, D.N. Furlong, Y. Okahata, 2. Assembly of Alternating Polyelectrolyte and Protein Multilayer Films for Immunosensing, Langmuir, 13 (1997) 3427-3433.

[77] A.A. Argun, J.N. Ashcraft, P.T. Hammond, Highly Conductive, Methanol Resistant Polyelectrolyte Multilayers, Advanced Materials, 20 (2008) 1539-1543.

[78] C. Picart, Polyelectrolyte Multilayer Films: From Physico-Chemical Properties to the Control of Cellular Processes, Current Medicinal Chemistry, 15 (2008) 685-697.

[79] E. Kharlampieva, V. Kozlovskaya, S.A. Sukhishvili, Layer-by-Layer Hydrogen-Bonded Polymer Films: From Fundamentals to Applications, Advanced Materials, 21 (2009) 3053-3065.

[80] E. Vazquez, D.M. Dewitt, P.T. Hammond, D.M. Lynn, Construction of Hydrolytically-Degradable Thin Films via Layer-by-Layer Deposition of Degradable Polyelectrolytes, Journal of the American Chemical Society, 124 (2002) 13992-13993.

[81] O. Etienne, C. Gasnier, C. Taddei, J.-C. Voegel, D. Aunis, P. Schaaf, M.-H. Metz-Boutigue, A.-L. Bolcato-Bellemin, C. Egles, Antifungal Coating by Biofunctionalized Polyelectrolyte Multilayered Films, Biomaterials, 26 (2005) 6704-6712.

[82] J. Orivel, V. Redeker, J.-P. Le Caer, F. Krier, A.-M. Revol-Junelles, A. Longeon, A. Chaffotte, A. Dejean, J. Rossier, Ponericins, New Antibacterial and Insecticidal Peptides from the Venom of the Ant Pachycondyla goeldii, The Journal of Biological Chemistry, 276 (2001) 17823-17829.

[83] J. Choi, M.F. Rubner, Influence of the Degree of Ionization on Weak Polyelectrolyte Multilayer Assembly, Macromolecules, 38 (2004) 116-124.

[84] S.L. Clark, P.T. Hammond, The Role of Secondary Interactions in Selective Electrostatic Multilayer Deposition, Langmuir, 16 (2000) 10206-10214.

[85] N.S. Zacharia, D.M. DeLongchamp, M. Modestino, P.T. Hammond, Controlling Diffusion and Exchange in Layer-by-Layer Assemblies, Macromolecules, 40 (2007) 1598-1603.

[86] J. Zhang, N.J. Fredin, J.F. Janz, B. Sun, D.M. Lynn, Structure/Property Relationships in Erodible Multilayered Films: Influence of Polycation Structure on Erosion Profiles and the Release of Anionic Polyelectrolytes, Langmuir, 22 (2005) 239-245.

[87] A.L. Barry, W.A. Craig, H. Nadler, L.B. Reller, C.C. Sanders, J.M. Swenson, Methods for Determining Bactericidal Activity of Antimicrobal Agents; Approved Guideline, M26-A, Clinical and Laboratory Standards Institute, 19 (1999) 1-29.

[88] J. Selinummi, J. Seppälä, O. Yli-Harja, J.A. Puhakka, Software for Quantification of Labeled Bacteria from Digital Microscope Images by Automated Image Analysis, Biotechniques, 39 (2005) 859-863.

[89] C. Porcel, P. Lavalle, V. Ball, G. Decher, B. Senger, J.-C. Voegel, P. Schaaf, From Exponential to Linear Growth in Polyelectrolyte Multilayers, Langmuir, 22 (2006) 4376-4383.

[90] L. Jourdainne, Y. Arntz, B. Senger, C. Debry, J.-C. Voegel, P. Schaaf, P. Lavalle, Multiple Strata of Exponentially Growing Polyelectrolyte Multilayer Films, Macromolecules, 40 (2007) 316-321.

[91] C. Picart, J. Mutterer, L. Richert, Y. Luo, G.D. Prestwich, P. Schaaf, J.C. Voegel, P. Lavalle, Molecular Basis for the Explanation of the Exponential Growth of Polyelectrolyte Multilayers, Proceedings of the National Academy of Sciences of the United States of America, 99 (2002) 12531-12535.

[92] P. Lavalle, C. Gergely, F.J.G. Cuisinier, G. Decher, P. Schaaf, J.C. Voegel, C. Picart, Comparison of the Structure of Polyelectrolyte Multilayer Films Exhibiting a Linear and an

Exponential Growth Regime: An in Situ Atomic Force Microscopy Study, Macromolecules, 35 (2002) 4458-4465.

[93] A. Ishwar, K. Jeong, A. Panitch, O. Akkus, Raman Spectroscopic Investigation of Peptide-Glycosaminoglycan Interactions, Applied Spectrscopy, 63 (2009) 636-641.

[94] Y. Wang, B. Agerberth, A. Löthgren, A. Almstedt, J. Johansson, Apolipoprotein A-I Binds and Inhibits the Human Antibacterial/Cytotoxic Peptide LL-37, The Journal of Biological Chemistry, 273 (1998) 33115-33118.

[95] S. Pacor, A. Giangaspero, M. Bacac, G. Sava, A. Tossi, Analysis of the Cytotoxicity of Synthetic Antimicrobial Peptides on Mouse Leucocytes: Implications for Systemic Use, Journal of Antimicrobial Chemotherapy, 50 (2002) 339-348.

[96] J.E. Parrillo, Pathogenetic Mechanisms of Septic Shock, New Englang Journal of Medicine, 328 (1993) 1471-1478.

[97] R.E.W. Hancock, R. Lehrer, Cationic Peptides: A New Source of Antibiotics, Trends in Biotechnology, 16 (1998) 82-88.

[98] Y.J. Gordon, E.G. Romanowski, A.M. McDermott, A Review of Antimicrobial Peptides and Their Therapeutic Potential as Anti-Infective Drugs, Current Eye Research, 30 (2005) 505-515.

[99] K. Chua, B.P. Howden, Treating Gram-Positive Infections: Vancomycin Update and the Whys, Wherefores and Evidence Base for Continuous Infusion of Anti-Gram-Positive Antibiotics, Current Opinion in Infectious Diseases, 22 (2009) 525-534.

[100] L. Zhao, P.K. Chu, Y. Zhang, Z. Wu, Antibacterial Coatings on Titanium Implants, Journal of Biomedical Materials Research Part B: Applied Biomaterials, 91B (2009) 470-480.

[101] S. Radin, J.T. Campbell, P. Ducheyne, J.M. Cuckler, Calcium Phosphate Ceramic Coatings as Carriers of Vancomycin, Biomaterials, 18 (1997) 777-782.

[102] M.L. Veyries, G. Couarraze, S. Geiger, F. Agnely, L. Massias, B. Kunzli, F. Faurisson, B. Rouveix, Controlled Release of Vancomycin from Poloxamer 407 Gels, International Journal of Pharmaceutics, 192 (1999) 183-193.

[103] S. Radin, P. Ducheyne, Controlled Release of Vancomycin from Thin Sol-Gel Films on Titanium Alloy Fracture Plate Material, Biomaterials, 28 (2007) 1721-1729.

[104] J.M. Andrews, Determination of Minimum Inhibitory Concentrations, Journal of Antimicrobial Chemotherapy, 48 (2001) 5-16.

[105] S.L.R. Barker, D. Ross, M.J. Tarlov, M. Gaitan, L.E. Locascio, Control of Flow Direction in Microfluidic Devices with Polyelectrolyte Multilayers, Analytical Chemistry, 72 (2000) 5925-5929.

[106] D.M. Lynn, R. Langer, Degradable Poly(β-Amino Esters): Synthesis, Characterization, and Self-Assembly with Plasmid DNA, Journal of the American Chemical Society, 122 (2000) 10761-10768.

[107] J.L.H. Johnson, S.H. Yalkowsky, Reformulation of a New Vancomycin Analog: An Example of the Importance of Buffer Species and Strength, AAPS PharmSciTech, 7 (2006) E33-E37.

[108] P.T. Hammond, Recent Explorations in Electrostatic Multilayer Thin Film Assembly, Current Opinion in Colloid & Interface Science, 4 (1999) 430-442.

[109] N.A. Kotov, Layer-by-Layer Self-Assembly: The Contribution of Hydrophobic Interactions, Nanostructured Materials, 12 (1999) 789-796.

[110] N. Cini, T.l. Tulun, G. Decher, V. Ball, Step-by-Step Assembly of Self-Patterning Polyelectrolyte Films Violating (Almost) All Rules of Layer-by-Layer Deposition, Journal of the American Chemical Society, 132 (2010) 8264–8265.

[111] A.P.R. Johnston, E.S. Read, F. Caruso, DNA Multilayer Films on Planar and Colloidal Supports: Sequential Assembly of Like-Charged Polyelectrolytes, Nano Letters, 5 (2005) 953-956.

[112] T. Cserháti, E. Forgács, Use of Liquid Chromatography for the Determination of Interactions Between Bioactive Compounds, Biomedical Chromatography, 9 (1995) 157-161.

[113] M.P. Gasper, A. Berthod, U.B. Nair, D.W. Armstrong, Comparison and Modeling Study of Vancomycin, Ristocetin A, and Teicoplanin for CE Enantioseparations, Analytical Chemistry, 68 (1996) 2501-2514.

[114] C.-Y. Lai, B.G. Trewyn, D.M. Jeftinija, K. Jeftinija, S. Xu, S. Jeftinija, V.S.Y. Lin, A Mesoporous Silica Nanosphere-Based Carrier System with Chemically Removable CdS Nanoparticle Caps for Stimuli-Responsive Controlled Release of Neurotransmitters and Drug Molecules, Journal of the American Chemical Society, 125 (2003) 4451-4459.

[115] R.R. Pfeiffer, Structural Features of Vancomycin, Reviews of Infectious Diseases, 3 (1981) S205-S209.

[116] D.H. Williams, M.S. Searle, J.P. Mackay, U. Gerhard, R.A. Maplestone, Toward an Estimation of Binding Constants in Aqueous Solution: Studies of Associations of Vancomycin Group Antibiotics, Proceedings of the National Academy of Sciences of the United States of America, 90 (1993) 1172-1178.

[117] M. Schäfer, T.R. Schneider, G.M. Sheldrick, Crystal Structure of Vancomycin, Structure, 4 (1996) 1509-1515.

[118] K. Kishimoto, J.M. Manning, Adherence of Vancomycin to Proteins, Journal of Protein Chemistry, 20 (2001) 455-461.

[119] M. Switek, D. Valensin, C. Migliorini, E. Gaggelli, G. Valensin, M. Jezowska-Bojczuk, Unusual Binding Ability of Vancomycin Towards Cu2+ Ions, Dalton Transactions, (2005) 3808-3813.

[120] M.H. Wilcox, T.G. Winstanley, R.C. Spencer, Binding of Teicoplanin and Vancomycin to Polymer Surfaces, Journal of Antimicrobial Chemotherapy, 33 (1994) 431-441.

[121] C.-K. Lee, S.I. Sandler, Vancomycin Partitioning in Aqueous Two-Phase Systems: Effects of pH, Salts, and an Affinity Ligand, Biotechnology and Bioengineering, 35 (1990) 408-416.

[122] C. Picart, J. Mutterer, L. Richert, Y. Luo, G.D. Prestwich, P. Schaaf, J.-C. Voegel, P. Lavalle, Molecular Basis for the Explanation of the Exponential Growth of Polyelectrolyte Multilayers, Proceedings of the National Academy of Sciences of the United States of America, 99 (2002) 12531-12535.

[123] L. Jourdainne, Y. Arntz, B. Senger, C. Debry, J.-C. Voegel, P. Schaaf, P. Lavalle, Multiple Strata of Exponentially Growing Polyelectrolyte Multilayer Films, Macromolecules, 40 (2006) 316-321.

[124] P. Bieker, M. Scholˋnhoff, Linear and Exponential Growth Regimes of Multilayers of Weak Polyelectrolytes in Dependence on pH, Macromolecules, 43 (2010) 5052-5059.

[125] E. Kharlampieva, J.F. Ankner, M. Rubinstein, S.A. Sukhishvili, pH-Induced Release of Polyanions from Multilayer Films, Physical Review Letters, 100 (2008) 128303.

[126] A.S. Antipas, D.G. Vander Velde, S.D.S. Jois, T. Siahaan, V.J. Stella, Effect of Conformation on the Rate of Deamidation of Vancomycin in Aqueous Solutions, Journal of Pharmaceutical Sciences, 89 (2000) 742-750.

[127] J.-D. Hecq, L.P. Boitquin, D.F. Vanbeckbergen, J. Jamart, L.M. Galanti, Effect of the Freezing Conditions and Microwave Thawing Power on the Stability of Cefuroxime in Dextrose 5% Infusion Polyolefin Bags at 4 °C, The Annals of Pharmacotherapy, 39 (2005) 1244-1248.

[128] M.J. Wood, R. Lund, M. Beavan, Stability of Vancomycin in Plastic Syringes Measured by High–Performance Liquid Chromatography, Journal of Clinical Pharmacy and Therapeutics, 20 (1995) 319-325.

[129] W. Mawhinney, C. Adair, S. Gorman, B. McClurg, Stability of Vancomycin Hydrochloride in Peritoneal Dialysis Solution, American Journal of Health-System Pharmacy, 49 (1992) 137-139.

[130] T.E.A.H. Küpper, S. Bettina, R. Burkhard, A.-V. Hemmerling, S. Volker, S. Juergen, Drugs and Drug Administration in Extreme Environments, Journal of Travel Medicine, 13 (2006) 35-47.

[131] J.M. Anderson, A. Rodriguez, D.T. Chang, Foreign Body Reaction to Biomaterials, Seminars in Immunology, 20 (2008) 86-100.

[132] M.J.S. Langman, J. Weil, P. Wainwright, D.H. Lawson, M.D. Rawlins, R.F.A. Logan, M. Murphy, M.P. Vessey, D.G. Colin-Jones, Risks of Bleeding Peptic Ulcer Associated with Individual Non-Steroidal Anti-Inflammatory Drugs, The Lancet, 343 (1994) 1075-1078.

[133] J. Page, D. Henry, Consumption of NSAIDs and the Development of Congestive Heart Failure in Elderly Patients: An Underrecognized Public Health Problem, Archives of Internal Medicine, 160 (2000) 777-784.

[134] W.A. Ray, C.M. Stein, J.R. Daugherty, K. Hall, P.G. Arbogast, M.R. Griffin, COX-2 Selective Non-Steroidal Anti-Inflammatory Drugs and Risk of Serious Coronary Heart Disease, The Lancet, 360 (2002) 1071-1073.

[135] N. Jessel, P. Schwinté, R. Donohue, P. Lavalle, F. Boulmedais, R. Darcy, B. Szalontai, J.C. Voegel, J. Ogier, Pyridylamino-β-Cyclodextrin as a Molecular Chaperone for Lipopolysaccharide Embedded in a Multilayered Polyelectrolyte Architecture, Advanced Functional Materials, 14 (2004) 963-969.

[136] Renée C. Smith, M. Riollano, A. Leung, Paula T. Hammond, Layer-by-Layer Platform Technology for Small-Molecule Delivery, Angewandte Chemie International Edition, 48 (2009) 8974-8977.

[137] S.Y. Wong, Q. Li, J. Veselinovic, B.-S. Kim, A.M. Klibanov, P.T. Hammond, Bactericidal and Virucidal Ultrathin Films Assembled Layer-by-Layer from Polycationic N-Alkylated Polyethylenimines and Polyanions, Biomaterials, 31 (2010) 4079-4087.

[138] C. Doria, C.P. Fischer, C.G. Wood, P. Mark Li, S. Marra, J. Hart, Phase 3, Randomized, Double-Blind Study of Plasma-Derived Human Thrombin Versus Bovine Thrombin in Achieving Hemostasis in Patients Undergoing Surgery, Current Medical Research and Opinion, 24 (2008) 785-794.

[139] M. Sabel, W. Stummer, The Use of Local Agents: Surgicel and Surgifoam, European Spine Journal, 13 (2004) S97-S101.

[140] T. Białopiotrowicz, B. Jańczuk, Surface Properties of Gelatin Films, Langmuir, 18 (2002) 9462-9468.

[141] M.C. Berg, L. Zhai, R.E. Cohen, M.F. Rubner, Controlled Drug Release from Porous Polyelectrolyte Multilayers, Biomacromolecules, 7 (2005) 357-364.

[142] J. Andersson, J. Rosenholm, S. Areva, M. Lindén, Influences of Material Characteristics on Ibuprofen Drug Loading and Release Profiles from Ordered Micro- and Mesoporous Silica Matrices, Chemistry of Materials, 16 (2004) 4160-4167.

[143] R. Langer, N.A. Peppas, Advances in Biomaterials, Drug Delivery, and Bionanotechnology, AIChE Journal, 49 (2003) 2990-3006.

[144] J.L. Sondeen, A.E. Pusateri, V.G. Coppes, C.E. Gaddy, J.B. Holcomb, Comparison of 10 Different Hemostatic Dressings in an Aortic Injury, Journal of Trauma-Injury Infection & Critical Care, 54 (2003) 280-285.

[145] N.R. Goldsack, R.C. Chambers, K. Dabbagh, G.J. Laurent, Molecules in Focus Thrombin, The International Journal of Biochemistry & Cell Biology, 30 (1998) 641-646.

[146] E.W. Davie, J.D. Kulman, An Overview of the Structure and Function of Thrombin, Seminars in Thrombosis and Hemostasis, 32 (2006) 3-15.

[147] I. Erel-Unal, S.A. Sukhishvili, Hydrogen-Bonded Multilayers of a Neutral Polymer and a Polyphenol, Macromolecules, 41 (2008) 3962-3970.

[148] A. Karshikov, W. Bode, Electrostatic Properties of Thrombin: Importance for Structural Stabilization and Ligand Binding, Seminars in Thrombosis and Hemostasis, 19 (1993) 334-343.

[149] J.W. Fenton, M.J. FAsco, A.B. Stackrow, Human Thrombins: Production, Evaluation, and Properties of Alpha-Thrombin, The Journal of Biological Chemistry, 252 (1977) 3587-3598.

[150] J.P. Van Buren, W.B. Robinson, Formation of Complexes Between Protein and Tannic Acid, Journal of Agricultural and Food Chemistry, 17 (1969) 772-777.

[151] P. Gaffney, T. Edgell, The International and "NIH" Units for Thrombin- How do they Compare?, Journal of Thrombosis and Haemostasis, 74 (1995) 900-903.

[152] R. Sood, Clinical Haematology: Bleeding Disorders, Medical Laboratory Technology Methods and Interpretation, Jaypee Brothers Medical Publishers, 1999, pp. 247.

[153] G.J. Gabriel, A. Som, A.E. Madkour, T. Eren, G.N. Tew, Infectious Disease: Connecting Innate Immunity to Biocidal Polymers, Materials Science and Engineering: R: Reports, 57 (2007) 28-64.

[154] A.K. Marr, W.J. Gooderham, R.E.W. Hancock, Antibacterial Peptides for Therapeutic Use: Obstacles and Realistic Outlook, Current Opinion in Pharmacology, 6 (2006) 468-472.

[155] O. Etienne, C. Picart, C. Taddei, Y. Haikel, J.L. Dimarcq, P. Schaaf, J.C. Voegel, J.A. Ogier, C. Egles, Multilayer Polyelectrolyte Films Functionalized by Insertion of Defensin: A New Approach to Protection of Implants from Bacterial Colonization, Antimicrobial Agents and Chemotherapy, 48 (2004) 3662-3669.

[156] K. Kuroda, G.A. Caputo, W.F. DeGrado, The Role of Hydrophobicity in the Antimicrobial and Hemolytic Activities of Polymethacrylate Derivatives, Chemistry-a European Journal, 15 (2009) 1123-1133.

[157] R.F. Epand, B.P. Mowery, S.E. Lee, S.S. Stahl, R.I. Lehrer, S.H. Gellman, R.M. Epand, Dual Mechanism of Bacterial Lethality for a Cationic Sequence-Random Copolymer that Mimics Host-Defense Antimicrobial Peptides, Journal of Molecular Biology, 379 (2008) 38-50.

[158] B.P. Mowery, S.E. Lee, D.A. Kissounko, R.F. Epand, R.M. Epand, B. Weisblum, S.S. Stahl, S.H. Gellman, Mimicry of Antimicrobial Host-Defense Peptides by Random Copolymers, Journal of the American Chemical Society, 129 (2007) 15474-15476.

[159] C.C. Zhou, X.B. Qi, P. Li, W.N. Chen, L. Mouad, M.W. Chang, S.S.J. Leong, M.B. Chan-Park, High Potency and Broad-Spectrum Antimicrobial Peptides Synthesized via Ring-Opening Polymerization of alpha-Aminoacid-N-carboxyanhydrides, Biomacromolecules, 11 (2010) 60-67.

[160] G.N. Tew, D.H. Liu, B. Chen, R.J. Doerksen, J. Kaplan, P.J. Carroll, M.L. Klein, W.F. DeGrado, De Novo Design of Biomimetic Antimicrobial Polymers, Proceedings of the National Academy of Sciences of the United States of America, 99 (2002) 5110-5114.

[161] J. Lin, S.Y. Qiu, K. Lewis, A.M. Klibanov, Bactericidal Properties of Flat Surfaces and Nanoparticles Derivatized with Alkylated Polyethylenimines, Biotechnology Progress, 18 (2002) 1082-1086.

[162] J.C. Tiller, C.J. Liao, K. Lewis, A.M. Klibanov, Designing Surfaces that Kill Bacteria on Contact, Proceedings of the National Academy of Sciences of the United States of America, 98 (2001) 5981-5985.

[163] B. Dizman, M.O. Elasri, L.J. Mathias, Synthesis and Antibacterial Activities of Water-Soluble Methacrylate Polymers Containing Quaternary Ammonium Compounds, Journal of Polymer Science Part A-Polymer Chemistry, 44 (2006) 5965-5973.

[164] S.Y. Wong, Q. Li, J. Veselinovic, B.S. Kim, A.M. Klibanov, P.T. Hammond, Bactericidal and Virucidal Ultrathin Films Assembled Layer-by-Layer from Polycationic N-Alkylated Polyethylenimines and Polyanions, Biomaterials, 31 (2010) 4079-4087.

[165] L.M. Timofeeva, N.A. Kleshcheva, A.F. Moroz, L.V. Didenko, Secondary and Tertiary Polydiallylammonium Salts: Novel Polymers with High Antimicrobial Activity, Biomacromolecules, 10 (2009) 2976-2986.

[166] M.A. Gelman, B. Weisblum, D.M. Lynn, S.H. Gellman, Biocidal Activity of Polystyrenes that are Cationic by Virtue of Protonation, Organic Letters, 6 (2004) 557-560.

[167] M.F. Ilker, K. Nusslein, G.N. Tew, E.B. Coughlin, Tuning the Hemolytic and Antibacterial Activities of Amphiphilic Polynorbornene Derivatives, Journal of the American Chemical Society, 126 (2004) 15870-15875.

[168] A.C. Engler, H.I. Lee, P.T. Hammond, Highly Efficient "Grafting onto" a Polypeptide Backbone Using Click Chemistry, Angewandte Chemie-International Edition, 48 (2009) 9334-9338.

[169] A.C. Engler, D.K. Bonner, H.G. Buss, E.Y. Cheung, P.T. Hammond, The Synthetic Tuning of Clickable pH Responsive Cationic Polypeptides and Block Copolypeptides, submitted, (2010).

[170] C. Xiao, C. Zhao, P. He, Z. Tang, X. Chen, X. Jing, Facile Synthesis of Glycopolypeptides by Combination of Ring-Opening Polymerization of an Alkyne-Substituted N-carboxyanhydride and Click "Glycosylation", Macromolecular Rapid Communications, 31 (2010) 991-997.

[171] P.J. Belshaw, S. Mzengeza, G.A. Lajoie, Chlorotrimethylsilane Mediated Formation of Omega-Allyl Esters of Aspartic and Glutamic Acids, Synthetic Communications, 20 (1990) 3157-3160.

[172] W.H. Daly, D. Poche, The Preparation of N-Carboxyanhydrides of Alpha-Amino-Acids Using Bis(Trichloromethyl)Carbonate, Tetrahedron Letters, 29 (1988) 5859-5862.

[173] B. Carboni, A. Benalil, M. Vaultier, Aliphatic Amino Azides as Key Building-Blocks for Efficient Polyamine Syntheses, The Journal of Organic Chemistry, 58 (1993) 3736-3741.

[174] M. Calas, G. Cordina, J. Bompart, M. BenBari, T. Jei, M.L. Ancelin, H. Vial, Antimalarial Activity of Molecules Interfering with Plasmodium Falciparum Phospholipid Metabolism. Structure-Activity Relationship Analysis, Journal of Medicinal Chemistry, 40 (1997) 3557-3566.

[175] O.M. Merkel, M.A. Mintzer, J. Sitterberg, U. Bakowsky, E.E. Simanek, T. Kissel, Triazine Dendrimers as Nonviral Gene Delivery Systems: Effects of Molecular Structure on Biological Activity, Bioconjugate Chemistry, 20 (2009) 1799-1806.

[176] W.C. Johnson, Protein Secondary Structure and Circular-Dichroism - A Practical Guide, Proteins-Structure Function and Genetics, 7 (1990) 205-214.

[177] P.I. Haris, D. Chapman, The Conformational-Analysis of Peptides Using Fourier-Transform IR Spectroscopy, Biopolymers, 37 (1995) 251-263.

[178] T. Ikeda, H. Hirayama, H. Yamaguchi, S. Tazuke, M. Watanabe, Polycationic Biocides with Pendant Active Groups: Molecular Weight Dependence of Antibacterial Activity, Antimicrobial Agents and Chemotherapy, 30 (1986) 132-136.

[179] A. Ivankin, L. Livne, A. Mor, G.A. Caputo, W.F. DeGrado, M. Meron, B. Lin, D. Gidalevitz, Role of the Conformational Rigidity in the Design of Biomimetic Antimicrobial Compounds, Angewandte Chemie International Edition, 49 (2010) 8462-8465.

[180] J. Cho, F. Caruso, Polymeric Multilayer Films Comprising Deconstructible Hydrogen-Bonded Stacks Confined between Electrostatically Assembled Layers, Macromolecules, 36 (2003) 2845-2851.

[181] A. Zhuk, S. Pavlukhina, S.A. Sukhishvili, Hydrogen-Bonded Layer-by-Layer Temperature-Triggered Release Films, Langmuir, 25 (2009) 14025-14029.

[182] L. Feuz, P. Strunz, T. Geue, M. Textor, O. Borisov, Conformation of Poly(L-lysine)-Graft-Poly(ethylene glycol) Molecular Brushes in Aqueous Solution Studied by Small-Angle Neutron cattering, The European Physical Journal E: Soft Matter and Biological Physics, 23 (2007) 237-245.

Appendix A

Fitting Data That Transitions Between Two Linear Regimes

A.1 Instantaneous Transition

For a variable t which varies with n, and where the trend shows two linear regions with different slopes connected at a transition value n_o, we can use following simple relation

$$t = X_1 n_o + \frac{1}{2} X_1 \left\{ (n - n_o) - |n - n_o| \right\} + \frac{1}{2} X_2 \left\{ (n - n_o) + |n - n_o| \right\} \tag{1}$$

where, n_o is the value of n where the slope changes from X_1 to a higher value X_2.

Here, if $n < n_o$, $|n - n_o| = -(n - n_o)$, equation (1) reduces to:

$$t = X_1 n$$

If $n > n_o$, $|n - n_o| = (n - n_o)$, equation (1) reduces to

$$t = (X_1 - X_2) n_o + X_2 n$$

Note, since $|n - n_o| = \sqrt{(n - n_o{}^2)}$, we can also rewrite (1) as

$$t = X_1 n_o + \frac{1}{2} X_1 \left\{ (n - n_o) - \sqrt{(n - n_o)^2} \right\} + \frac{1}{2} X_2 \left\{ (n - n_o) + \sqrt{(n - n_o)^2} \right\} \tag{2}$$

A.2 Smooth Transition

For a variable t which varies with n, and where the trend shows two linear regimes with different slopes, and where one linear regime with lower slope smoothly transitions to the second linear region with higher slope, we can use following simple relation:

$$t = X_1 n_o + \frac{1}{2} X_1 \left\{ (n - n_o) - \sqrt{(n - n_o)^2 + dn} \right\} + \frac{1}{2} X_2 \left\{ (n - n_o) + \sqrt{(n - n_o)^2 + dn} \right\} \tag{3}$$

where, n_o, denotes a value for n related to where transition from one region to another region occurs. The parameter, d $(d \geq 0)$, controls how gradually the transition happens. The lower the

value of d, the narrower the transition region ($d = 0$, indicates abrupt change and (3) simplifies to (2)).

We can rearrange and write (3) as

$$t = X_1 n_o + \frac{1}{2}(X_1 + X_2)(n - n_o) - \frac{1}{2}(X_1 - X_2)\sqrt{(n - n_o)^2 + dn} \qquad (4)$$
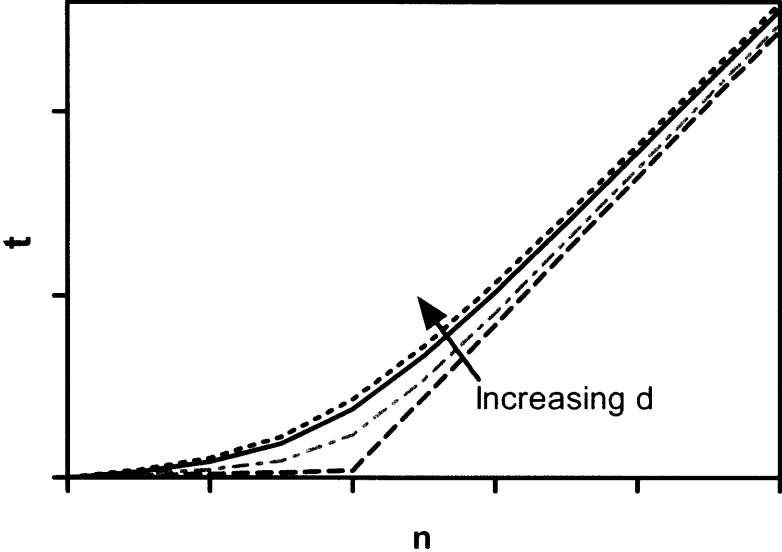

Figure A-1: Two phase linear transition.

Appendix B

Effect of Wash Ionic Strength on Vancomycin Films

Vancomycin containing films were constructed with the same architecture as films described in Chapter 3, (poly 2/polyanion/vancomycin/polyanion)$_n$ on (LPEI/SPS)$_{10}$. All deposition solutions had the same concentration, pH, and ionic strength as the films constructed in Chapter 3. However, instead of rinsing in solutions with the same ionic strength as the deposition solutions (0.1 M sodium acetate buffer, pH 5.0), the rinse steps were carried out in deionized water (18.2 MΩ, Milli-Q Ultrapure Water System, Millipore). The pH of this water was not adjusted and was tested at the start of the deposition process to be approximately pH 5. Additionally, no salt was added to this water rinse. Figure B-1 shows the growth profiles of these films, while Figure B-2 shows the release profiles of 60 tetralayer films.
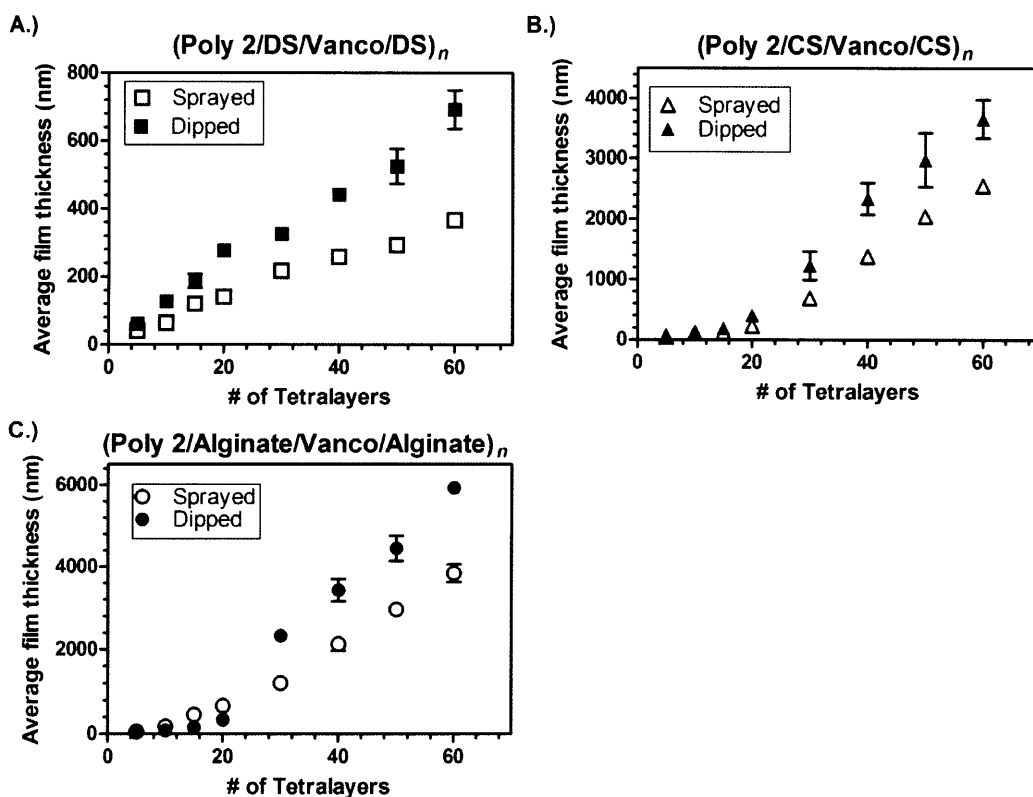

Figure B-1: Growth profiles for: (poly 2/polyanion/vancomycin/polyanion)$_n$. Rinse steps following each deposition were conducted in deionized water (no ionic strength of pH adjustment).

Except for the dextran sulfate dipped films, the films constructed with unadjusted water rinse steps, loaded more vancomycin for the same number of tetralayers as those that were rinsed at the same pH and ionic strength as the deposition solutions. However, all films released vancomycin rapidly (in the first 4 to 8 hours).
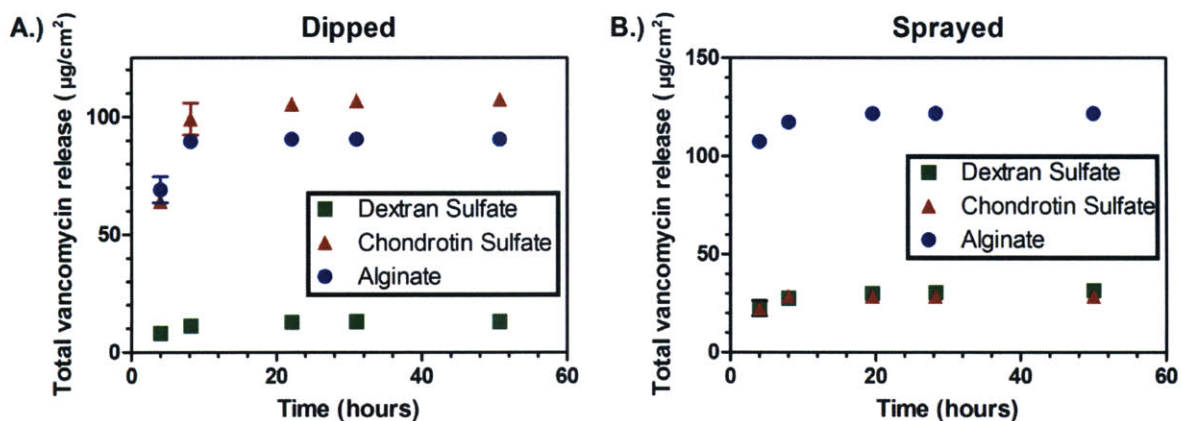

Figure B-2: Vancomycin release from dipped and sprayed 60 tetralayer films with water rinse steps.

Appendix C

Antimicrobial Polypeptide Surface Coatings

C.1 Calculation of Thickness

Thickness of solvent cast polypeptides was estimated by assuming that the polymer is a rigid rod α-helical peptide [182], as shown below (Equations 1-6). Figure C-1 shows a schematic of the polypeptide dimensions.
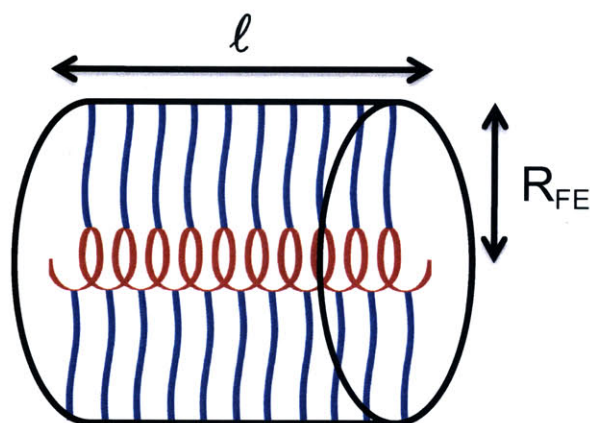

Figure C-1: Polypeptide schematic.

The length of the polypeptide, ℓ, was estimated by calculating how many turns each polymer has (3.62 repeat units per turn) and multiplying it by the distance between turns on an α-helical backbone (1.5 Å per turn). The polymer radius, R_{FE}, was estimated by assuming the polypeptide side chains protruded out from the α-helical backbone in a fully extended chain conformation. The surface area, A_{PP}, covered by a single polypeptide was estimated by multiplying ℓ by $2R_{FE}$ (the polymer diameter). The total area covered by polypeptides if they were packed as cylinders in a single monolayer, A_{SC}, was calculated by multiplying A_{PP} by the concentration of polymer solution, C_{PS}, and the volume casted, V_{PS}, as well as Avogadro's number, and dividing this by the molecular weight of the polypeptide, MW_{PP}. The number of polypeptide monolayers, L, was estimated by dividing the disc area, A_D, by A_{SC}. The thickness, h, was estimated by multiplying the number of polypeptide layers by $2R_{FE}$.

$$n_{turns} = \frac{DP}{3.62}$$ (1)

$$l = 1.5\text{Å} \times n_T$$ (2)

$$A_{PP} = l \times 2R_{FE}$$ (3)

$$A_{SC} = \frac{A_{PP} \times C_{PS} \times V_{PS} \times N_A}{MW_{PP}}$$ (4)

$$L = \frac{A_D}{A_{SC}}$$ (5)

$$h = L \times 2R_{FE}$$ (6)

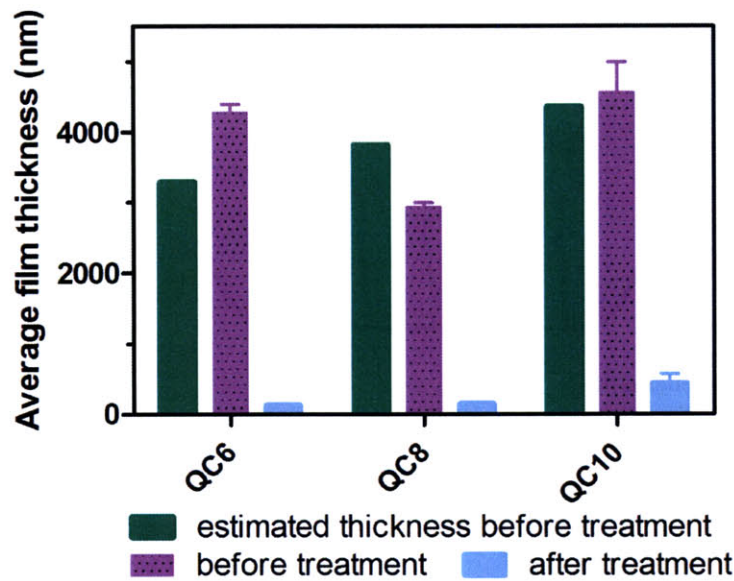## C.2 Substrate Coating Experiments

Figure C-2: Average polypeptide film thickness.

Figure C-2 shows thicknesses following solvent casting of PPLG DP=75 substituted with QC6, QC8, and QC10 polypeptide films before and after bacteria culture media treatment (data shown here corresponds to incubation in CaMHB). The predicted thickness values before treatment based on the above model are also shown. The estimated polypeptide thickness was within 30% of the measured film thickness. Morphology of films before and after treatment is shown for the QC10 polypeptide solvent cast substrates in the following atomic force microscopy images.
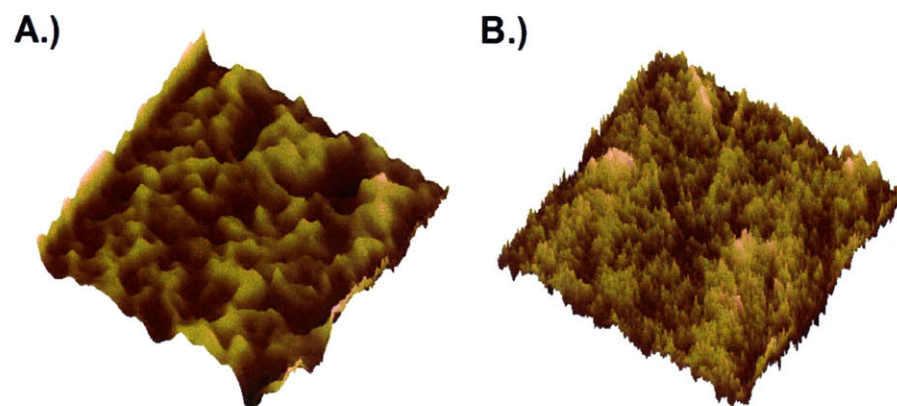
Figure C-3: QC10 solvent cast substrate morphology (10 μm x 10 μm). A.) Before media treatment (maximum z-scale = 22.1 nm). B.) After media treatment (maximum z-scale = 1.7 nm).